Additively Manufactured, Cost-Efficient Sensors for Ions and Bacteria in Fluids

Christian Pfeffer

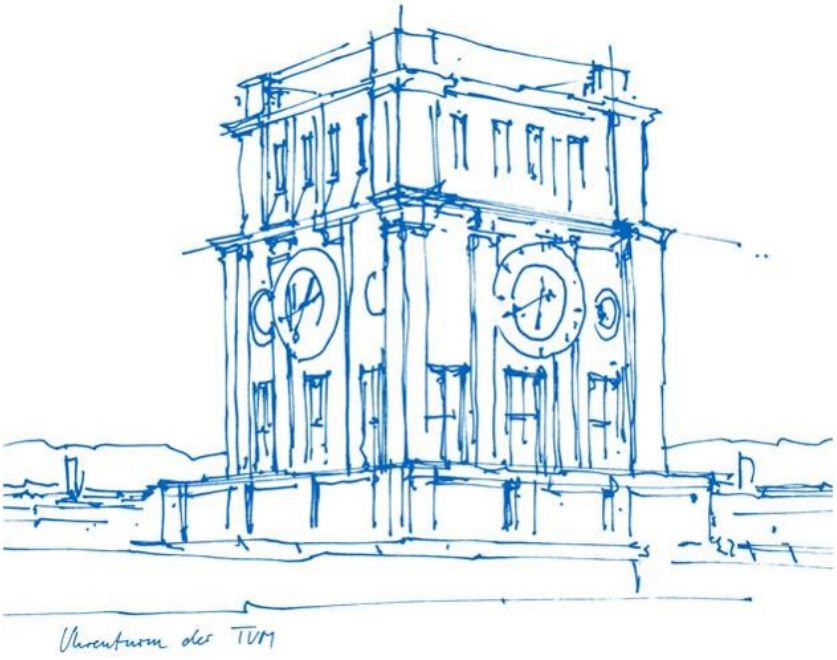

Technische Universität München

TUM School of Computation, Information and Technology

Additively Manufactured, Cost-Efficient Sensors for Ions and Bacteria in Fluids

Christian Pfeffer

Vollständiger Abdruck der von der TUM School of Computation, Information and Technology der Technischen Universität München zur Erlangung des akademischen Grades eines

Doktors der Ingenieurwissenschaften
(Dr.-Ing.)

genehmigten Dissertation.

Vorsitz:	Prof. Dr. rer. nat. Bernhard Wolfrum
Prüfer*innen der Dissertation:	1. Prof. Dr.-Ing. Ralf Brederlow
	2. Prof. Dr. rer. nat. Bernhard Wolf

Die Dissertation wurde am 04.05.2022 bei der Technischen Universität München eingereicht und durch die Fakultät für Elektrotechnik und Informationstechnik am 17.09.2022 angenommen.

A true scientist is curious about everything. It's not just about their own field of research, it's about everything that's happening around them.

Attributed to Mayim Bialik

Abstract

In a smart and connected world, sensor system represent a vital bridge between the analog, real world and the digital world. Especially chemistry is hard to measure or evaluate if the needed sensor systems are too complex, too expensive for the application, or simply not-well understood.

In this work, cost-efficient electrochemical sensor systems are explored. Electrochemical Impedance Spectroscopy (EIS) is used to derive ionic concentrations in fluids as well as pathogen detection in aquaos solution. Additive Manufacturing is used to reduce costs drastically. Our approach compromises significant progress by circumventing the urgent need of an additional reference electrode.
In the first part, the plan, design, layout, and fabrication of ionic sensors are presented. Finite-Elements Simulations are used to model the systems and study their electrostatical behaviour. Next, the approach of EIS for sensor applications is experimentally verified and characterized. Finally, an enhanced equivalent circuit model based on experimental results is presented for future integration of read-out electronics to this kind of ionic sensor. A dynamic range of the EIS-sensor of $(71.3 \pm 0.7)\mathrm{M}\Omega$ is reported. The lower frequency range up to 1 kHz is identified to be superior in its usability for ionic sensing. Noteworthy, the system covers the biologically relevant concentration range of Sodium in the mM -range. A theoretical detection limit of 10^{-8} M is indicated proving sufficient sensitivity for biotech applications.
In the second part, bacteria sensors based on EIS are considered. The sensor system is studied regarding its design, modeling and material choices, and possible wiring configurations. Specifically, a mathematical tool is developed to evaluate and differentiate manifold sensor designs. Finally, experimental proof that shows that bacterial loads consisting out of E. Coli colonies down to 10^4 Colony-Forming Units (CFU) per ml can be measured by our approach. The bacterial detection limit for this method could be improved by two to three orders of magnitude indicating a significant performance increase through the optimized sensor design.

The results demonstrate that cost-effective, EIS-based sensors can be fabricated using additive manufacturing methods. In general, targets like E. Coli bacteria as well as ions like Sodium can be detected. Further steps include the system's behaviour in field-like environments depending on the application area. Cross-sensitivies towards other bacterial strands like Pseudomonas aeruginosa or Legionella pneumophila or chemically- similar ionic species have to be researched. Long-term studies that exceed the observed life-time of 6 months are recommended to realize a possible product.

Zusammenfassung

In einer 'smarten' Welt der ständigen Konnektivität nehmen Sensoren eine besondere Rolle ein. Sie stellen die Brücke zwischen der Welt des digitalen Zwillings und der echten, analogen Welt dar. Die Chemie um uns herum ist bisher kaum vermessbar, da mögliche Sensorsysteme zu komplex und zu teuer für die Anwendung sind.

In dieser Arbeit werden kosteneffiziente elektrochemische Sensorsysteme erforscht. Elektrochemische Impedanzspektroskopie (EIS) erlaubt es, Ionenkonzentration oder bakterielle Schädlinge in Lösungen zu messen. Dabei werden Verfahren aus dem Bereich "Additve Fertigung" benutzt um eine kostengünstige Herstellung der Sensoren zu gewährleisten. Unser Ansatz fällt durch das Umgehen einer sonst notwendigen und umständlichen Referenzelektrode auf.

Im ersten Teil der Arbeit wird die Planung, das Design, das Layout sowie die Herstellungen der ionischen Sensoren präsentiert. Finite-Elemente-Methode (FEM-) Simulationen modelieren das System und untersuchen ihr elektrostatisches Verhalten. Der Ansatz der Impedanzspektroskopie für die Sensoranwendung wird experimentell verifiziert und charakterisiert. Weiterhin wird ein verbessertes Ersatzschaltbild zur Modelierung eines ionischen Sensors vorgestellt, welches zur zukünftigen Entwicklung und Anpassung einer integrierbaren Ausleseschaltung dienen kann. Der nutzbare Dynamikumfang des ionischen Sensors ist $(71.3 \pm 0.7)\mathrm{M}\Omega$. Der niedrigere Frequenzbereich bis 1 kHz der Anregungsfrequenz ist für EIS-Messungen wegen seines höheren, nutzbaren Signals prädestiniert. Bemerkenswert ist, dass das System Natrium Ionen in dessen biologisch relevanten Bereich (mM) messen und unterscheiden kann. Ein theoretisches Detektionslimit wird auf 10^{-8} M abgeschätzt, sodass der Ionensensor ausreichend Sensitivität für biotechnlogische Anwendungen bietet.

Im zweiten Teil werden auf EIS-basierende Bakteriensensoren betrachtet. Das Sensorsystem wird zunächst entworfen, modelliert und auf Materialauswahl sowie mögliche Konfigurationen bei der Kontaktierung untersucht. Insbesonders wird ein mathematisches Model (und dessen Implementierung in Matlab) entwickelt, welches erlaubt, beliebige Sensordesigns zu evaluieren und in ihrer Performance zu unterscheiden. Abschließend wird ein experimenteller Beweis zur Messbarkeit von E. Coli Kolonien bis zu 10^4 KBE (Kolonie-bildende Einheit) gezeigt. Das optimierte Sensordesign führt zur signifikanten Verbesserung des Detektionslimits für das ausgewählte Bakterium.

Die Resulate zeigen, dass kostengünstige EIS-basierte Sensoren über Druckverfahren herstellbar sind. So können sowohl Ziele wie E. Coli Bakterien als auch einzelne Ionen wie Natrium detektiert und quantifiziert werden. Zukünftige Arbeiten sollen das Langzeit-Verhalten der Sensoren in schwierigeren Umgebungen entsprechened der Anwendung untersuchen. Quersensitivitäten zu anderen Bakterienarten wie Pseudomonas aeruginosa, Legionella pneumophila oder eben anderen Ionensorten als auch die Lebenszeiten der Sensoren im Medium (bisher mehr als 6 Monate) müssen unter-

sucht werden um ein mögliches Produkt auf den Markt bringen zu können.

Contents

List of Figures

List of Tables

List of Symbols

Symbol	Description	Unit
a	Nozzle Diameter	µm
a_{red}	Activity for Reduced Ions	
a_{ox}	Activity for Oxidized Ions	
$\alpha_{a,c}$	Transfer Coefficients in Anodic and Cathodic Direction	
C	Concentration	M
$c_{r,o}$	Concentrations of Redox Couple "R" and "O"	mol $\cdot$ m^{-3}
$\mathbf{C}$	Capacitance Matrix	F
D	Electric Displacement Field	C $\cdot$ m^{-2}
δ	Dynamic Range	MΩ
E	Electric Field or Electrode Polarisation	V/m
E_0^F	Formal Potential of Redox Couple	V
$\lvert E_{RMS}\rvert$	Magnitude of the Electrical Field (root-mean square)	V/m
ϵ_0	Permittivity of free space	
ϵ_m	Permittivity of media	
ϵ_p	Permittivity of particle	
E_0	Electrode potential under standard conditions	V
f	Inverse Thermal Voltage	V^{-1}
F	Faraday Constant	96485 C $\cdot$ mol^{-1}
γ	Activity Coefficient	
γ	Surface Tension	N/m
k_0	Heterogenous Rate Constants	m $\cdot$ s^{-1}
σ	Conductivity	mS/cm
ϕ	Phase	rad
Oh	Ohnesorg Number	
ν	Dynamic Viscosity	Pa $\cdot$ s
ρ	Density	kg m^{-3}
τ	Lifetime	s
ω_0	Reciprocal of Time Constant	s^{-1}
Ω	Solid (room) angle	sr

P	Polarization	$C \cdot m{-}2$
p	Complex Frequency Variable	
Q	Electrical Charge Matrix	C
R	Gas Constant	8.3145 J mol^{-1} K^{-1}
S	Sensitivity	$M\Omega$ mM^{-1}
T	Temperature	K
V	Volume	m^3
V_{ij}	Electric Field Gradient	$V \cdot m{-}2$
U_0	Unit Step Voltage	V
W_e	Electrical Energy	J
Y	Admittance Matrix	Ω^{-1}
z	Charge of Principal Ion	
Z	Impedance	Ω

Table 1: List of Symbols Used in this Work

Acronyms

AAS	Atomic Absorption Spectrometry
AC	Alternating Current
BSA	Bovine Serum Albumin
CFU	Colony-Forming Unit
CMOS	Complementary Metal-Oxide-Semiconductor
CMUT	Capacitative Micromachined Ultra-Sonic Transducer
DC	Direct Current
DOD	Drop-On-Demand
EIS	Electrochemical Impedance Spectroscopy
ELISA	Enzyme-linked Immunosorbent Assay
ESD	Electrostatic Discharge
E. Coli	Escherichia Coli
HSI	Hyperspectral Imaging Technique
IDA	Interdigitated Electrode Array
IoT	Internet of Things
ISM	Ion-selective Membrane
ITO	Indium-Tin-Oxide
FEM	Finite Element Method
FBAR	Film Bulk Acoustic Resonator
FTIR	Fourier Transform Infrared Spectroscopy
MEMS	Micro-Electromechanical Systems

PBS Phosphate-Saline-Buffer

PCA Principal-Component-Analysis

PCR Polymerase Chain Reaction

PDMS Polydimethylsiloxane

PEN Polyethylennaphthalat

PVC Polyvinyl Chloride

QCM Quartz Crystal Microbalance

QF Qualtity Factor

RE Reference Electrode

SAW Surface Acoustic Wave

SNR Signal-to-Noise Ratio

SERS Surface-Enhanced-Raman Spectroscopy

ISFET Ion-Selective-Field-Effect-Transistor

UV Ultra-violett

Chapter 1

Introduction

1.1 The Role of Sensors in the Era of IoT

The United Nations defined UN Sustainable Development Goals in 2015. They introduced guidelines for researcher and engineers around the globe [1]. Sensors play a critical role for current and future technologies as they allow to measure the physical world. Hence, sensors provide valueable data that can be used to gain valueable insights for real-life applications.

Figure 1.1: Sustainable Development Goals of the United Nations. This PhD project tries to make a contribution to the highlighted goals in red. Adapted and modified from [2].

This work encompasses two sensor systems that involve aspects from the UN goals (see figure 1.1). Figure 1.2 gives a quick overview on the two projects involving Electrochemical Impedance Spectroscopy.

On the one side, a chemical sensor is developed measuring ion concentrations in fluids. The low-cost approach involves novel fabrication methods about additive manufacturing. One highlight is the versatility of the system regarding the ion of interest. At the time of writing, theoretical and experimental proof is presented for Na^+ and H^+, but can be further extended to other cations and likely anions as well. Further advantages are size reduction, and a possibility to integrate the read-out electronics.

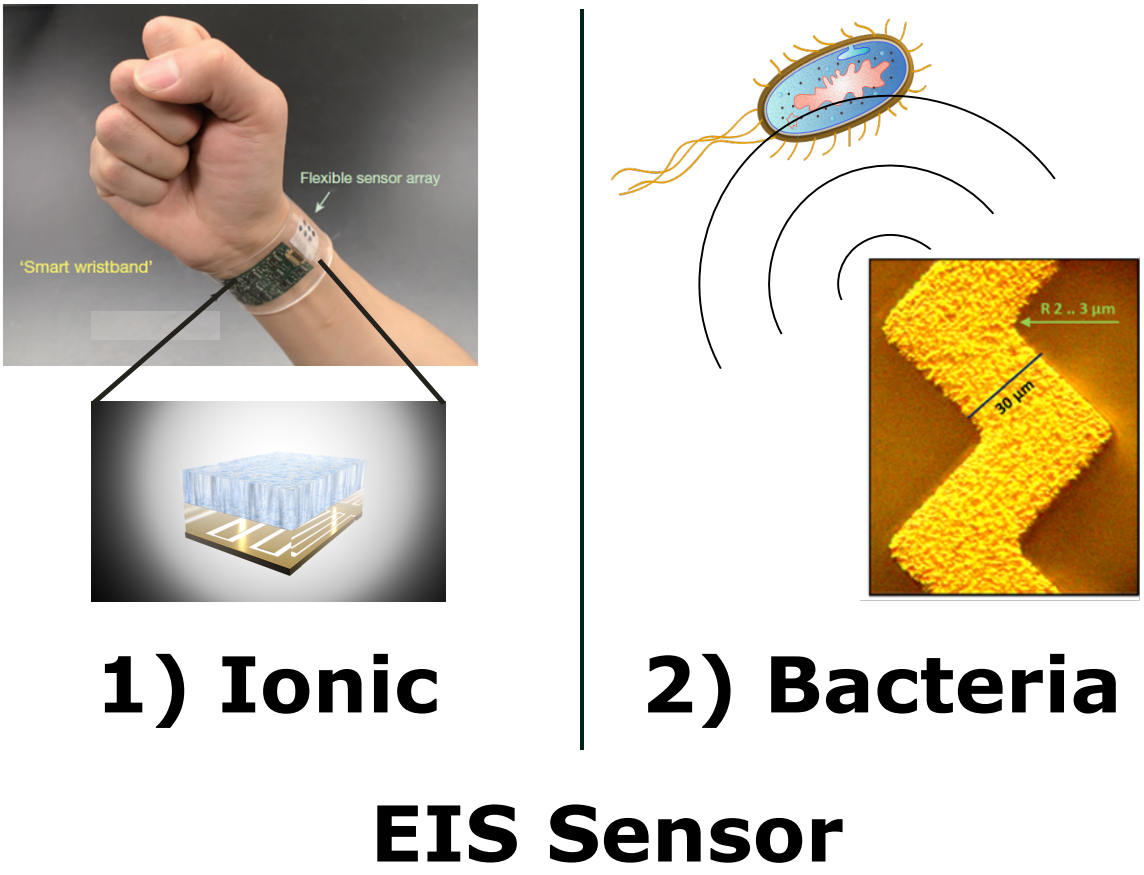

Figure 1.2: Two sensor projects emcompassing this thesis. On the left hand side, a fully additive manufacturable ionic sensor serves the purpose of Biotech applications like sweat monitoring. On the right side, a microfabricated sensor uses Electrochemical Impedance Spectroscopy for pathogen detection in fluids. Adapted and modified from [2, 3].

On the other side, a sensor system for bacterial detection is presented. Based on Finite-Elements Simulations, electrical fields are calculated in a electrode design study. The theoretical behaviour of bacteria in these fields is studied, and a model is shown on how their polarization and movement in the field can be used to derive a detection scheme. Backed-up by experimental data, this approach allows valueable insights about pathogen detection in fluids.

1.2 Sensor Applications

Possible applications for the presented sensor systems are:

- Body Fluid Monitoring for Disease Detection
- Water Quality Monitoring
- Soil Quality
- Bacterial Detection in Air Condition
- Bacterial Detection in Public Spaces

A few scientific problems arouse when trying to realize these applications. In on the on hand side, the behaviour of miniaturized electrochemical and its limits remain unclear. The commonly used potentiometric measurement scheme allows high resolution, but is mostly limited to thick-film fabrication methods like dipping, prone to manufacturing deviations and suffers from drift. Hence, a calibration is needed by trained personell. Bulky read-out circuits have not yet been integrated with very few exceptions (e.g. [3]). Life times below six month are common and are tackled. Furthermore, packaging is not straight forward as the sensor and all contacts are exposed to liquids that can lead to undesired short-circuits.

1.3 Goal of This Work

The approach of this work aims to solve and significantly enhance the knowledge about the mentioned problems. First of all, an enhanced impediometric instead of potentiometric measurement scheme is implemented in order to circumevent drift and the urgent need of calibration. Vast Finite-Elements simulations are performed to predict distribution of electrical field lines and find suitable sensor geometries. Advances in material science and additive manufacturing are used to create progress. Inkjet-printing can help to minimize deviations in the manufacturing process. In this context, novel non-PVC based inks have been developed and optimized for Ink-jet printing. The ultimate goal is to broaden the understanding of biotech and life science sensors.

This work is divided into the following chapters. Chapter 2 presents the state of art. More details and some theoretical basics on the approach taken are given in this part. Both projects share the use of the detection method Impedance Spectroscopy. Chapter 3 describes the manufacturing of the sensors, the involved materials, and theoretical background on the numerical simulations as well as the used measurement equipment. Results on ionic detection and on bacterial detection are set out in chapter 4 and 5. The sixth chapter summarizes and discusses the findings. In Chapter 7, the author

draws conclusions and offers an outlook on how this technology can go to market and have a real-life impact eventually.
The technology in this project can be used for other applications as well. The introduction explained the framework of this work giving details about motivation, applications, the scientific problem and the approach taken. In the next chapter, the state of the art in this field is reviewed and differences to the authors approach are presented.

Chapter 2

State of the Art: Microscopic Ionic Sensor

2.1 Overview

This chapter starts with an overview, followed by the physical and chemical principles behind the systems. Finally, a range of examples are given and directly compared to the approach taken here. This work comprises sensor systems for bacterial detection as well as ionic detection. Firstly, ionic or chemical sensors are discussed.

2.2 Definition of Chemical Sensor

IUPAC defines a chemical sensor to be "a device that transforms chemical information, ranging from the concentration of a specific sample component to total composition analysis, into an analytically useful signal" [4]. Even though first chemical sensors have already been published in 1978, many Internet-of-Things (IoT) applications remain unreachable due to size and costs of production. The ionic sensor presented in this work fulfils this definition as well as the one of a biosensor.

2.3 Definition of Biosensor

Sensors for bacterial detection are categorized as "biosensor". A biosensor is defined in more general terms as "a device that uses specific biochemical reactions mediated by isolated enzymes, immunosystems, tissues, organelles or whole cells to detect chemical compounds usually by electrical, thermal or optical signals" [5]. Figure 2.1 shows the stages of a biosensor.
The samples of interest contain specific ionic species like Na^+. The recognition elements are macromolecules, called ionophores in the scope of this project and will be

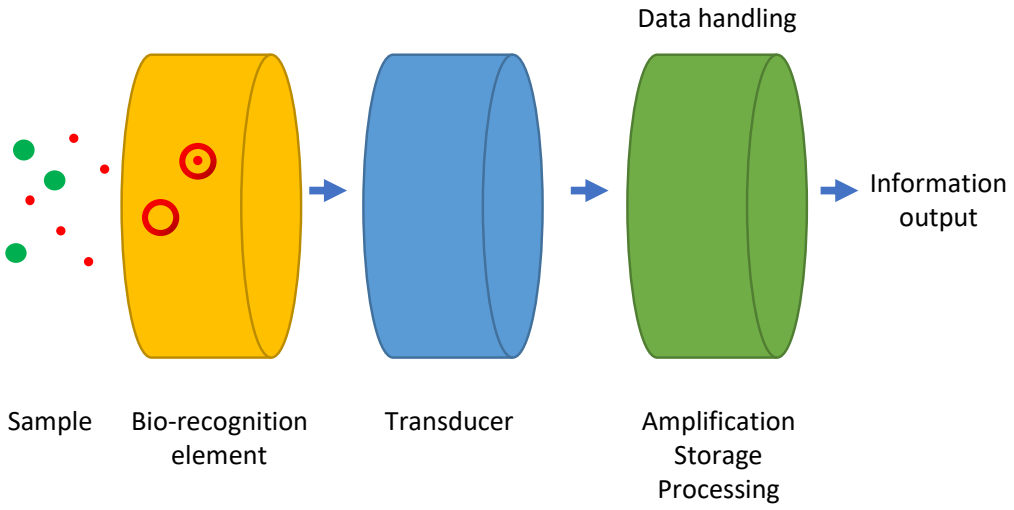

Figure 2.1: General Working Principle of a Biosensor. Adapted from [6, 7]

detailed in section 2.6. The desired information are concentrations of ionic species in fluids, or the quantity of bacteria in a solution, respectively.

2.4 Requirements

The need of calibration, trained personnel, limits in feature size lead to high prices and consequently rule out many applications. Hence, this project does not focus on the highest possible analytical resolution but instead really tries to push the cost efficiency into new heights (see figure 2.2). The main reason for this boundary condition is that chemical sensors have been developed a few decades ago. However, the high prices prevented that the rich chemical information in our everyday's lives are exploited. A scale-able fabrication technique allow high quantities of producible sensors and lead to a higher cost-efficiency. This correlates with a size reduction of the used systems as well as the possibility of integrating the read-out electronics. The fabrication of the sensors plays the main role in the cost calculations. Also, sensitivity, selectivity and life time interplay in the trade-off. This project evolved around trying to maximize the first two parameters allowing single-use applications that are comparatively accessible. This approach offers the potential to tackle life time issues later on enhancing the realm of possible applications.
A special focus is laying on the fabricational part of the sensor. Additive Manufacturing is a vital part of it and is detailed in chapter 4.1.

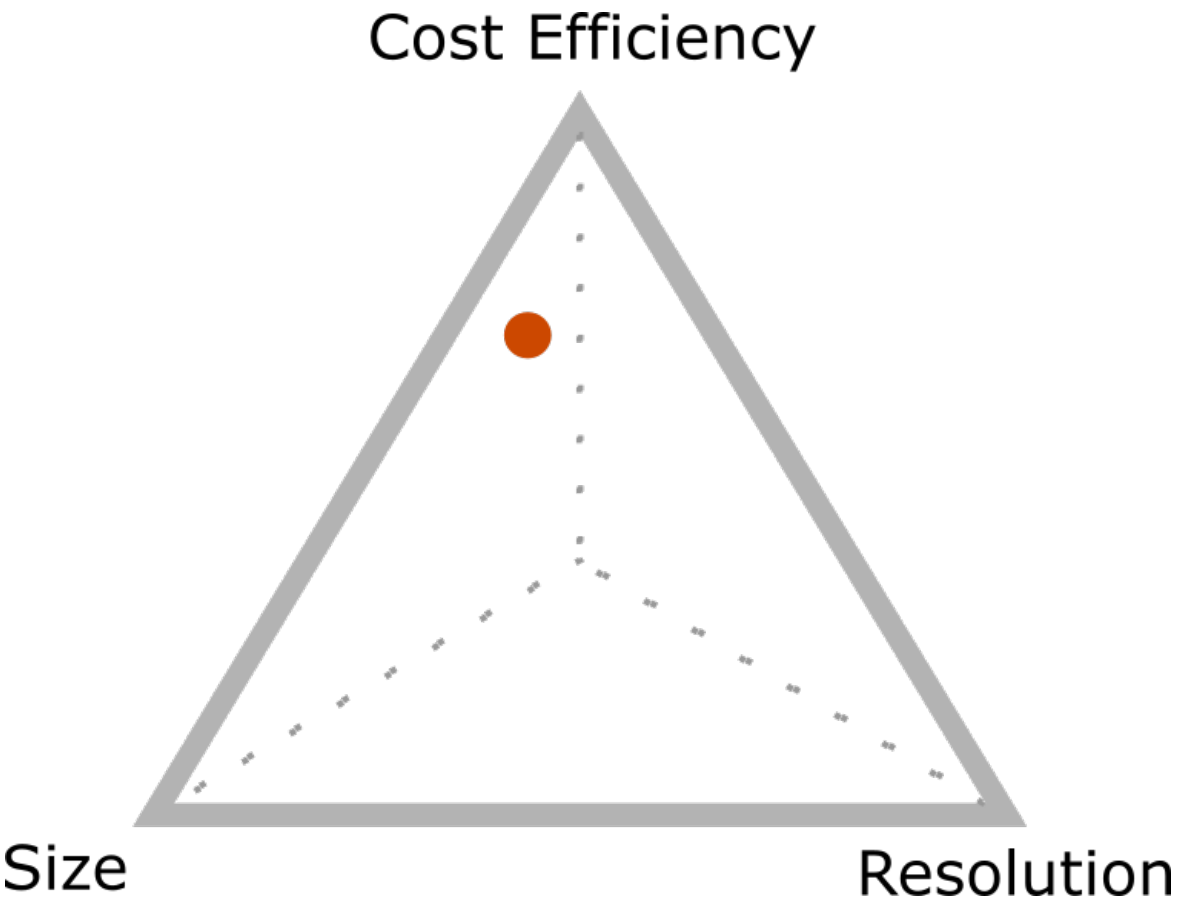

Figure 2.2: Trade-off in Conception of Integrated, Chemical Sensor Systems. The red dot symbolizes the taken approach in this work.

Figure 2.2 sets the spotlight towards low cost as high-resolution measurements can be performed with off-the-shelf potentiometric ion-selective electrodes (ISE). This gold standard is inferior in cost and size and limit the application space [8]. The desired applications highly drive the systems design and requirements. The physical limits lead to trade-offs that have to taken into consideration and that cannot be circumvented. Table 2.2 shows a few ways on how to realize a chemical sensor systems. However, the physical and chemical principles behind the sensors are presented first.

2.5 Transduction Principles

A transducer converts a signal in one form of energy to a signal in another [9]. In our case, the inputs are ether ion concenctrations or bacteria concentrations in fluids. Some form of electronical signal is desired as output [10].

2.5.1 Charge based

2.5.1.1 Potentiometric

The most prominent way to measure ions in fluids is to directly measure the influence of the ion's charge. The fluid itself can have a measureable potential E that an experimenter can tap that follows the well-known Nernst potential in eq. 2.5.1 by Walther Nernst.

$$E = E_0 + \frac{RT}{z_i F}\frac{a_{red}}{a_{ox}} = E_0 + \frac{2.303RT}{z_i F} log(\gamma N) \tag{2.5.1}$$

The second part of eq. 2.5.1 is the Nikolsky modification that describes specifically Ion-Selective-Electrodes (ISE) and micro-ISE [11, 12]. E_0 describes the potential of the electrode under standard conditions. R is the gas constant (8.31 $\frac{J}{K \cdot mol}$) and T is the thermodynamic temperature (in Kelvin). z_i is an integer with sign and magnitude corresponding to the charge of the principal ion and F stands for the Faraday constant (9.659104 $\frac{C}{mol}$). Next, a_i are the activities of the involved ions and differ for oxidized and reduced ions, respectively. In the second part is γ described as an activity coefficient and N stands for the concentration of the principal ion (please see [11, 12]). Logically, the overall potential origins from manifold ions and surface effects. Thus, a physical separation of the ions is done to specifically target the ion-of-interest. Ion-selective-membranes on electrodes are used to only allow for a certain type of ion and its potential to be measured. The Nernst-Equation is then used to derive the target ion's concentration in the solution. It is important to state here, that using this method a defined overall potential is needed. A reference electrode like Ag/AgCl can force this potential to a defined value. Therefore, a 3-electrode setup is indespensable. The reader is kindly referred to extensive reviews about current solid-contact ion-selective sensors [13, 14].

Since the 1970's, Bergfeld came up with Ion-Selective-Field-Effect-Transistors (ISFET's). This approach takes advantage of transistors and the change in current through them to obtain the output signals. There are manifold variations, e.g. Extendend-Gate-ISFET's that can be studied in current reviews [15, 16, 17, 18], but it will not be detailed here. ISFET belong to the category of potentiometric sensors and rely on defined potentials of the fluid-of-interest, consequently. Combined with functional organic layers, ISFET's have been used for environmental monitoring [19, 20, 21]. Mobile [22], and especially printable [23] labs have been proposed and studied mainly in terms of drug delivery and cancer research.

2.5.1.2 Amperometric

For rough concentrations (e.g. sea water) amperometric methods are used that directly measure the current flowing between electrochemical electrodes. The target has to

have the ability to be oxidized or reduced, and the reactions directly lead to current as output variable. One of the earliest biosensor of this kind dates back to 1962 when L.C. Clark introduced a glucose meter [10, 24]. A sensitive layer of Glucose-Oxidase acts as a transducer element on top of a Clark (or Oxygen) electrode. The reduction of the functional material leads to a measurable current as output variable. The current is directly proportional to the concentration of glucose (or oxygen), respectively [25].

2.5.1.3 Impediometric or Conductometric

So far, the introduced transduction mechanism rely on large pertubations of the system: Forcing potential steps (or sweeps), and current steps to an electrochemical systems brings it into a situation far off from equilibrium [26]. The next approach allows for staying closer to the steady-state conditions using the the impedance Z in eq. 2.5.2.

$$Z(\omega) = Z_{Re} - jZ_{Im} \tag{2.5.2}$$

Please note that the phase ϕ and magnitude $|Z|$ are the more practical variables for EIS in eq. 2.5.3.

$$|Z| = (Z_{Re})^2 + (Z_{Im})^2 \; and \; \phi = arctan(\frac{Z_{Im}}{Z_{Re}}) \tag{2.5.3}$$

By applying only AC signals with very small amplitude to the system a few advantages arise, as cited in [26, 27]:

- High-precision measurements possible
- Small-signal model: Linearization of E-I characteristics allows simplification of kinetic and diffusional processes
- Measurement over long time
- No need for additional reference electrode

Hence, Electrochemical Impedance Spectroscopy (EIS) offers an elegant method on how to gain information about complex, non-linear system of interest. It is a versatile technique used for various purposes, e.g. in the case of single-ion-detection like Ca^{2+} or Mg^{2+} [28]. Also, thin-film enzyme based sensor can be realised with this approach [29]. Further examples are presented in the table 6.1. Compared to the potentiometric "gold standard" of thick-film Ion-Selective-Electrodes (ISE), the mandatory need of an additional reference electrode can be omitted. Some disadvantages include:

- Precise fabrication method is required
- Assuming steady-state conditions measurements can take longer

- Bleaching of ionophores is possible

Impediometric sensors on solid-state micro-electrodes for Potassium [30] have been reported. The concept of using an acrylate-based dielectric reference membrane for potentiometric measurements is presented by Bananezhada in 2019 [31].

ISCOM

In the late 1990's, the first Ion-Selective Conductometric Microsensors have been reported using PVC membranes [32, 33, 34, 35]. The reference electrode, with Ag/AgCl being the most prominent one, can be omitted in this approach and allows for further minituarization of the sensor system as the reference electrode itself is very challenging to reduce in size [8]. They have not been as widely followed up compared to potentiometric sensors but driven by the mentioned core advantage in recent years researchers presented more often related-work [28, 30, 36]. The theory is explained in more detail in section 5.2.
The presented literature is based on Polyvinyl chloride (PVC)-based membranes. These are commercially available in membrane cocktails that include a solvent that evaporates and eventually hardens the mixture into solid-state. A major drawback with PVC membranes are inhomogeneities that can arise from the evaporation process. Hence, other base matrix materials are searched that can offer more control over the process in section 2.6.4.

2.5.2 Optical Sensors

In the world of (electro)-chemistry optical approaches play an essential role. The measurement of light absorbed or emitted as consequence of a biochemical reaction is called optical biosensor [37]. The reader is kindly refered to a general review about this topic [38]. Optical sensors tended to have short life times (below 15 days of operation) but significant advances have been made in the lab-on-chip field integrating optical devices. An extensive review about optical lab-on-chip technologies and their limitations can be found in [39]. Depending on the analyte, detection limits down to 10 pM are reported. However, the necessary light source suffers from noise that might arise from light intensity fluctuation or temperature fluctuations [39]. Direct electrochemical measurements are preferred due to their ability to miniaturize the system and omit expensive optical parts.
It is worth to note some destructive analysis techniques, like flame atomic absorption spectrometry or flame atomic emission spectrometry. Burning the material emits characteristic light that can be used to derive the quantity of an analyte [40]. However, the focus of this work lays in non-destructive techniques.

2.5.3 Microelectromechanical, Gravimetric and other Approaches

2.5.3.1 Thermistor

Heat can also be used as a transducer element. Thermistors can be used for single-ion detection of heavy metals, offering detection limits below 1.0×10^{-3} M [41, 42, 43]. Another rather exoctic approach is to use mechanosensitive piezo channels proteins [44]. Proteins react to ions show mechanical or electrical forces that could be used a transducer element.

2.5.3.2 Surface Acoustic Wave Transducers (SAW)

Rayleigh reported about surface acoustiv waves back in 1885 [45]. Surface acoustic wave (SAW) transducers can be enhanced with selective coatings that react with the chemical analyte. The propagation of an acoustic wave across the surface of the device is affected by any perturbation [46]. A phase shift, frequency-shift, or time-delay in the output electrical signal can be detected consequently [46] and used for sensing. Furthermore, other surface acoustic wave devices can be utilized for chemical sensing. In recent years, first approach about nanopores filled with specific ions came up. The reader is kindly referred to an review to this novel approach [47].

2.5.3.3 Quartz Crystal Microbalances (QCM)

A completely different approach can be taken by gravimetry. Some ions like Sodium can be physically separated by ion-exchange resins, bound to to a well-known counter-ion like Sulfate, and consequently measured by high-precision weights. Some authors report detection limits down to 2 µg for this method [46].

Quartz crystal microbalances (QCM) QCM sensors are mainly used for gas sensors but can also be used with crown ethers binding to alkali metals. Taking advantage of the piezoelectric effect combined with functional layers can achieve Sodium detection in a biologically relevant range [48]. A clear disadvantage is the destructive nature of this type of method [40]. A fine, recent review about gravimetric biosensing can be found here [46].

2.5.3.4 Film Bulk Acoustic Resonator (FBAR)

This CMOS-based approach exploits the QCM theory further. A bulk wave propagating inside a piezoelectric thin film is generated when the piezoelectric thin film is placed between electrodes and applying a high-frequency signal, resulting in frequencies typically in the GHz-range [49, 50, 46]. Using the inverse piezoelectric effect, the

defined resonance frequency of standing acoustic waves changes with the additional weight of a bound target analyte [49, 50, 46]. The authors report detection limits in the range of µM [46].

2.5.3.5 Micro-electromechanical Systems (MEMS)

Silicon Capacitive Resonators (or micro-scale resonating tips) can be employed for chemical detection of e.g. Copper ions in water samples. When in contact with the sample, the resonant structure is oxidized and changes the resonant frequencies accordingly. The shift in frequency can be correlated to the physical amount of the analyte.The authors report detection limits of 4 µM [51].

2.5.3.6 Capacitive Micromachined Ultra-sonic Transducer (CMUT)

A combination of the techniques above are arrays of capacitive micromachined ultrasonic transducer (CMUT) arrays [52]. The technique evolves around capacitive transduction for mass load detection mainly for gas sensing [46] but it can be also used for fluids [53].

2.6 Ion-selective-Sensor Systems

2.6.1 Overview on Ionophores

Solid-state chemical sensors are studied since a few decades and a variety of publications is available [13]. The heart of the ionic sensors is the interaction between the an target ion and its corresponding ionophore separating the target from other ionic species present in the medium. This chapter tries to summarize the existing ionophores.
A short version of the table that displays the available target ions is given in 2.1. Heavy metals like Silver or Cadmium can be of interest for environmental monitoring as they can be toxic in certain concentration ranges. Alkali metals can be important biomarkes in body fluids like sweat and can contribute to health monitoring devices[13].
An extensive research about available and developed ionophores is given in the appendix in table A.1. The reader is kindly refered to the appendix to view the table. The working principle of ionophores is explained in chapter 4.1. When reviewing the table one notices that there are several ionophores for certain targets like Sodium. The abundance of the ion-specific macro molecules can be explained by nature itself - in the 1980's researcher began to discover that Sodium transfer plays a vital role in cell-to-cell communication [54]. In this context, biology does not rely on a single mechanism but rather provides a few different proteins that differ in their properties like target selectivity and cross sensitivities [35]. This highlights the urgent need to

adapt to the application requirements from a system perspective and hence, selecting the best performing ionophore to the expected environment of exposition.

List of Possible Target Ions Available by Developed Ionophores

Ammonium	Erbium	Perchlorate
Bisulfite	Flouride	Phtalate
Cadmium	Hydrogen	Potassium
Calcium	Lithium	Silver
Bromo-Calcimycin	Magnesium	Sodium
Carbonate	Manganese	Tin
Cesium	Mercury	Thulium
Chloride	Nickel	Zinc
Copper	Nitrate	
Cyanide	Nitrite	

Table 2.1: List of Possible Target Ions Available by Developed Ionophores

In this work, Sodium Ionophore X (Selectophore) is chosen [55]. It's low detection limit of down to $3.5 \cdot 10^{-6}$ M as well as its low (the lower the better) selectivity coefficient of -2,7 towards Potassium are the strength of this ion-specific molecule [55]. However, these values refer to potentiometric measurements and can only hint the ionophore's performance in impediometric systems.

2.6.2 Commercially Available Solutions

The gold standard for ion detection in fluids are the commercially available PVC-membrane-based potentiometric sensors, commonly refered to "Ion-Selective-Electrodes (ISE)" [56]. Hach is an example among other suppliers for various target ions [57]. Moreover, Fisher Scientific offers half cells which are also following the same working principle [58].
Mettler Toledo offers glass as sensor material and, similar to an pH electrode, changes the glass membrane to be sensitive to Sodium [59]. The detection limit is 10^{-7} M and covers the biologically relevant range. Sodium stands out between other target ions because of its small ionic size and its abundance in glass compositions. Glassy electrodes change the tap-able potential when in contact with Sodium ions, however, this method of detection offers rather low selectivity [60] and usually comprise the use of reference solutions to make the measurement scheme more robust and sensitive.

For other ions like NH_4 Xylem Inc. provides potentiometric ISE [61]. The macroscopic

sizes, the urgent need for an additional reference electrode and calibration, as well as high costs of at least 500 Euro incl. read-out devices are the downsides of the commercial systems.

2.6.3 Comparison

In this section, a number of ion-sensitive systems are presented in table 2.2. Depending on the target ion the presented detection methods reveal that the most used technique is potentiometric. Apart from the central disadvantage of the reference electrode, most scientific literature is focused around this method due to its superior detection limit (10^{-12}) and ease-of-use.

For very high molarities, like in sea salt water, the amperometric method is used and appreciated for its robust available setups but comes at the price of modest resolutions. As opposed to gravimetric methods are prone to selectivity issues , require sophisticated read-out circuitry so far and usually are lab-bound techniques. An exeption are SAW sensors that become more interesting due to its CMOS-compatibility and its rapid development in industry.

The optical approach may not be suited perfectly for electrochemical measurements. Its advantages are the intrinsic robustness, also in challenging environments. The existence of manifold flourescent dyes and their increasing importance in Biotech might be a key for success for future sensor applications.

Micromechanic or gravimetric approachs are still niche but they hold promise to exactly target the low-cost markets. This is due to CMOS compability and its extraordinary technological development. As technological processes in fabrication are highly optimized, Surface acoustic wave transducers (SAW), Micro-electromechanical systems (MEMS) and capacitive micromachined ultra-sonic transducer (CMUT) can fill the gap between existing, very precise potentiometric approaches and low-resolution, low-cost miniaturized chemical sensors. Their detection limits are currently in the mM-range which can be enough for sweat-analysis, for instance.

Table 2.2: Comparison of State of the Art Portable Ionic Sensors

Transducer	**Measurement Technique**	**Properties**	**Detection Limit**	**Year and Reference**
Ion-selective Membrane	Potentiometric (with additional reference electrode)	Gold Standard, Thick-film, Carbon Electrode Material for enhanced detection limits	1.6×10^{-7} M for K^+ and 4.0×10^{-11} M for Ag^+	2009 [62]
Ion-selective Membrane	Potentiometric (with additional reference electrode)	Additional inner filling solutions for enhanced detection limits	down to 1×10^{-10} M for Ca^{2+}	2009 [63]
Glass membrane	Potentiometric	Durable, limited to single-ions like H, or Na, hard to miniaturize	1×10^{-5} for Na^+ M	2021 [64]
Crystalline membranes	Potentiometric	Macroscopic, Available for some ions, like F^+	down to 1×10^{-10} for F^+	2013 [65]
Ion-Exchange Resin Membrane	Potentiometric	Specific Design allows for bigger selection of target ion, Low chemical and physical durability	down to 1×10^{-7} for Pb	2021 [66]
Enzyme Electrodes	Potentiometric	Two-step mechanism, product leads to electrically measurable signal, high specificity, low durability		n.a.

Table 2.2 Continued From Previous Page - Comparison of State of the Art Portable Ionic Sensors

Transducer	**Measurement Technique**	**Properties**	**Detection Limit**	**Year and Reference**
Glucose-meter	Amperometric	Single-time use (cost-effective), Continuous Monitoring challenging, Requires specific enzyme like Glucose-Oxidase	2-10 x10^{-6}M	1962 [24]
Cobalt Phthalocyanine Carbon electrode	Amperometric	Destructive Measurement Technique, short lifetime and single-use only	2x10^{-6}M	2011 [67]
Multi-enzyme	Amperometric/ Multi	Cascade, cyclic and competitive enzyme systems	0.1x10^{-6}M (Phosphate)	2020 [68, 69]
Ion-selective Membrane	Impediometric	Screen-printed, Acrylic-based Membrane	1.6x10^{-6}M	2006 [70]
Ion-selective Membrane	Potentiometric	Inkjet- or Screen-Printed, for Sodium or Nitrate		2010, 2019, 2020 [31, 71, 72, 73]
Membrane-less	Impediometric	Enzyme-based, high specificity, limited in application	several	2008 [29]
Conducting Polymers	Conductometric and Amperometric	Enzyme-based	several	2020 [74, 37]
Ion-selective Membrane	Conductometric	PVC-based membrane, multi-ion	down to $5x10^{-6}$ M	[33]

Table 2.2 Continued From Previous Page - Comparison of State of the Art Portable Ionic Sensors

Transducer	**Measurement Technique**	**Properties**	**Detection Limit**	**Year and Reference**
Ion-selective Membrane	Impediometric	Solid-state micro-electrodes, PVC-based membrane	0.01 mM	2016-2018 [30, 36]
Mass	Gravimetry	Destructive and lab-bound technique	2 µM	1996 [40]
Chromoionophores	Optical	Big in size and cost-intensive due to optical parts	nM to pM	2020 [75]
Crown Ether	Optical	Big in size and cost-intensive due to optical fiber	100 µM	1987 [76]
Crown Ether	Gravimetry	QCM-based	mM	2019 [48]
Crown Ether	Film Bulk Acoustic Resonater	QCM-based, MEMS-optimized technology, CMOS compatible	µM	2016, 2018 [49, 50]
Silicon Capacitive Resonators	Micro-electromechanical system	CMOS-compatible but low selectivity	4 µM	2008 [51]
Capacitive micro-machined ultrasonic transducer	Gravimetry	MEMS-technology, arrays allow for high sensitivity	n.a.	2009 [53]

2.6.4 New Approach

In general, potentiometric or amperometric methods allow insights on electrode reactions by imposing large pertubations (like potential steps) to a system pushing it far off from equilibrium [26]. The complete opposite represents Electrochemical Impedance Spectroscopy (EIS). Very small pertubations of alternating signals of small amplitude give insights in a steady-state system that behaves much more at equilibrium and is only slightly disturbed. To be exact, this non-destructive approach permits the use of the small signal approximation. Ultimately, complex non-linear current-potential characteristics can be linearized and dramatically simplified this way [26]. Bard et al. summarize the advantages of EIS to have theoretically better resolution, the possibility of measuring over wide time- and frequency ranges and consequently significant reduction of complexity in terms of diffusional and kinetic processes [26].

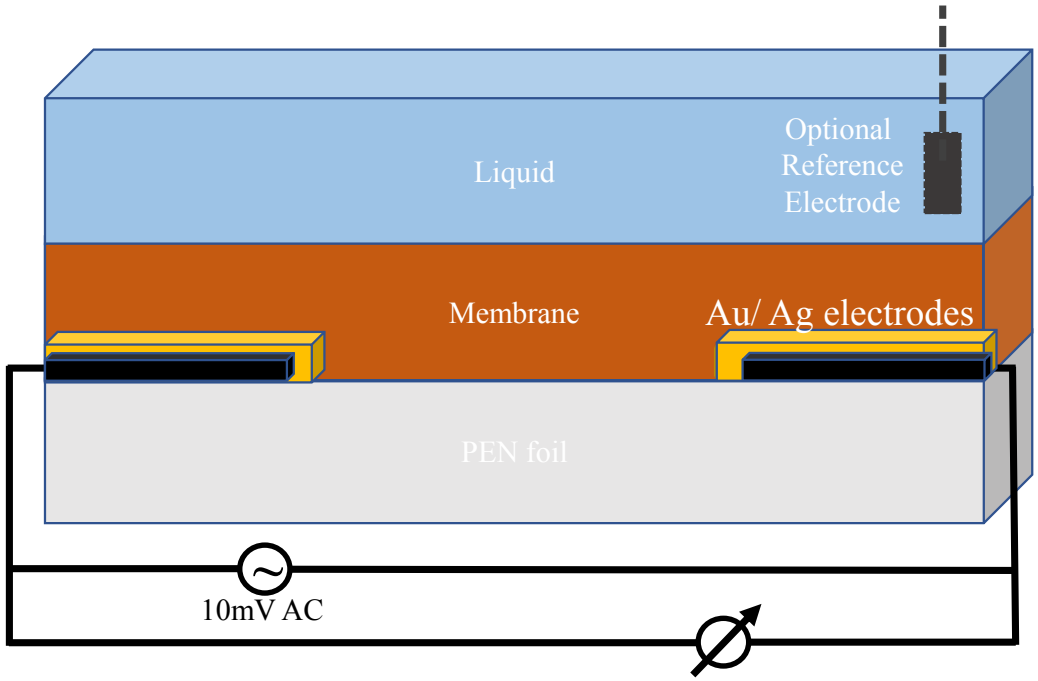

Figure 2.3: Schematic Cross-section of the Ionic Sensor Stack and Measurement Setup. The bottom-up approach of the ionic sensor comprises printed Ag/Au electrodes on top of a substrate (PEN) and are surrounded by a functional, dielectric membrane. The readout circuit needed for electrochemical impedance spectroscopy is hinted conceptionally. To obtain a constant potential in the fluid-of-interest a pseudo Pt-mesh reference electrode can be added. As the electrodes are not in direct contact with the fluid, a two-electrode measurement is preferred in order to circumvent the urgent need of the additional reference electrode. Published in [77], ©IEEE 2021.

Being able to circumvent the need of a reference electrode is another main advantage, as many biotech applications have issues with Ag leaking from the most commonly

used Ag/AgCl reference electrodes.

Figure 2.3 shows the concept including the EIS method, the use of an ion-selective membrane and an optional reference electrode. EIS can be performed in a two- and three-electrode setup. For our sensor systems there is scientific evidence, that both setups do no differ severely. When having an additional reference electrode, the fluid's potential can be forced to be the same as the one created from a Ag/AgCl reference [78, 35, 26]. Logically, this enhanced control over the system is favorable. However, the two-electrode setup offers a more simple setup and might be good enough to achieve the desired resolutions and low cross sensitivity. This hypothesis is tested and discussed in chapter 7.4.1.

2.6.5 Measurement Scheme

The approach is closed off with a description on the measurement scheme. In brief, EIS uses small sinusoidal AC-signals (of 10mV) as input variable. The output variables are the overall magnitude of the impedance |Z| and the phase given at any excitation frequency. The output variables rely on a change in the dielectric displacement field of the functional membrane. It is assumend to be induced by the entirety of Ionophore' polarizations when the target ion is located in a local energetic minimun within the pocket. The theory is detailed in chapter 5. However, the magnitude of the impedance |Z| itself can be used to derive the desired ion concentrations. Figure 7.6 outlines that the small-signal model (low excitation amplitude) allows for linear regression to link |Z| to the concentration of Sodium proportionally. Even though highly non-linear processes act on the electrochemical sensor this approximation appears to be a good work-around and can be realized by picking a preferable excitation frequency with minimal Signal-to-Noise Ratio (SNR). Details can be found in chapter 8.1.

Chapter 3

State of the Art: Bacterial Detection In-Situ

This chapter describes the second project that uses micro-electrodes and Electrochemical Impedance Spectroscopy (EIS) for pathogen detection in liquids. The state-of-the-art divides into conventional method, label-based and label-free techniques. The movement (and consequent accumulation) of bacteria is a crucial part of the new approach and thus it will be discussed in one section. Before presenting the approach taken in this thesis the limitations of current techniques are briefly brought up.

3.1 Conventional Method

3.1.1 Label- based Techniques

3.1.1.1 Immunoassays

Immunoassays are based on antigen-antibody bindings [79, 80]. Real-time pathogen detection is not possible [79].

3.1.1.2 DNA-based Assays

If antibodies are not sufficiently present in the sample fluid DNA-based assays can be used to achieve higher sensitivity.

3.1.1.3 Enzyme-linked Immunosorbent Assay (ELISA)

High-throughput, well plate-based bioanalytical techniques like Enzyme-linked Immunosorbent Assay (ELISA) can track various target analytes. Toxins produced from the pathogen's genes can be used as target as well as nucleic acids, viruses and cells [80]. An extensive review can be found in [79].

3.1.1.4 Polymerase Chain Reaction (PCR)

The gold standard is a technique based on Polymerase Chain Reaction (PCR). Very high sensitivity and selectivity can be achieved as various biological traces can be defined as targets.
The drawbacks include "costly instruments, and amplification, isolation, and quantification of DNA technology make it a complex method to perform" [79]. Reviews about real-time PCR gives an overview about detectable bacterial species [81] and its advantages and disadvantages [82]. PCR requires trained personnel to operate the full procedure and belongs to the lab-bound technqiues so far [83, 79]. An important application area is the food industry [84]. Fast response times of below ten minutes have been reported by some authors [85].
Figure 3.1 shows the process on how real-time PCR is utilized to detect bacterial strands. The process includes several steps that require manual labour especially in the preparation and extraction of the samples. Excellent sensitivity and selectivity are given. However, the samples are destroyed after the measurement and in-situ measurement are still out-of-reach.

3.1.2 Label-free techniques

3.1.2.1 Count Method of Culturing and Colony

The most prominent way is the count method of culturing and colony [79, 87, 88]. Samples are given in a petri-dish with a medium providing an optimal breeding ground for pathogens. After several days, visible colonies are counted and rough quantities can be infered from that data. Specialized image-processing software can be used to automatize the process of counting [89].

3.1.2.2 Electrochemical Method

The Electrochemical Methods include the following types of detection:

- Amperometric
- Potentiometric
- Capacitative
- Impediometric
- Conductumetric

A very extensive, current review about electrochemical biosensors for pathogen detection can be found in [80]. Tissues or even single cells have been researched in the last twenty years focusing on metabolic traces like changes in pH or Oxygen in the

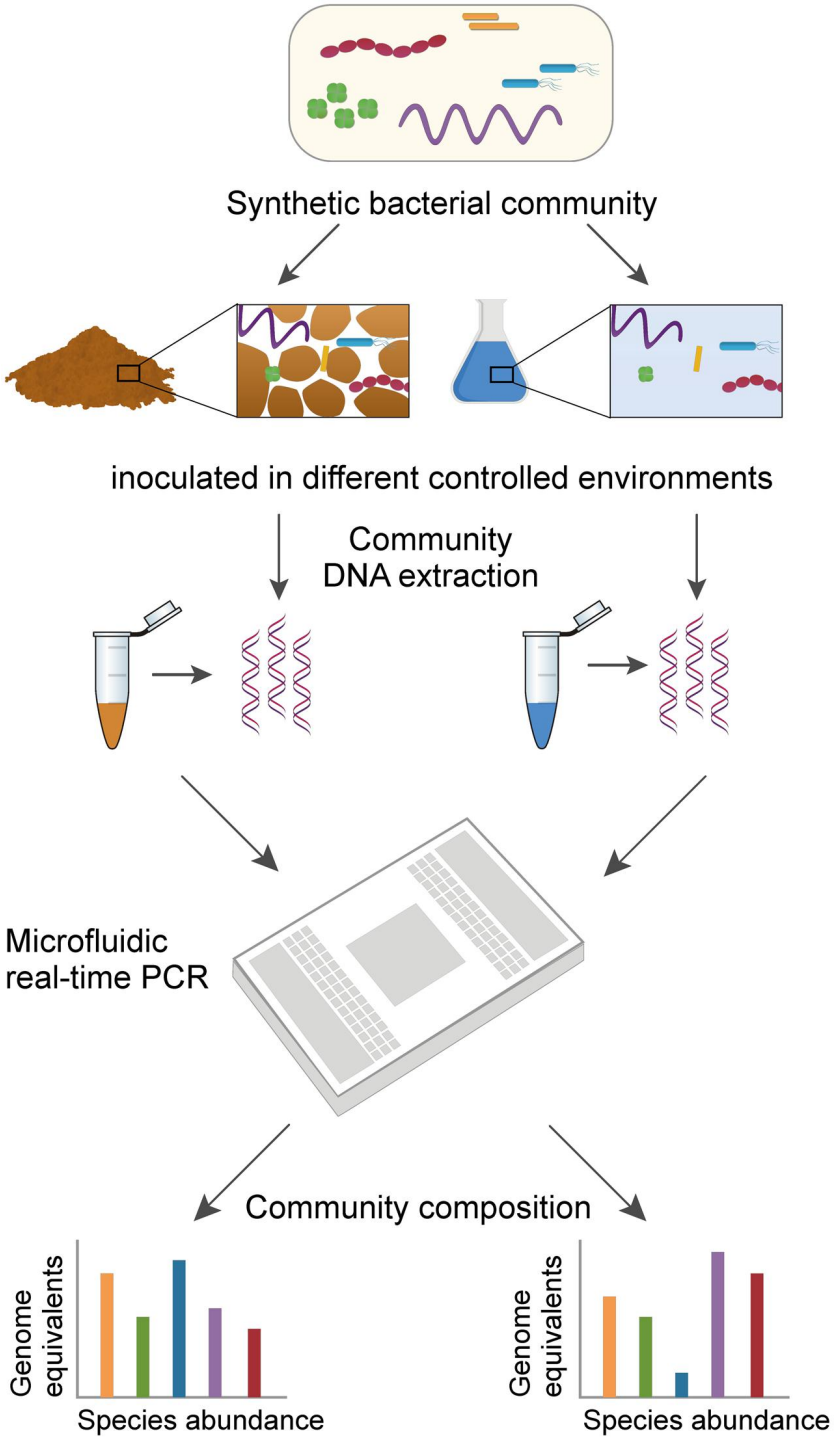

Figure 3.1: Concept of Polymerase Chain Reaction for Pathogen Detection. The preparation of the sample as well as the DNA extraction are manual steps. The results of the real-time PCR are matched to a data base in order to identify the pathogen. Adopted from [86].

immediate environment [90, 91, 92, 93, 94, 95, 96]. These efforts have been combined with fluorescent probes [97] to enhance specitivity, for instance. In general, CMOS-based ISFETS can also be used to monitor a cell's behaviour [98]. Impedance-based techniques for bacterial detection have been researched [99, 100] and some FEM simulations have been to used to model the behaviour [101]. An interesting application for impediometric pathogen detecting is the possibility to track tooth decay (Caries) on a macroscopic level [102].

3.1.2.3 QCM-based Biosensors

Quartz Crystal Microbalance (QCM) -based techniques are a mechanical detection method [103]. The mass-change of a biosensor can be used to detect E.Coli for instance (please see [104]).

3.1.2.4 SAW-based Biosensors

Surface Acoustic Wave (SAW) based interdigital transducer can be used to detect pathogens [105, 79]. A significant contribution to can be found in [106] and the reader is kindly refered to an extensive review about this topic [79].

3.1.2.5 Nanomaterials

Another important approach in pathogen detection is taking advantage of nanomaterials, like nanoparticles, nanotubes, nanowires and nanomechanical switches [107, 108, 77]. Present nanofabrication technology is able to reach the small size of an active sensor area comparable to those of bacteria or other target pathogens, and hence significantly improving the sensitivity and detection limit of a sensor [107, 108, 77, 109]. For instance, Elkin et al. coated carbon nanotube surfaces with bovine serum albumin (BSA) to enhance the solubility of the nanotubes in aqueous solution [107, 108, 77, 109]. Then, the authors developed nanotube-protein conjugates with pathogen-specific antibodies to detect E. coli O157:H7 [80, 109, 77]. Direct measurement of conductance between two electrodes with a nano-sized gap represents a highly sensitive technique in biosensing [107, 108, 109, 77]. Even more importantly, it is possible to detect a pathogen cell larger than a small biomolecule, such as a virus or an antigen [80, 109, 77]. Recent advances include efforts to used carbon nanotubes with flourescent dyes to label pathogens and detect them optically [110].

Distinct groups have shown field effect transistors (FET) fabricated with nanotubes to be used as highly sensitive immunosensors [111, 108, 109, 77].

3.1.2.6 Instrumental Techniques for Detection of Bacteria

Flow Cytometry
Flow cytometry uses optical signals to detect and differentiate pathogen [112]. The method can be improved by using fluorescent labels but the labelling can be also circumvented with advanced image processing and neural networks [113].

Gas Chromatography and Mass Spectroscopy
The high precision of chromatography and mass spectoscopy can be used to detect bacterial compounds. The identification of distinct bacterial strands is possible [114],

Electrochemical Collision Event
Microscopy, the measurement of optical density and smart cell culturing is used to identify bacterial cells. For instance, the number of collision events of bacterial cells on Ultra-Micro-Electrodes correlates directly to a current over time. The authors report currents in the range of pA and confirm their experimental finding with FEM simulations [84, 115].

3.1.2.7 Spectroscopic Techniques

Fourier Transform Infrared Spectroscopy (FTIR)
Infrared light can excite molecules. The resulting vibrations lead to an absorbance spectrum which is characteristic for pathogens [84, 116].

Raman Spectroscopy
Raman spectroscopy works in a similar manner. The inelastic scattering of light creates a highly specific footprint of the (biological) target [117]. Authors report detection limits of 10^3 CFU/ml [84]. Surface-Enhanced-Raman Spectroscopy (SERS) can be used to derive quantity of pathogen bacteria [118]. Optical approaches involving surface plasmons are published but detection limits are higher 10^5 CFU/ml [119].

Hyperspectral imaging techniques (HSI)
Several excitation wavelenghts in the near- and mid-infrared as well as enhanced image processing allow for the cost-effective and fast detection of pathogens [120].

THz radiation
Originally, Tera Hertz radiation showed poor transmission in aqueous solutions and hindered the use of this part of the electro-magnetic spectrum for pathogen detection [84]. In the last years, functionalized and patterned metamaterials for sensing allow the use in many environments [121]. The method is contactless, non-invasive and allows for on-site detection - with and without labels [84].

3.1.3 Movement of bacteria

In general, the movement of bacteria in liquips by applying external electric fields is called "Electrophoresis". Mostly capillary effects are exploited for bacterial detection or quantification [122, 123, 124]. The gold standard of this field appears to be Pulsed-field gel electrophoresis. A current review about this techniques is given in [125] but as this field deals usually with lab-bound approaches [126] the focus of this work are mobile, impediometric approaches.

There are publications that explore the effects of bacteria like E. Coli when using Impedance Spectroscopy (please see [127]). Depending on whether direct or alternating current potentials are created the bacterial load in the fluid will behave differently [128]. Similar to electrophoresis that uses Agar Agar gel (like gelatine), bacterial strands can be moved in liquid media by applyling DC potentials [129]. In contrast, alternating electric fields can not only penetrate and polarize bacteria cells, but also be used for gathering and detection [130].

Therefore, the state of the art divides into the two phases of operation before reviewing the landscape of bacterial sensors [131]. Firstly, the attraction of bacteria and their adhesion on the active sensor surface is regarded. Applying DC potentials on electrodes to move and attract microorganism in solution has been studied and is scientifically proven [132, 133, 134, 135, 131].
Next, bacterial detection via EIS (using AC potentials) is introduced in a series of projects. A recent review sums up the literature around pathogen detection very well [80]. In general, the utilization of microfabrication of bacterial sensors enhanced the efforts and paved the way for the integration of multiple processes in sequence for one-step sensing or in parallel aiming for high throughput screening [136, 109, 131].

3.1.3.1 The Role of Microfluidics

Lab-on-chip offers a convenient, cost-effective approach that is compatible with microfluidics. Additionally, electrical(-chemical) methods lack the urgent need of a label for sensing specific target bacteria cells [132, 133, 134, 135, 131, 109]. Boehm et al. fabricated a microfluidic pathogen sensor that measures the impedance in a fixed-volume chamber that contains cells [109, 137]. Micro-electrodes out of Platinum are utilized to discriminate two bacterial strains E. Coli and M. Catarrhalis in single minutes leveraging a change in impedance. By contrast, Carbonaro et al. have developed a promising, on-chip artificial pore that could be exploited to detect bacterial pathogenic cells [138, 139, 131].

Cheng et al. show a microfluidic sensor system out of two parallel glass slides and a thin PDMS gasket [140, 131]. After cells were attached to the glass surface modified with proteins specific to the target cells, they were lysed to monitor a change in conductivity that correlates with the number of cells. A lower detection limit was presented as 20 cell/uL [109, 131]. Electrochemical impedance spectroscopy is itself a label-less sensing technique that highly depends on the exact environment it is used in. A more challenging enviroment are biofluids due to its variety of potential interfering species. For instance, Liao et al. published a microfluidic, electrochemical sensor array in order to detect uropathogens in human body fluids [141, 131]. In line with the development of impedance-based sensor, the electrical impedance output can be generally amplified when using a parallel set of electrode configuration like interdigitated array microelectrodes (IDA) [109, 77]. Increasing the number of parallel electrodes and extending the active surface area can lower the detection limit and even response times in some cases [109, 142]. Laczka et al. report a bacterial cell detection limit of 1500 cells/mL [142]. In contrast, Lei et al. takes advantage of an capacitative approach [143, 109].
Yang et al. take advantage of IDA microelectrodes to detect Salmonella Typhimurium in milk. The microelectrodes, fabricated out of indium-tin-oxide (ITO), measure a change in impedance during bacterial cell growth [109, 144, 131]. A suspension with a bacteria concentration of 10^5 CFU/mL could be experimentally identified in less than 2.2 hours. In contrast, Lu et al. utilized IDA electrodes out of gold to detect bacterial cells in an otherwise insulating environment. The inter-electrode spacing is reduced to 2µm in these devices. This makes the attachment of single bacteria across two adjacent electrodes possible. Interestingly, the current flowing correlated with the number of bacterial cells forming a conducting bridge between electrodes adjacent to each other [109, 131]. While the sensor is extremely sensitive to detect a single bacteria, whole films are more challenging as it requires a clear knowledge on the conducting mechanism of the bacterial cells on the electrode surface posing a many-body problem [109, 131].

3.1.3.2 Fabrication and Role of Electrode Geometry

As nanofabrication technology advances, the fabrication and assembling of new micro sensors has become a straightforward process [109, 131]. Nevertheless, reliability, repeatability, durability, and ease-of operation are crucial aspects for lab-on-a-chip pathogen sensors [109, 131] and require good knowledge about the physical effects that can occur. In addition, the integration of a complex process within a single chip is still not straightforward [109] - especially when chemical surfaces effects occur affecting the input parameters. The reader is kindy refered to an excellent review about microbial biosensors in general [145].
As geometrical parameters tremendously influence the EIS sensor performance [142],

the community started to use FEM simulations in order to foster the understanding of this kind of biosensor [146]. As the fields are specific to the used design, many open questions remain. For instance, what electrode dimensions perform best? What is the role of the substrate and its material properties on the sensing scheme? What are the detection limits of an EIS bacterial sensor?

Summing up, the generated output is highly dependent on the geometry of the cells. Hence, we present a systematic approach on how to evaluate arbitrary designs that eventually lead to a high-performance bacterial sensor. In brief, the limitations of biotechnical pathogen sensors are presented in the next section.

3.2 Comparison

PCR and corresponding methods excel with the fastest measurement times (down to 1h) and the lowest detection limit (10^1 CFU/ml). DNA-based assays can compete in terms of sensitivity but offer the advantage of better portability and possible in-site measurements [84]. Spectroscopic techniques like THz radiation can also offer this key advantage and offer great potential for the future. Depending on the application, the electrochemical biosensors can compete in terms of costs and sensitivity towards pathogens. However, PCR and optical methods are slightly better in terms of selectivity.

3.3 Limitations

To the best of the author's knowledge, there are no commercially available in-situ sensors for bacterial loads. So far, the gold standard is to multiply the pathogens in agar in a petri dish. This process comprises the following challenges:

- No in-situ measurements possible
- Time consuming (several days)
- Laboratory required
- Trained personnel required
- Specific but also error-prone

3.4 New Approach

In this work, a systematic study on bacterial, electrochemical impediometric sensors intends to give rise to an in-situ pathogen sensor. As the design aspects are absolutely essential for the further development of EIS biosensors FEM simulations are performed.

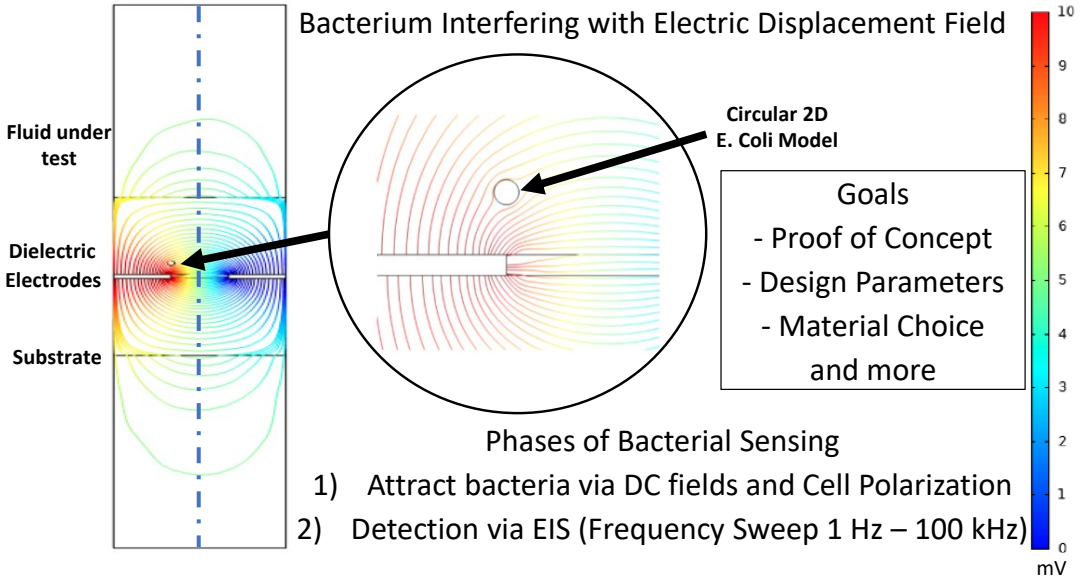

Figure 3.2: Concept of Bacteria Interacting with the applied Displacement Field - FEM simulation in 2D: In 2D, the displacement field between two electrodes in a sensor stack is simulated. The field evolves when an external potential is applied to the electrodes. Bacteria are modelled as circles in 2D assuming an averaged dielectric constant inside. The polarizable bacteria interacts with the displacement field that spans between the electrodes. In a first step, bacteria is attracted by applying DC potentials to the electrodes. In a second step, the read-out follows via electrochemical impedance spectroscopy (EIS) by applying AC potentials with in a frequency sweep. The colour scale indicates low potentials (blue) to high potentials (red). Published in [131], more details in chapter 6.

In general, the investigation comprises two steps that can be seen in figure 3.2 and is inspired by [131]. Firstly, the attraction of bacteria to the sensor surface by DC potentials is explored. Secondly, classical impedance spectroscopy is performed for detection and represents the method of choice for read-out. A pathogen-like model and its behaviour in an electrical field is researched (see 3.2**a** and **b**). In a two-dimensional electrostatic case several layouts are investigated and the displacement of the fields is explored with and without bacteria in the electrode's proximity.

The goals are to illuminate and verify the physical concepts behind the sensor, exploring an optimized attraction method for cells in fluids, as well as finding the best geometry for EIS measurements. The role of electrode configuration and periodicity is addressed, and a new mathematical tool for the evaluation of arbitrary, complex sensor models in 3D is presented. Finally, novel layout and design recommendations for future EIS biosensors are given [131].

Chapter 4

Methods and Materials

After describing the new approaches for the ionic as well as the bacterial sensor and their state of the art, the used materials and methods are presented in this chapter. The content is based on the author's publication [77]. The focus lays on the chemical formulation of the novel ink-jet printable inks, its development and role of its constituents. We sum up with measurement devices, the used experimental setup and some technical details.

4.1 Additive Manufacturing and Materials

On the substrate (flexible Polyethylennaphthalat [PEN] foil, untreated Teonex Q65HA, purchased at Pütz Folien GmbH), electrodes are printed using a conductive silver nanoparticle ink (Orgacon SI-20x, Agfa, Mortsel, Belgium) [131]. The printable, UV-curable (Dose: 1 Jcm^{-2}) Ion-Selective-Membrane (ISM) can be drop-casted as well as printed, and is based on the main constituent Butyl Acrylate (detailed in chapter 4.2.1 and in [131]). The ISM is doped with ion-selective ionophore Na-X (all from VWR chemicals). The chemical structure of the ionophore is presented in figure 4.1. The mentioned ionophore has been chosen due to good selectivity coefficients towards other ions, its detection limits in the µM-range and its response time of less than 20s in corresponding potentiometric measurements [55]. In addition, the chosen ionophor offers the possibility to be used in optodes as well [55].

4.2 Inkjet Deposition Platform, Encapsulation and Fabrication

A high-end inkjet-printing system from Ceradrop (F-series, Limoges, France) is utilized for fabrication and shown in Fig. 4.2A) . The working principle of the deposition platform is portrayed in Fig. 4.2B), and will be explained briefly and is based on a

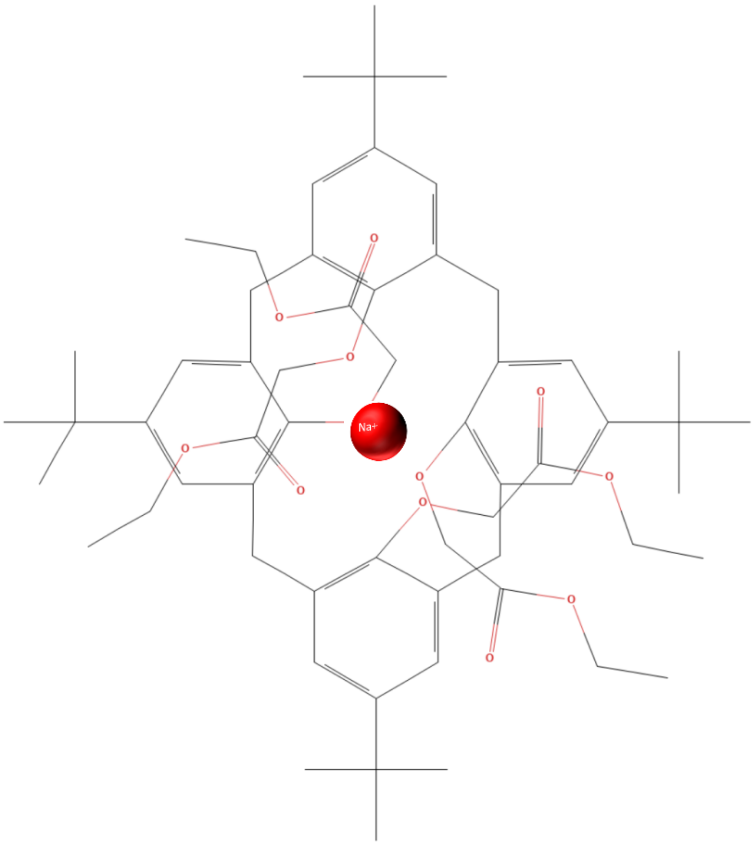

Figure 4.1: Structure of used Ionophore Natrium-Ionophor X by Supelco and Sigma Aldrich / Merck, 4-tert.-Butylcalix[4]aren-tetraessigsäure-tetraethylester. The red dot symbolizes an bound Sodium Ion in the center. Adopted from [147] and [55] .

inkjet review [150] as well as [151, 152, 153, 154, 155, 156]. The used platform is also described as DOD (Drop-On-Demand) Inkjet system [157].

First, the costum-made ink (see chapter 4.2.1 is filled into disposable printing cartridges (DMC, 1 pl, Fujifilm Dimatix, Santa Clara, USA) [158]. A piezoelectric element converts the electrical signal (2 kHz AC square wave) into a mechanical force pushing out droplets [150]. Even though the mechanical accuracy of the printing system is in the range of single µm (given by the deposition platform manufacturer [148]) the achieved printing resolution lays in the 10 to 20 µm range (lateral resolution).

In order to achieve such low lateral resolution the printing process has to be stable and each droplet has to be accounted in its spreading of the impact on the substrate (as indicated in Fig. 4.2B) . An appropriate workflow for DOD printing is described here and allows for the recreation of arbitrary printing structures.

The opening, "nozzle", defines the volume of a single droplet and is given by the cartridge itself. The droplet lands on the substrate which is heated to 50°C. The ink droplets can be heated by the printhead heater and purposefully have been matched to the same temperature [156]. The reasoning behind this is the attempt to keep the

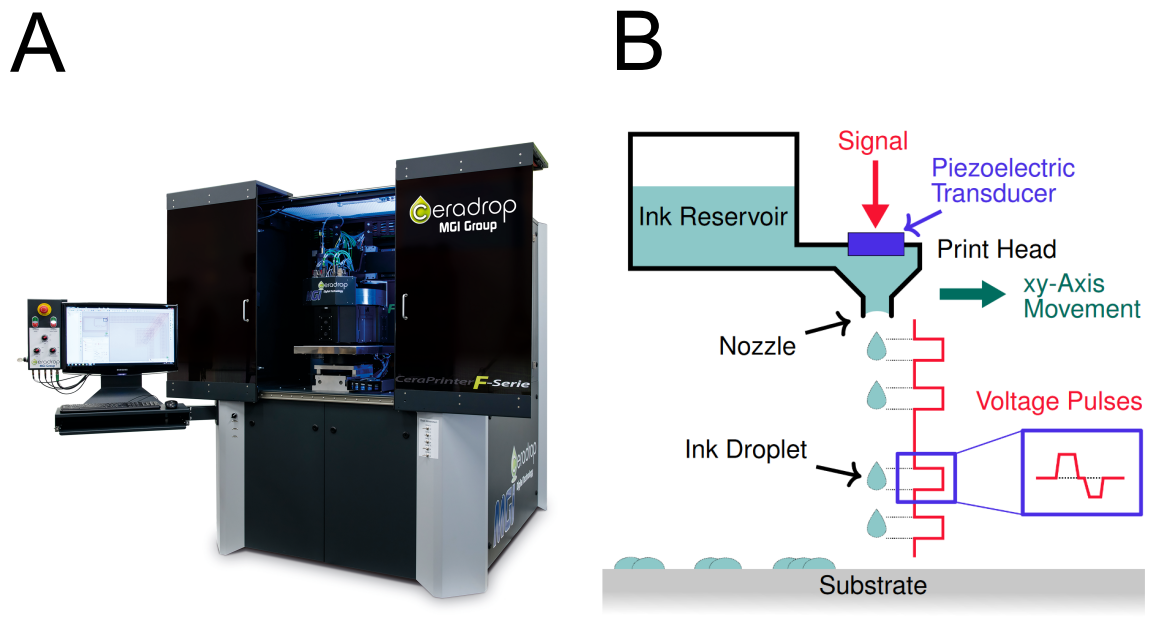

Figure 4.2: Inkjet Deposition Platform and Working Principle. A) A CeraPrinter F-Serie (- a Hybrid Digital Materials Deposition Platform) is used for the printing of the electrode material and the functional membrane of the ionic sensor system. From [148]. B) Working Principle of Inkjet Deposition Platform. A piezoelectric transducer converts an electrical signal into a mechanical force pushing the ink through a nozzle. Reprinted with permission from [149].

surface energy of the droplet as similar as possible to the substrate surface energy [156]. The impact of the droplet widens its lateral dimension and the drop spacing have to be adjusted accordingly [153]. Consequently, a maximum drop spacing δ_{sp} of 19.5 µm has been used.

In general, the drop spacing δ_{sp} is an important parameter for DOD printing. It can be calculated via eq. 4.2.1 using the experimentally measureable contact angle θ_a, its corresponding diameter d_{con}, and the diameter of the drop-in-flight a (which is similar to the nozzle diameter and is defined by the cartridge) [155, 159, 160].

$$\delta_{sp} = \frac{2\pi a^3}{3d_{con}^2 \cdot (\frac{\theta_a}{sin^2(\theta_a)} - \frac{cos(\theta_a)}{sin(\theta_a)})} \tag{4.2.1}$$

Equation 4.2.1 refers to a continuous printing regime avoiding isolated drops. Interestingly, the contact diameter d_{con} can not only be derived via rather challenging experimental length measurements but also it can be derived theoretically in eq. 4.2.2 using the parameters described above [155].

$$d_{con} = a \cdot \sqrt[3]{\frac{8}{tan(\frac{\theta_a}{2}) \cdot (3 + tan^2(\frac{\theta_a}{2}))}} \tag{4.2.2}$$

Based on eq. 4.2.1 and eq. 4.2.2, the total bead width w of the 'end' printing product can be calculated when assuming stable printing conditions and volume conservation in eq. 4.2.3 [155, 161, 159, 149].

$$w = \sqrt{\frac{2\pi a}{3\delta_{sp} \cdot (\frac{\theta_a}{sin^2(\theta_a)} - \frac{cos(\theta_a)}{sin(\theta_a)})}} \tag{4.2.3}$$

The described set of equations represent the necessary theoretical backbone to the workflow for printing structures with a minimal spatial dimension of the total bead width w. Depending on the bead width, the drop spacing can be calculated. As the the drop spacing has to be in the right range the reader is advised to do the calculation first. If the drop spacing is too big, non-continuous, isolated drops appear on the substrate [155]. If the drop spacing is too small, however, bulging of the droplets occurs [155]. This means that the vertical height differs tremendously from the desired value and affects lateral elongation as well. The overlap of single droplets is desired in DOD printing. Nevertheless, the stacking of too many droplets results in unstable printing results [162, 159, 163, 164].
Next, the post-processing of the samples is described. The printed samples are sintered for one hour at 150°C – similar to [165]. In order to encapsulate the sensor, glass rings are glued with Polydimethylsiloxane (PDMS) and thermally cured in the oven at 120°C for one hour (see Fig. 7.4 and [77]). The encapsulation serves the purpose of packaging and is necessary to pipette ionic testing solutions onto the active sensor area. Using this approach, the experimenter can avoid open bare electrodes to the solution and consequently undesired electrochemical reactions. Fig. 7.4 presents three identical, printed sensors encapsulated with glass rings, and the ion-selective membrane and printed electrodes below in the center. As testing solutions, fresh $NaNO_3$, KNO_3 or, respectively, K^+ in H_2O in AAS-Standard (VWR chemicals) are utilized, and diluted with high purity DI-water [77]. EIS measurements are taken with a Biologic VSP 300 potentiostat and a custom-made adapter. A 10 mV AC-signal is applied (if not stated otherwise), and the setup is confined in a faraday cage to minimize external noise. The sensor samples have been pre-wetted for three hours in the $NaNO_3$ AAS-Standard to shorten response times [77]. Finite-Element-Method Simulations via COMSOL Multiphysics® software [166] are performed in order to choose the best materials and topology in terms of dielectric properties, adhesion, printability, stability and costs of the sensor system [77].

4.2.1 Ink Formulation

Next, details on the formulation of the developed membrane materials are explained. In table 4.1, the functional active membrane ink is presented. Butyl Acrylate is the main component and gives rise to the later cross-linked polymer matrix. Due to its

Table 4.1: Newly Developed Ion-sensitive Acrylate Ink

Component	wt%	Volume [µl]
Butyl Acrylate	75,1	3755
2-Ethylhexyl Acrylat	20,7	1035
1,6-Hexandiol Diacrylate	0,2	50
Potassium tetrakis(4-chlorophenyl)borate	1	50
Omnirad 2100 photoactive catalyst	1	50
Sodium X ionophore	2	50
Total	100	5000

low viscosity high-precision nozzles and low-volume cartridges can be used and allow for resolution of the printing process down to the µm-range.

The crosslinker is 1,6-Hexandiol diacrylat and drives the polymerization process of the acrylate building blocks or chains. Since a very precise, repeatable process is the goal, only very discrete energy inputs in form of ultra-violett radiation are desired. Keeping the control over the deposited energy (Dose: 1 Jcm^{-2}) can be done using short and precise UV pulses. The UV-sensitive molecule is the commercially available Omnirad 2100 photoactive catalyst. Lastly, a lipophilic ion exchanger, called Potassium tetrakis(4-chlorophenyl)borate is added to fine-tune the membrane's conductivity (inspired by [167]). More details can be found in [168].

4.2.2 Calibration to Deposition Platform

A high-end deposition platform, the involved cartridges and nozzle sizes need the right viscosity to be successfully printed. The presented formulation is based on the assumption that the viscosity or inverse of the Ohnesorg (Oh) number should be in the range of $1 - 15$ [169]. The Ohnesorg number can be described by equation 4.2.4 [170].

$$Z = \frac{1}{Oh} = \frac{\sqrt{\gamma \rho a}}{\nu} \tag{4.2.4}$$

The Ohnesorg (Oh) number consists out of the surface tension γ in units of N/m, ρ describes the density in units of kg/m^3, and a represents the nozzle diameter of the print head in m, and ν is the dynamic viscosity in units of $\mathrm{Pa} \cdot \mathrm{s}$ [170, 168]. More details on the fluid dynamics involved can be found in literature [150, 170, 157].

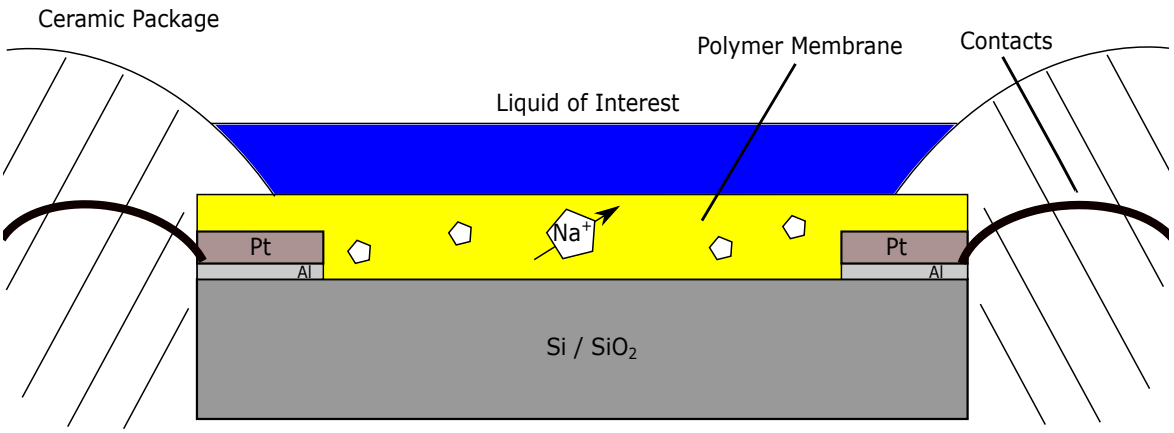

Figure 4.3: Alternative Solid Substrate Approach. The functional polymer membrane can be dropcasted onto a solid, silicon substrate. A ceramic package seals the active sensor area. Adapted and modified from [171].

4.2.3 Alternative Approach of Substrate for Ionic Sensor

So far, the shown layer stack in Fig. 2.3 is the blueprint of the fully printable ionic sensor. The ionic sensor consist of an functional polymer layer and a polymer substrate which has the big benefit of better printability of the other layers.

An alternative approach is presented in figure 4.3. The presented approach of a solid state substrate, in this case Si/ SiO_2, has the advantage of being CMOS-compatible. Specifically, the electrodes can be precisely fabricated on the substrate. Platinum has been used as electrode material in this alternative approach [172].
A disadvantage is the more complex and more costly packaging (ceramic package from an external service manufacturer) as liquids are involved. Hence, the focus lays on a fully printable ionic sensor.

Nevertheless, the approach is used to verify some properties of the functional polymer membrane and its results are shown in Fig. 7.9 and Fig. 7.10.

4.3 Finite Elemente Method

The AC DC Module of COMSOL Multiphysics © v5.5 is utilized for FEM Simulations [166]. In order to evaluate arbitrary EIS sensor structures the mathematical tool of a quality factor is developed. The quality factor can be mathematically defined via the electric field norm of the gradient. The quality factor assumes a precise volumes of interest, detailed in section 6.5 for further reading [131].

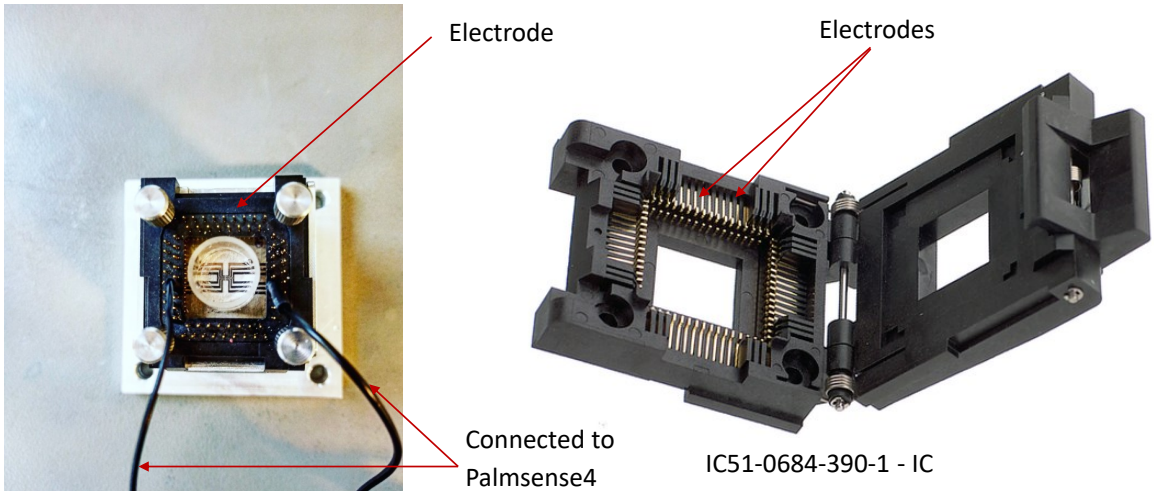

Figure 4.4: Experimental Setup for Sensor Connections and Adapter. A home-made adapter with an Yamaichi IC socket is used to clamp the printed samples.

4.4 Evaluation and Measurement Equipment

An optical Zeiss Metallux microscope is utilized to create photographs of the fabricated structures. Figure 4.4 shows the used IC-Testsocket $IC51-0684-390-1$, Clam Shell PLCC-68, Yamaichi Electronics. The designed sensor structures and its feedlines are customized to the footprint of this device. Short wiring ensures low additional parasitic capacitances.

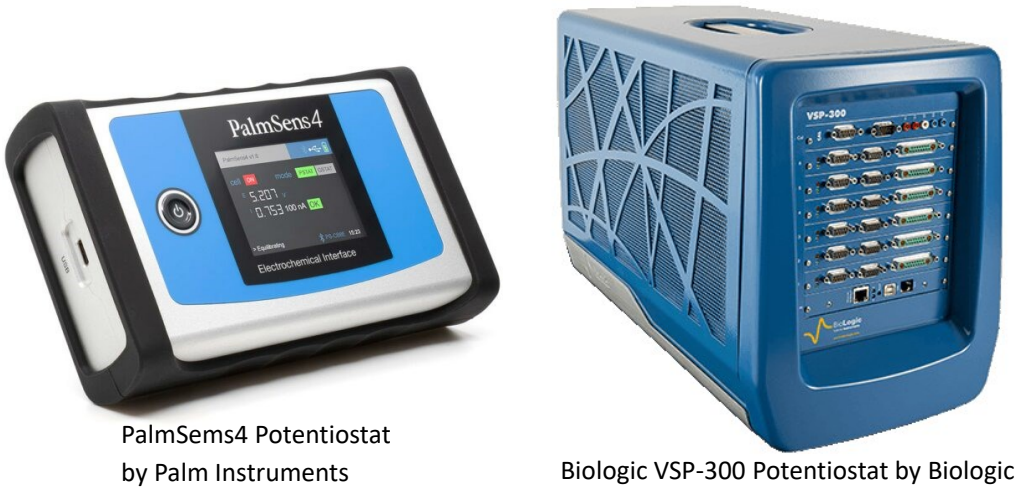

Figure 4.5: Experimental Measurement Devices. Both devices allow for multi-channel measurements. The Biologic offers a low-current option and additional algorithms for error correction. From [173, 174].

The socket of the adapter is made out of milled Aluminum and can be tightened with additonal screws. The measurements were performed in an Electrostatic Discharge (ESD)-protected environment.
The electrochemical impedance spectroscopy (EIS) has been performed on a Biologic

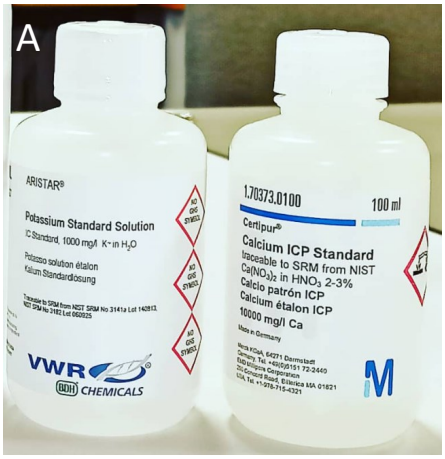

	C_{Na^+} [mM]	$V_{Solution}$[ml]	V_{DI}[ml]	V_{Total}[ml]	Dilution factor
S_{sd}	43	43	0	0	0
S_1	21.7	$25_{S_{sd}}$	25	50	1/2
S_2	10.85	25_{S_1}	25	50	1/2
S_3	4,35	1_{S_1}	49	50	1/5
S_4	0.87	1_{S_3}	49	50	1/5

Figure 4.6: A) Standard Solutions and B) Dilution Process of $NaNO_3$. The measurement process includes the fabrication of well-defined test solutions. Atomic Absorbance Standards (AAS-) are used to ensure high purity of the sample. Based on [175].

VSP−300 and a PalmSense 4 Potentiostat, as can be seen in figure 4.5.
The fluids under test are created using dilution series on commercially availabe AAS-Standards that are pictured and detailed in Fig. 4.6 A) and B). In brief, the chemical preparation followed the well-known eq. 4.4.1 for calculating concentrations C from volumina V and keeping the overall molarity constant.

$$C_1 \cdot V_1 = C_2 \cdot V_2 \tag{4.4.1}$$

The main advantage of using a very precise stock solution and diluting it down with deionized water is to minimize errors of the pipetting process. Additionally, evaporation and corresponding errors are kept as low as possible by providing fresh samples from the stock buffer.

Chapter 5

Theory

In this chapter, the physical background of ionophores and Impedance Spectroscopy is explained. The theory relies heavily on the most-cited and extensive book about EIS by Barsoukov and Macdonald from 2005. The reader is kindly refered to this core literature for more details [78, 176]. First, the most important component of the functional membrane, Ionophores, are described.

5.1 Ionophores

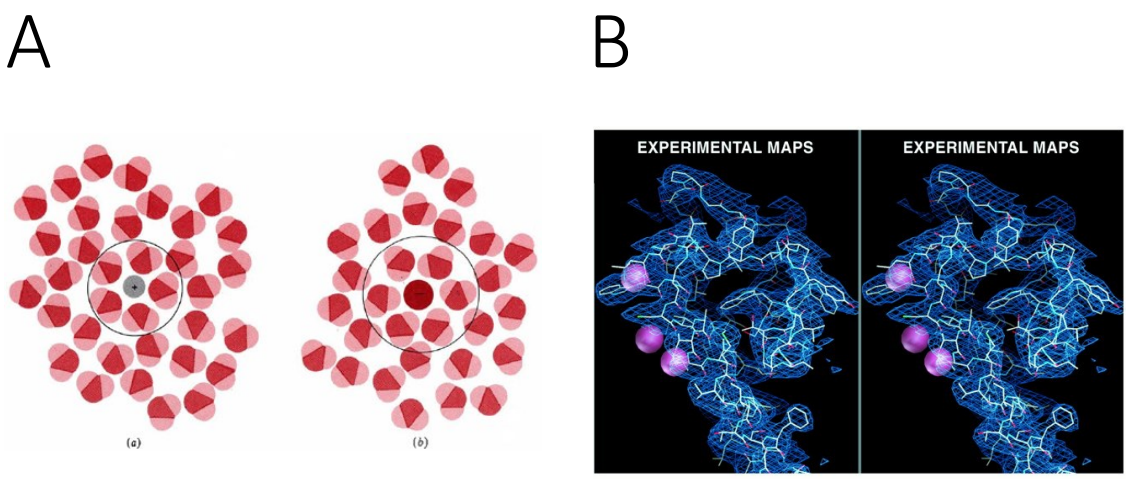

Figure 5.1: A) Hydration sphere of water molecules surrounding the charged ion in the center B) Experimental electron density map of an ionophore. The map is showing the inner helix, loop structures and selectivity filters; background: the pore helix and outer helix. Adapted and modified from [177] and [178].

Freely moving target ions in aqueous solution are usually surrounded by water molecules, the so-called hydration sphere (see figure 5.1 A). Independent of the charge of the ion,

water dipoles orient themselves around them [179, 180].
Ionophores strip off the hydration sphere and fit an ion with an corresponding ionic radius into their binding pocket. Without forming strong covalent bonds, the ion is situated in a local energetic minimum in the macroscopic ionophore as can be seen in figure 5.1 B (compare [179, 180]). In 1998, Doyle et al. described a K^+ Ionophore as inverted teepee with selectivity filters by molecular design. Inert hydrophobic linings, water filed cavities, helix dipoles play a vital role in lowering electrostatic energy barriers that a cation faces when being in proximity to the macromolecule. When the target ion strips off its hydration sphere carbonyl oxygen atoms of the ionophore take their respective place, come in very close proximity and eventually compensate the energetic loss of dehydration [178].

5.2 Impedance Spectroscopy

The ionophores are the transducer element in the sensor systems. Now, a theoretical background is presented linking the microscopic ionophores, their polarization to the applied experimental method Impedance Spectroscopy and their (macroscopic) output variables.

5.2.1 Fundamentals

According to Barsoukov and Macdonald, an "electric field can interact with a solid in two principal ways. These are, respectively, the reorientation of defects having electric dipole moments (usually complex defects) and the translational motion of charge carriers (usually simple defects such as vacancies, ionic interstitials, and defect electronic species" [78]. The first type leads to a displacement current which is defined by the electric displacement $\mathbf{D}$ in eq. 5.2.1,

$$\mathbf{D} = \epsilon_0 \mathbf{E} + \mathbf{P} \tag{5.2.1}$$

showing the electric field $\mathbf{E}$, ϵ_0 as the permittivity of free space and $\mathbf{P}$ being the polarization of the dielectric [78].
The second way of interaction also leads to a current that involves a real (exclusively DC-) conductivity σ in eq. 5.2.2.

$$i = \sigma \mathbf{E} \tag{5.2.2}$$

The concept of both presented EIS sensors is based on the first interaction. Assuming that ionophores are not symetrical in their molecular structure, the binding of the target ion leads to change in the polarization of the single macromolecule $\mathbf{p}$.

The entirety of the ionophores lead to macroscopic effects coming from the alternated polarization $\mathbf{P_s}$ in eq. 5.2.3

$$\mathbf{P_s} = \sum_i \mathbf{p_i} \tag{5.2.3}$$

We assume a single time constant for dielectric relaxation, and end up with two parts of the response. First, a extraordinary fast polarization with the high-frequency constant is given in 5.2.4.

$$\epsilon_\infty - 1 = \frac{\mathbf{P}_\infty}{\mathbf{E}\epsilon_0} \tag{5.2.4}$$

These are in the time range of 10^{-16}s and in the typical time frames of electrochemistry nearly instantanous. The second, a "time-dependent polarization $\mathbf{P'(t)}$ comes from the orientation of dipoles in the electric field" [78]. In a pseudo-static case, the total polarization $\mathbf{P_s}$ determines the static dielectric constant ϵ_s in equation 5.2.5 [78].

$$\epsilon_s - 1 = \frac{\mathbf{P}_s}{\mathbf{E}\epsilon_0} \tag{5.2.5}$$

Hence, eq. 5.2.6 can be written.

$$\mathbf{P}_s = \mathbf{P}_\infty + \mathbf{P'}(t = \infty) \tag{5.2.6}$$

Using the assumption of only first-order kinetics for $\mathbf{P'}$ and a single lifetime τ equation 5.2.7 is obtained.

$$\tau d\mathbf{P'}/dt = \mathbf{P}_s - \mathbf{P} \tag{5.2.7}$$

Now, a unit step voltage $u_0(t)$ is applied in eq. 5.2.8.

$$\mathbf{P} = \mathbf{P}_\infty u_0(t) + \mathbf{P'}(t) \tag{5.2.8}$$

Applying a Laplace transform on eq. 5.2.7 and eq. 5.2.8, and solving for $\{\mathbf{P}\}$ leads to eq. 5.2.9.

$$\{\mathbf{P}\} = \frac{\mathbf{P}_\infty}{(p + \omega_0)} + \frac{\omega_0 \mathbf{P}_s}{(p + p\omega_0)} \tag{5.2.9}$$

where ω_0 is the reciprocal of time constant τ and p as the complex frequency variable. By using a relation for the current density in eq. 5.2.10.

$$\{i\} = p\{\mathbf{P}\} - \mathbf{P}(t = 0) \tag{5.2.10}$$

and differentiating we end up to our final result [78]. The equation 5.2.11 shows the direct link between the current density i(t), the variables attributing to polarization

coming from the transducer element ionophore, their corresponding time constants and the insight, that decaying exponential functions describe the EIS process.

$$i(t) = \mathbf{P}_\infty \delta(t) + (\mathbf{P}_s - \mathbf{P}_\infty)\tau^{-1} exp(-t/\tau) \tag{5.2.11}$$

This mathematical derivation is elegant as it links the variable to be measured to the microscopic changes that occur in the EIS sensors - namely the polarization effects occuring on the bound or unbound ionophores. Remarkably, the equation 5.2.11 fulfils exactly the Debye equivalent circuit in figure 5.2.

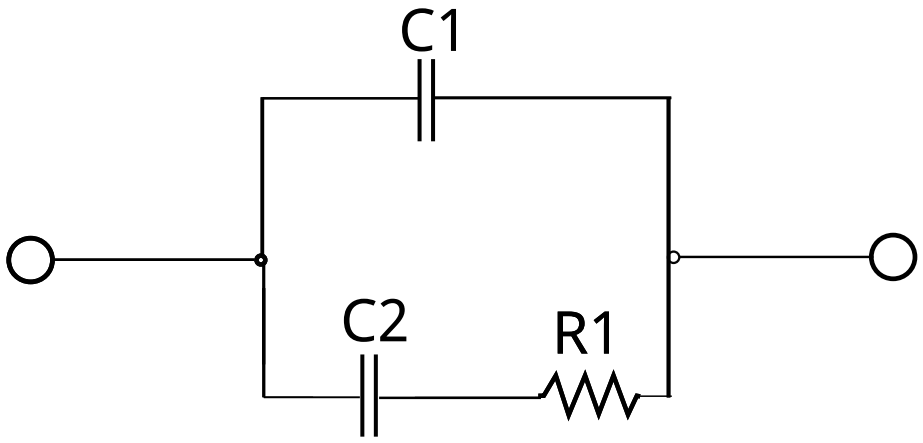

Figure 5.2: Debye Equivalent Circuit. First-order approximations of the polarization effects in a dielectric membrane appear to behave similar to the Debye equivalent circuit. Adapted and modified from [181, 182].

Peter J.W. Debye first described the Debye relaxation relations in 1929 [181, 182, 78]. The basic model can be used to to modern EIS systems and allows a framework for EIS data intepretation. In chapter 7.4.1, a finer model for the presented ion sensor is presented - including diffusional effects as well.

For the bacterial detection similar effects come into place. Dealing with much bigger dimensions (usually in the range of µm) also polarization effects occur. In chapter 6 the physics behind the sensing scheme are explained in detail.

5.2.2 ISCOM theory

For conductometric sensors, a theory is presented [32, 33, 34, 35]. The theory is closely related to the equations in chapter 5 but less detailed. Hence, the focus of this work lays in the utilization of EIS theory.

5.3 Sensitivity

The theoretical sensitivity of the impediometric EIS sensors is derived by the available dynamic range δ_{dr} and the concentration ranges in eq. 5.3.1.

$$S = \frac{\delta_{dr}}{\Delta \text{ (Measured } Na^{+} \text{ concentration range)}} \tag{5.3.1}$$

5.4 Basics of Finite Element Method

Electrical field distributions are described by the Maxwell equations [183]. The software COMSOL © provides a numerical solution solving the under-laying differential Maxwell equations for an arbitrary model that expands in space [131]. The most important equations are presented in this chapter. For more details, the reader is kindly referred to the corresponding literature [184, 185, 186, 187, 188]. First of all, the scalar field of the electric potential is calculated. Then, the second derivative of the potential gives the electric field gradient V_{ij}, see eq. 5.4.1 [131, 77].

$$V_{ij} = \frac{\partial^2 V}{\partial x_i \partial x_j} \tag{5.4.1}$$

The length of a gradient is defined via the norm in eq. 5.4.2. In the case of a polarizable bacterium in an electric field, the gradient corresponds to a mechanical force acting on it [131, 77].

$$||V_{ij}|| = \sqrt{\Delta E_x \cdot \Delta E_x + \Delta E_y \cdot \Delta E_y + \Delta E_z \cdot \Delta E_z} \tag{5.4.2}$$

Directed towards the electrodes that span the electric field, these forces directly correlate to the length of the gradient and shall be maximized in the later application by creating fields as inhomogeneous as possible (see [131]).

5.4.1 Electrode Configurations and Lumped-Element Model

The studied sensor systems in this work contain multiple electrodes. To obtain possible electrode configurations, a Lumped-Element Model is assumed in the FEM simulations. Voltages are forced on up to four electrodes in the models, hence a 4x4

admittance matrix $\mathbf{Y}$ is obtained in eq. 5.4.3. These equations are based on [189, 176].

$$\begin{bmatrix} I_1 \\ I_2 \\ I_3 \\ I_4 \end{bmatrix} = \begin{bmatrix} Y_{11} & Y_{12} & Y_{13} & Y_{14} \\ Y_{21} & Y_{22} & Y_{23} & Y_{24} \\ Y_{31} & Y_{32} & Y_{33} & Y_{34} \\ Y_{41} & Y_{42} & Y_{43} & Y_{44} \end{bmatrix} \begin{bmatrix} V_1 \\ V_2 \\ V_3 \\ V_4 \end{bmatrix} \tag{5.4.3}$$

Obviously, the admittance matrix $\mathbf{Y}$ is the inverse of the impedance matrix (see eq. 5.4.4).

$$\mathbf{Z} = \mathbf{Y}^{-1} \tag{5.4.4}$$

COMSOL© assumes for an electrostatic case that the current is replaced with charge $\mathbf{Q}$ and the admittance matrix is replaced with a capacitance matrix $\mathbf{C}$ in eq. 5.4.5 [189].

$$\begin{bmatrix} Q_1 \\ Q_2 \\ Q_3 \\ Q_4 \end{bmatrix} = \begin{bmatrix} C_{11} & C_{12} & C_{13} & C_{14} \\ C_{21} & C_{22} & C_{23} & C_{24} \\ C_{31} & C_{32} & C_{33} & C_{34} \\ C_{41} & C_{42} & C_{43} & C_{44} \end{bmatrix} \begin{bmatrix} V_1 \\ V_2 \\ V_3 \\ V_4 \end{bmatrix} \tag{5.4.5}$$

This is needed to complete the theoretical backbone of the simulations. COMSOL© uses the energy density to calculate the the capacitance matrix $\mathbf{C}$. The electric energy density is integrated over the whole geometry and hence, the whole model that is predefined in the very beginning is taken into account by using the equations 5.4.6 and 5.4.7.

$$C_{ii} = \frac{2}{V_i^2} \int_\Omega W_e \, d\Omega \qquad V_j = \begin{cases} 0, & j \neq i \\ V_i, & j = i \end{cases} \tag{5.4.6}$$

$$C_{ij} = \frac{1}{V_i V_j} \int_\Omega W_e \, d\Omega - \frac{1}{2}\left(\frac{V_i}{V_j} C_{ii} + \frac{V_j}{V_i} C_{jj}\right) \qquad V_k = \begin{cases} 0, & k \neq i, j \\ V_i, & k = i \\ V_j, & k = j \end{cases} \tag{5.4.7}$$

W_e denotes for the electrical energy and Ω for the angle [189]. By using these few equations and material properties, the FEM simulation can fully derive the electrical field lines and their distribution in chapter 6 and 7.4.1.

5.4.2 Butler-Volmer Equation and Modification

The famous Butler-Volmer equation is used in Figure 6.8. It describes electrode kinetics but usually on redox-couples [190]. In this work, the equation is modified in its diffusion constants and heterogenous rate constants k_0 with the goal to describe rather bacteria cells than ionic species. Assuming that the direct contact between a polarized pathogen cell and the electrode acts similar like an electron transfer of an active redox couple. The Butler-Volmer equation is more than one hundred years old but a current review describes in a superb fashion [191]. The equation is given in 5.4.8 and describes the exchange current I:

$$I = k_0 \cdot F \cdot \{c_r \exp[\alpha_a f(E - E_0)] - c_0 \exp[-\alpha_c f(E - E_{eq})]\} \tag{5.4.8}$$

F is the Faraday constant. The small letter "f" describes the inverse thermal voltage (f = F/RT). c_r and c_0 are the concentrations of the redox couple "O" and "R". α_a and α_c are transfer coefficients in anodic and cathodic direction. E is the electrode polarisation and E_0^F the formal potential of redox couple [191].

5.4.3 Polarization and Movement of Bacteria

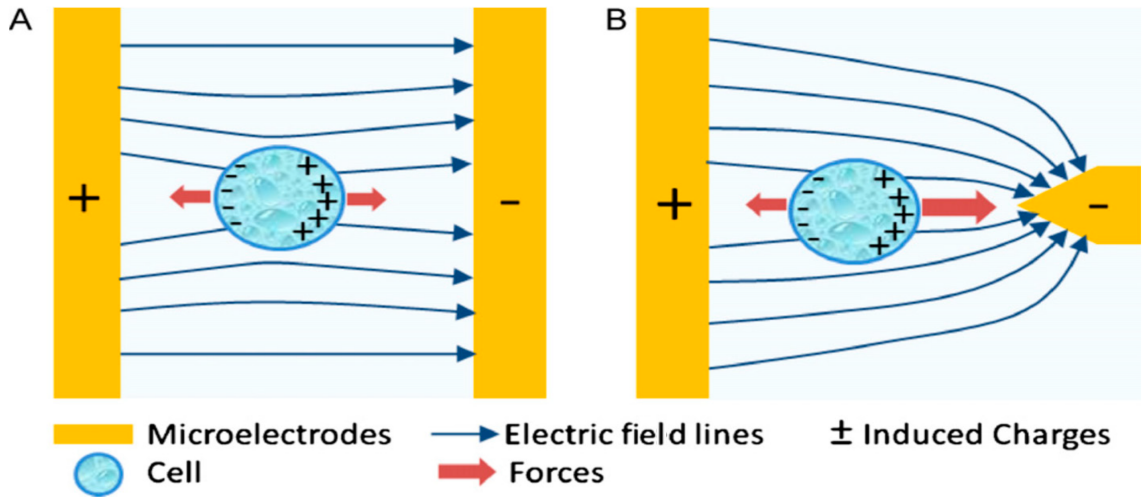

Figure 5.3: Schematic of Single Cell Bacteria in A) Uniform and B) Non-uniform Electric Field. The cell consists out of a great number of proteins, molecules and ions that can freely move within. An external field leads to a charge separation and consequently to moving force. DC fields can be used to move bacterial cells adequately. Adapted and modified from [192].

Physicist Herbert A. Pohl was the first to study systematically polarizable objects in electric fields [193, 194, 195]. The process called dielectrophoresis can be applied to

bacteria like E. Coli or biological cells as these objects are polarizable [196, 197]. In figure 5.3, a schematic of an polarizable bacteria in a DC field is given. Due to charge separation an effective force is acting on the dielectric object [192].
The reader is kindly referred to current review papers about this topic [198, 192, 199]. Summing up, DC fields can act a dielectrophoretic force F_{DEP} on spherical, dielectric bacteria [200], as can be seen in eq. 5.4.9.

$$\langle F_{DEP} \rangle = 2\pi r^3 \epsilon_m Re\Big\{ \frac{\epsilon_p^* - \epsilon_m^*}{\epsilon_p^* + 2\epsilon_m^*} \Big\} \nabla |\mathbf{E_{rms}}|^2 \tag{5.4.9}$$

The force in eq. 5.4.9 is time-averaged, ϵ_p^* and ϵ_m^* are the complex permittivities of the particle or medium, respectively [201]. The radius of the bacteria is given with r, and $|\mathbf{E_{rms}}|$ is the magnitude of the electrical field (root-mean square) [200]. In contrast, as shown in chapter 5.2, AC fields can be used to perform EIS on dielectric objects and consequently, to detect bacterial strands.

Chapter 6

Sensor Systems for Bacterial Detection

The previous chapter introduced the theoretical background for EIS detection of ions and directed movement of bacteria. This chapter details the design, simulation and evaluation approach for pathogen sensing and is based on the publication "Towards Easy-to-Use Bacteria Sensing: Modeling and Simulation of a New Environmental Impedimetric Biosensor in Fluids" published in MDPI Sensors in 2021 [131]. The main results are summarized and a few aspects are added. Firstly, the concept of measuring bacteria via electrochemical impedance spectroscopy is introduced and reviewed. Secondly, the choice of materials is studied before proceeding to the design aspects. Thirdly, the influence of periodicity in the electrodes is reviewed. Finally, a mathematical tool is presented that allows to evaluate arbitrary sensor geometries.

It is important to distinguish the purpose of alternating and direct currents when the system is electronically excited. For the purpose of bacteria sensing, two phases of the measurement scheme have to be considered:

1. **DC** excitation signals lead to polarization and consequent movement of the bacterial cells in fluids. This effect is used to gather the moveable objects in close proximity (100 µm and less) to the electrodes

2. **AC** excitation signals are used for actual detection of bacteria. A frequency sweep from 100 Hz to up to 1 MHz and the corresponding current response provide rich information about the quantity of pathogens

AC excitation signals are also the method of choice for ionic detection via EIS, which will be presented in chapter 6. For now, the focus lays on the bacterial strands exclusively.

6.1 Concept of EIS in Bacterial Sensing

The main idea of bacterial sensing in liquids is based on the fact that electrical field lines and their distribution depend on the electrical properties of the materials used. Assuming an electrostatical case as well as a more or less constant dielectric constants of the fluids we can deduct information on how the electrical field expands. Bacteria like E. Coli differ in their electronical properties [127], and can be modeled accordingly in Figure 6.1a). On the polymer substrate, electrodes are inkjet-printed. On top a functional dielectric membrane is deposited which is in direct contact to the fluid under test. Assuming an electrostatic case, an applied electrical field will penetrate the ellipsoidal shaped bacteria and will change accordingly. Figure 6.1 shows the concept that divides into two phases - an attraction phase as well as measurement part using Electrical Impedance Spectroscopy (EIS).

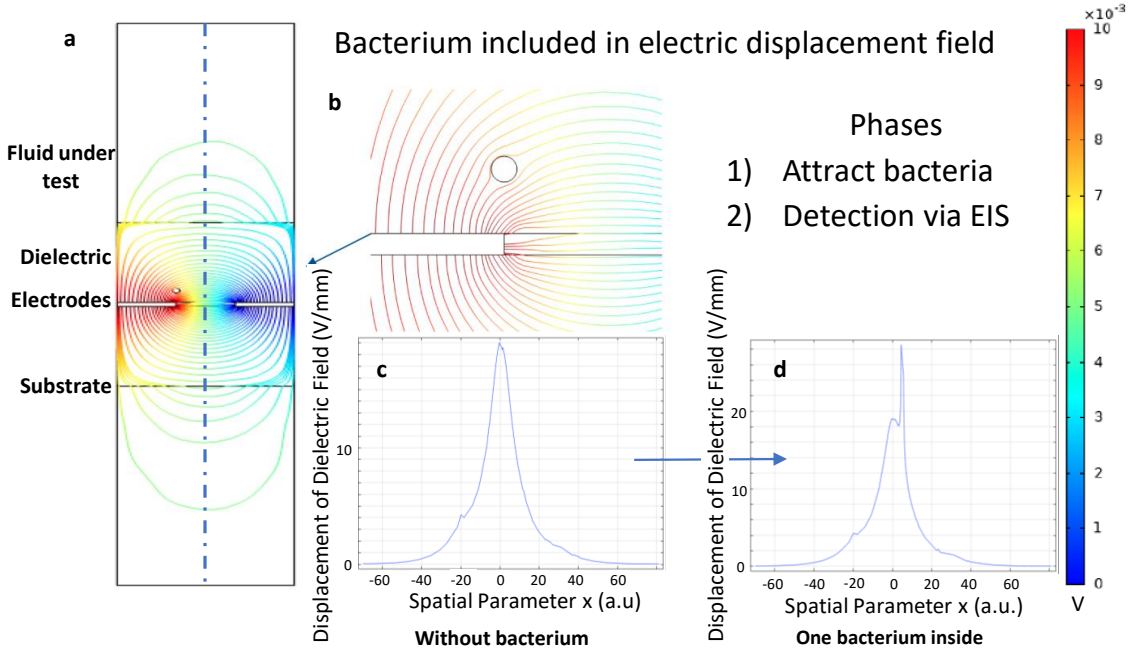

Figure 6.1: Interaction between Bacteria and the Electrical Field]: (**a**) A 2D two-electrode simulation of the displacement field when applying an external potential to the electrodes. (**b**) A circular model of a bacteria interacting with the displacement field between the electrodes. First, bacteria re attracted by applying DC potentials to the electrodes. In a second step, the read-out follows via electrochemical impedance spectroscopy (EIS) using AC potentials. (**c,d**) Displacement of the electric field in the center of the model in 1D with and without bacteria. The plot is evaluated along the dashed line in the model, starting from the center as indicated in (**a**).The color scale indicates low potentials (blue) to high potentials (red). Published in [131].

The FEM simulation solves the Maxwell equations for the problem above. The displacement of the dielectric field can be measured in a model with and without a single

bacteria and is validated when comparing 6.1 c) and d) indicating a possible signal to be exploited. When bacterial colonies are in close proximity to the electrode the dielectric displacement field changes. To gain more information on the dielectric properties of the functional membrane, Electrochemical Impedance Spectroscopy (EIS) is used for read-out purposes.

6.2 Material Choice

A major advantage of performing FEM simulations is the ability to prototype and test manifold materials. The bacteria sensor system does highly depend on the field distributions and densities that change when switching to other substrate materials, for instance. Figure 6.2 shows the effect of Al_2O_3, Glass or PET. The sensor is assumed to be surrounded by water above and below in this 2D model. Aluminumoxide shows denser field lines that lead to stronger forces acting on the bacteria, hence this substrate material is chosen.

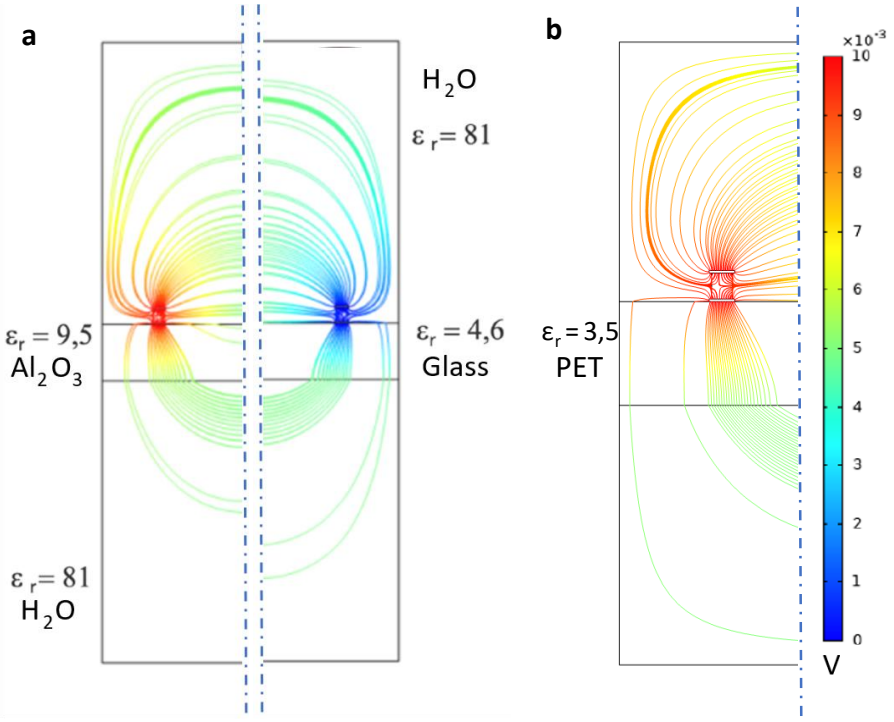

Figure 6.2: FEM Electric Field Simulations for Material Selection of Bacterial Sensor. (**a**) Field Distribution for Solid Substrates. The left side shows aluminumoxide as substrate material. The right hand side presents the corresponding simulation for the electrical field for borosilicate glass. (**b**) Field Distribution for Flexible Substrate PET (Polyethylene Terephthalate). The appropriate dielectric constants are assigned to the sensor stack's materials. The colour scale indicates low potentials (blue) to high potentials (red). Published in [131].

6.3 Design Aspects

Next, design aspects are studied. In figure 6.3 the best performing 3D designs are presented. As a substrate Aluminumoxide is chosen based on chapter 6.2. S-, T-, and Z-shaped electrodes are presented that use Polyimide as dielectric layer in between.

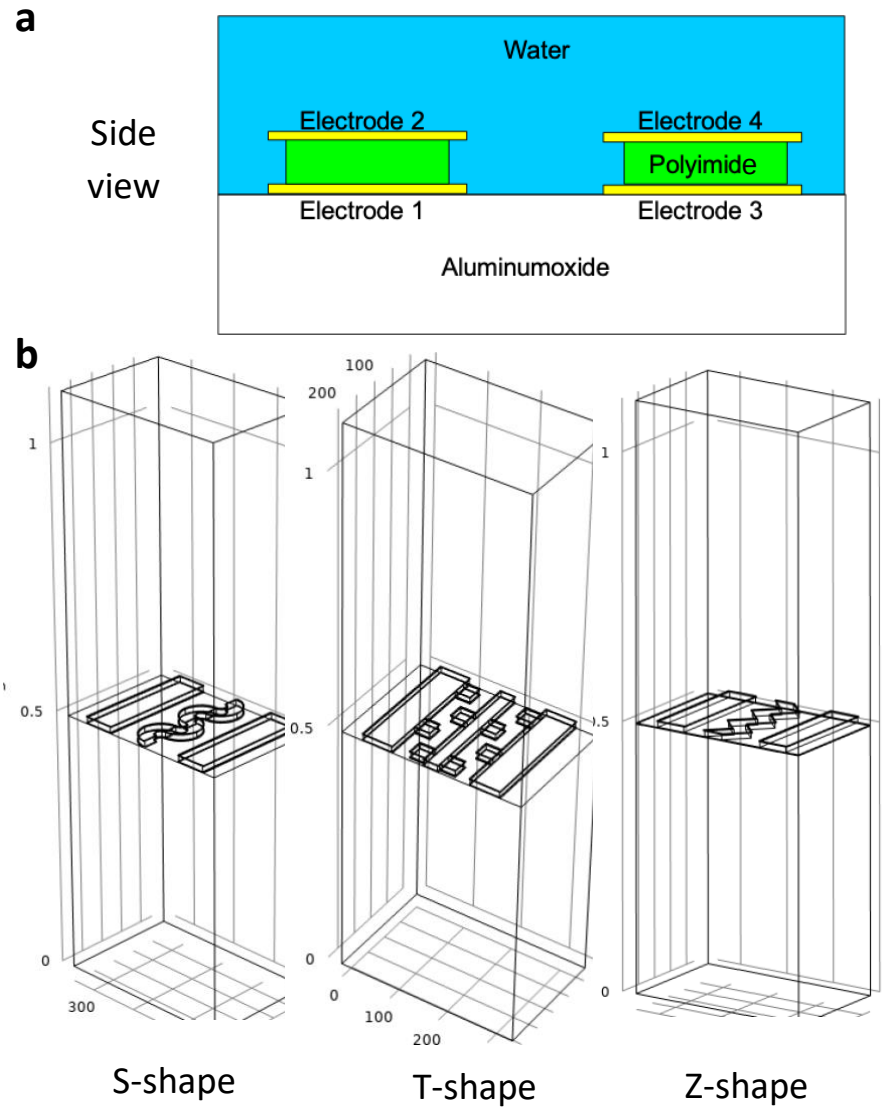

Figure 6.3: (**a**) Electrode Wiring and used Nomenclature in this Work. Polyimide acts as a insulating material between the stacked electrodes. (**b**) Designed 3D structures for Gathering and Detection of Pathogenic Cells. Published in [131].

In the simulations, the substrate is generally put on ground as this can be easily realized in real-life measurements as well. Also, 3D models that can be seen in 6.3b) are cut-out sectors of larger electrode designs as smaller sections need less computational power and time. The properties of larger scale (period) designs are discussed in the next chapter.

6.4 Periodicity

Larger electrode designs are studied here to gain an understanding of the effect of external, electric fields possibly interfering with the inner fields. In figure 6.4 a cross-view of an electrode array consisting of out of five electrodes can be seen. The reduction to a two-dimensional problem is sufficient here and serves the purpose of simplifying the issue.

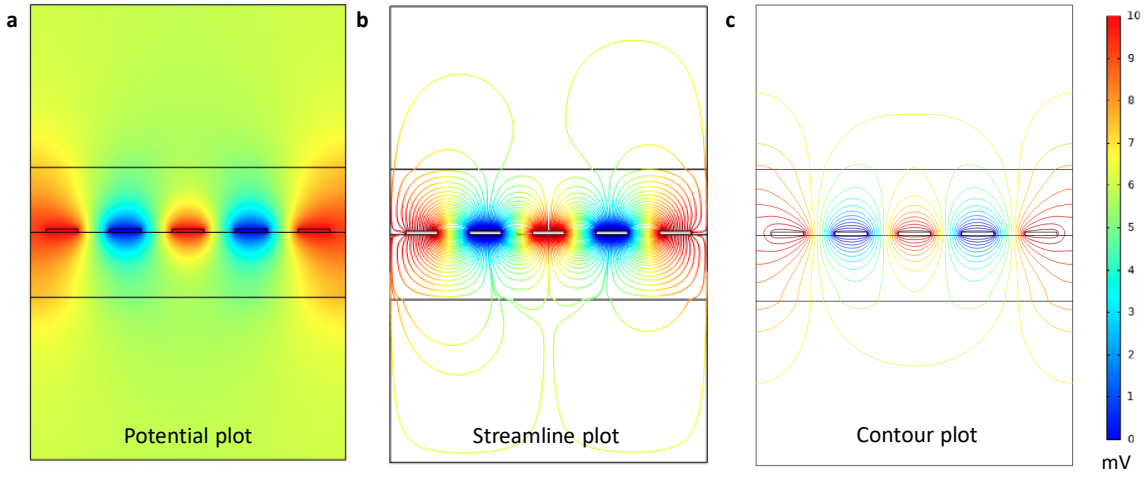

Figure 6.4: Periodicity of Multiple Electrodes: (**a**) Potential plot of five electrodes with two outer guard electrodes intended to shield external fields. (**b**) Streamline plot of electrical field lines and possible asymmetries between multiple electrodes of the bacterial sensor. The colour scale indicates low potentials (blue) to high potentials (red) but appears to be reversible for the purpose on estimating field distributions. The stack follows the same partitioning as in figure 6.1. Published in [131].

In figure 6.4 three types of visualizations are given for a electrode configuration of simply alternating between ground and 10 mV excitation voltage. The streamline and contour plot show that by using our geometrical dimensions and the corresponding material properties the field lines are quite dense and barely extend to further to the aquaous media above. A common strategy to shield external fields is to introduce "guard" electrodes. By putting the most outer electrodes on ground external field lines can be absorbed and the inner field effectively shielded. However, a significant outcome of this result is that there is no urgent need to realize this shielding method.

6.5 Quality Factor

The goal of this sensor system is to attract and detect bacteria. The ability to do so relies heavily on its geometrical design and the corresponding geometrical parameters. In order to optimize these parameters and the sensor signal, consequently, a mathematical tool to evaluate the sensor performance is presented [131]. Fig. 6.5 shows

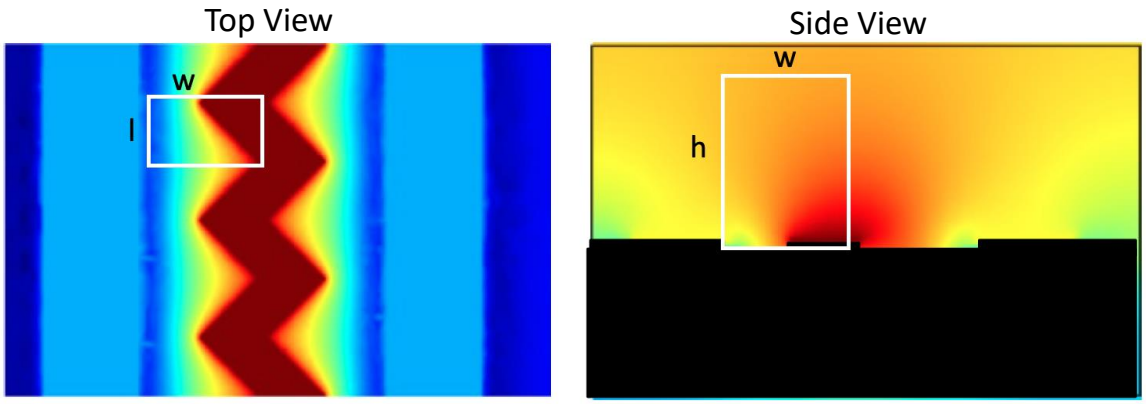

Figure 6.5: Towards Complete Mathematical Evaluation of 3D Simulations: Definition of Quality Factor. COMSOL Multiphysics © calculates a numerical solution to the underlying, (differential) Maxwell equations. The potential in each single point of the 3D volume of interest is determined and is utilized in order forecast electrical gradients in the mesh. W represents the distance from line contact edge to middle of "zigzag" contact; I denotes the distance from peak to valley; and h is the height of interest volume. Published in [131].

a potential plot with the same colour index as can be seen in fig. 6.4. A volume of interest is defined through the spatial parameters used. The length (l), width (w) and height (h) are defined in eq. 6.5.1.

$$V_{interest} = l \cdot w \cdot h \tag{6.5.1}$$

As stated in theoretical chapter 5.4, all electrical force gradients and their length are calculated from these potentials. The gradients correspond to the actual mechanical forces that act on bacteria swimming in the fluid. The complete computational space is divided into smaller pieces. In the 3D simulations, a mesh size of 1µm is used in the grid. The gradients in each of these boxes are geometrically summed up and then divided again by the volume of interest, as can be read in [131].
Firstly, the attraction of bacteria profits from higher gradients as the resulting forces are also stronger and directed towards the very proximity of the active sensor area. Secondly, the detection of the model used for E. Coli (EIS) also benefits from this metric. The closer the bacteria are located towards the electrodes the polarization effects become bigger and a better signal can be expected, as explained in chapter 5.2.

6.6 Complete Evaluation of 3D Simulation Models, the Role of Configurations and Excitation Amplitude

The concept of the quality factor allows a precise, mathematical tool to evaluate arbitrary electrode structures [131, 77].

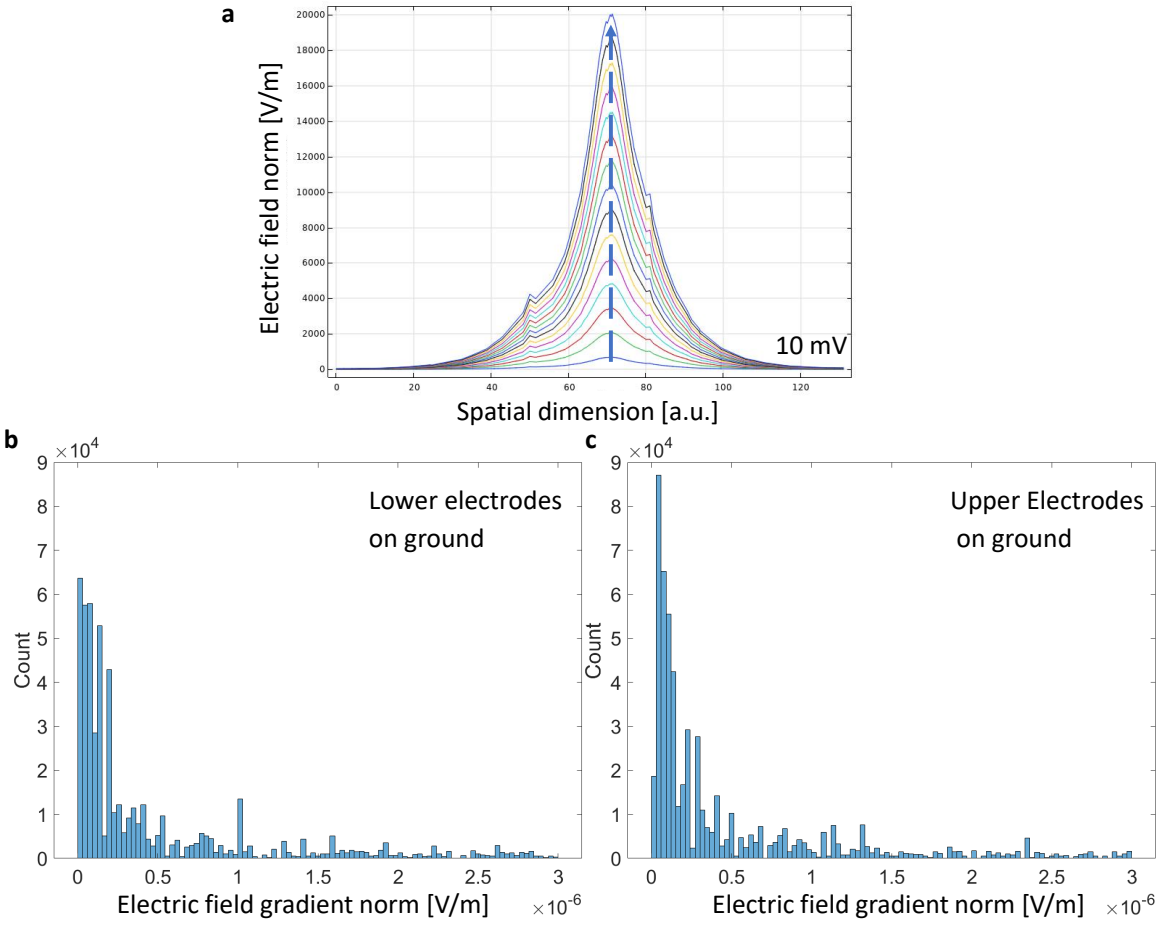

Figure 6.6: Simulated Distributions of Gradient Lengths across Volume of Interest, the Influence of the Electrode Configuration and the Role of Excitation Amplitude: (**a**) The FEM simulation illuminates the role of excitation amplitude for the gradient length ranging from 10 mV (bottom line) to 300 mV (step size 20 mV in a single, center point of the model. (**b**) In order to distinguish between the various designs, the mathematical tool of a quality factor is applied. The gathered data is presented in a histogram showing the full 3D distributions of gradient lengths in the simulated model ZF. The electrode potentials are configured in way that the bottom ones directly on the substrate are on ground. (**c**) Switching the configuration on the ZF design exhibits a divergent behaviour. Published in [131].

First, the role of the excitation amplitude is reviewed. In figure 6.6a) the electric field

norm is given in the very center of the presented sensor models (blue, dashed line) when applying a excitation signal with magnitudes between 10 mV and 300 mV. The colors indicate a step size of 20 mV.
It is worth to mention that 300 mV have not been exceeded in order to stay outside the electro-active window [131, 77]. The peaks appear to correlate linearly with the electrical field norm. Additionally, the side peaks can be reasoned with material interfaces like substrate-to-electrolyte, for instance.
The crucial advantage of the concept of the quality factor is the enhanced and more precise evaluation of the models especially when switching from 2D to 3D models. In figure 6.6b) and 6.6c) a full evaluation of the gradient lengths and their distribution is presented in a full 3D ZF model. This corresponds to a Z-like center electrode structure with a fully connected bottom electrode like presented in figure 6.3. Interestingly, different configurations lead to different outcomes in the quality factor. This is logic from a physical point-of-view. Numerical artifacts can be successfully counteracted by using an arithmetic mean of the quality factor.
"A higher quality factor can be interpreted as larger, average gradients in the overall volume units of the model" as stated in [131] and hence the concept is regarded as validated.

6.7 Comparison of presented 3D FEM models

Equipped with the mathematical tool of the quality factor, the authors seek the most useful electrode structure to trace microbes or germs in fluids. In chapter 6.3 S-, T-, and Z- FEM models are presented that are compared concerning their properties for the bacteria attraction and detection. In figure 6.7 cross sections of these 3D models with several configurations are given. The displayed potential distributions are compared especially in the surroundings of the electrodes. Remarkably, configurations with the bottom electrodes "E1" and "E3" on ground and top electrodes "E2" on the forced excitation potential of 10mV perform better.
The visual evaluation is followed by an mathematical scheming. Numerical results for the quality factor are shown in table 6.1.
The best performing electrode configuration is the ZF-structure consisting of a Z electrode structure and connected (or full) bottom electrodes.

6.8 Experimental Proof of Concept

Finally, experimental verfication of the concept is shown in Fig. 6.8. A Nyquist plot is shown for NaCl and various concentrations of E.Coli. The corresponding data is taken by the cooperation partner Domatec GmbH and uses the presented PalmSense potentiostat in section 4.1. The real and imaginary part of the EIS measurement of a

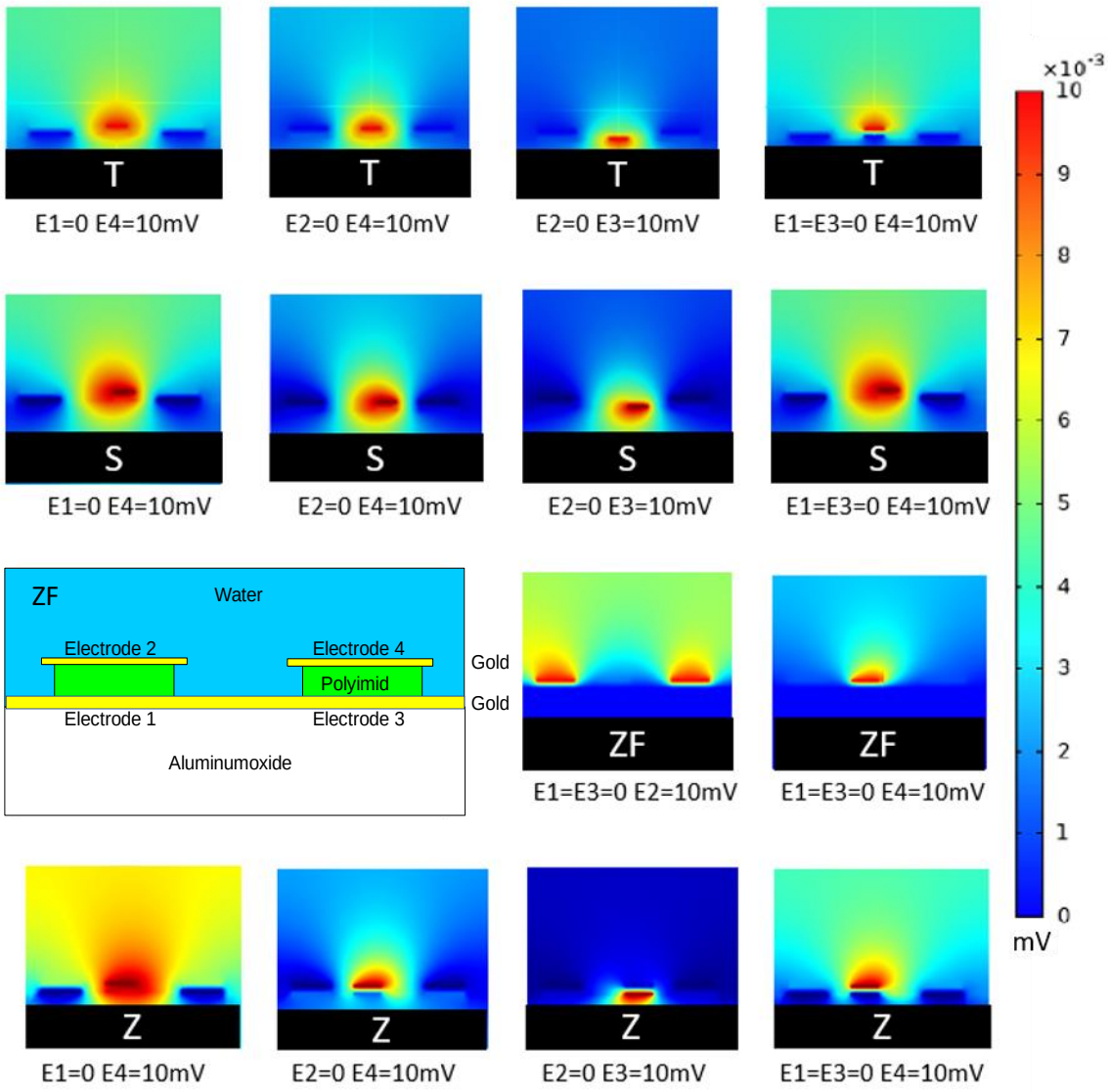

Figure 6.7: Comparison of Field Distributions on T-,S-, Z and ZF-shaped 3D Structure of the Active Sensor Layer. The range of simulated designs encompasses also a modified version of the Z-model with a full-length connected bottom electrodes (ZF-structure). The four electrode setup intends to stabilize the electric field from external fields. The nomenclature of the electrode configurations is given on the left side. Not mentioned electrodes are kept on floating potential. The colour scale indicates low potentials (blue) to high potentials (red). Published in [131].

Type	**Electrode Configuration**	**QF**	**Ranking**
S	E1=E3=0; E4=10mV	1.28014	7
S	E2=0; E4=10mV	1.66557	6
T	E1=E3=0; E4=10mV	1.95682	4
T	E2=0; E4=10mV	2.35999	3
Z	E1=E3=0; E4=10mV	1.83386	5
Z	E2=0; E4=10mV	2.93997	2
ZF	E1=E3=0; E4=10mV	3.23390	1

Table 6.1: Quality Factors for Selected and Presented Sensor Designs. If electrodes are not stated in a configuration they are kept on floating potential in the FEM simulation. Published in [131].

ZF-like sensor structure are plotted against each other. Sodium Chloride serves as a reference solution.
The plot in Fig. 6.8 shows clearly a useable signal for the detection and possibly quantification of pathogenic E. Coli strands. The imaginary part of the impedance dominates indicating a capacitative behaviour towards the pathogenic bacteria. The shown theoretical fit shows an effort for an analytical description of the EIS data. The underlying formula is the Butler-Volmer equation detailed in chapter 5. It assumes charge-like particles and ions instead of spatially extended single-cell bacteria like E. Coli. The difference in size between ions (1 nm ionic radius) and biological cells (1 µm) amounts to three orders of magnitude and hence is tried to be compensated by assuming heterogenous rate constant k_0 of $0,001$ cm/s and spatially randomly distributed single cell bacteria in the medium.
The theoretical behaviour is based on a linearized version of the Butler Volmer equation. In equation 6.8.1, the complex impedance is iteratively approximated using the solution resistance R_s, the polarization resistance R_p and the corresponding frequency ω [203]. Even though the Butler Volmer equation usually describes electrochemical reactions like Redox couples, the equation also describes diffusion of the reaction partner as well as the electron transfer rate constants k_f and k_b for forward and backward transfer [203]. The latter is the parameter to be optimized assuming the the forward and backward transfer rate is roughly the same.

$$Z(\omega) = R_s + R_p(1 + \frac{\lambda}{2\omega^\nu}) - R_p^2\lambda^2 C_d + \frac{jR_p\lambda}{2\omega^\nu} \tag{6.8.1}$$

The free parameter λ describes the propagation of the reaction partner (in our case E. Coli bacteria with CFU of $10^3/ml$ with the help of diffusion coefficients D_O and D_R in eq. 6.8.2. Originally, D_O and D_R are meant to describe the oxidation and reduction

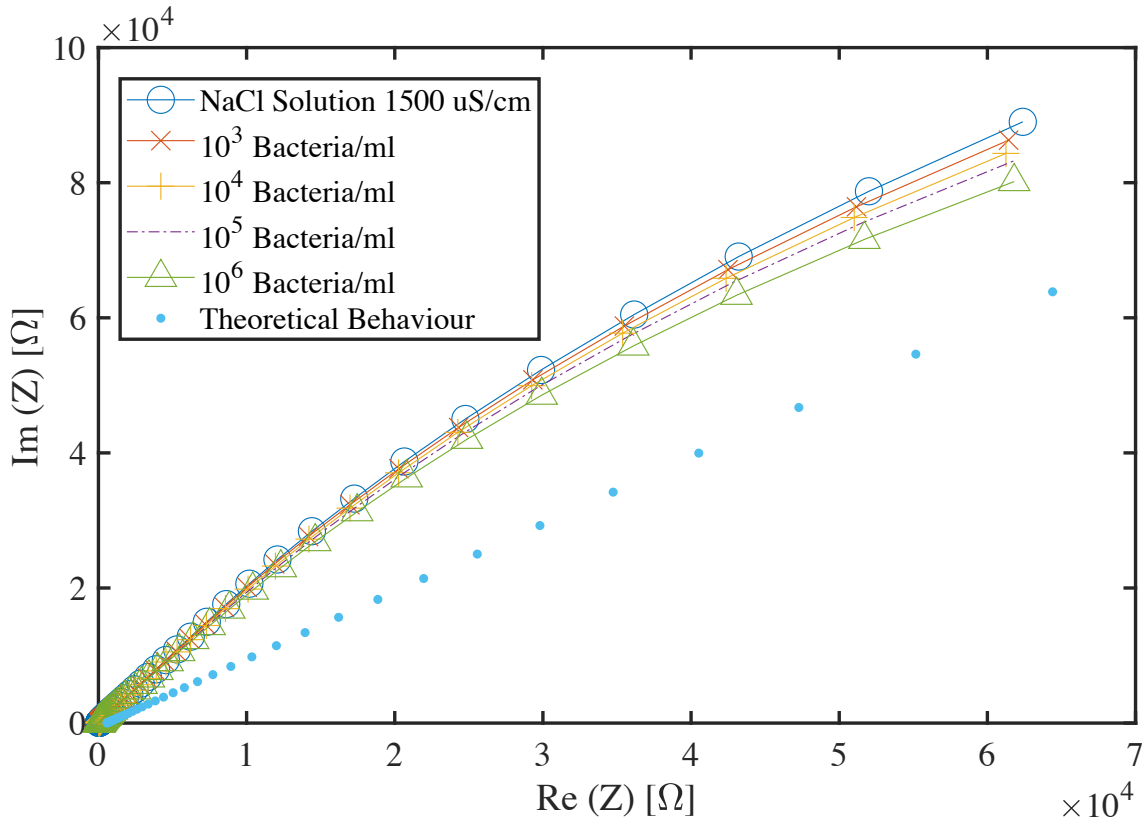

Figure 6.8: Experimental Proof of Concept of Bacterial Sensor. Nyquist plot showing the real vs. the imaginary part of the impedance Z. As base reference serves a defined NaCl solution. The other samples refer to colony-forming units (CFU) per ml. The theoretical behaviour is based on the Butler Volmer equation and fits to 10^3 CFU/ml. The experimental data was provided by the cooperation partner domatec GmbH, Raphael Oefelein, and plotted by the author [202].

partner [203] but here it is to used to approximate single bacteria coming to close proximity of bare electrodes in fluids. As the size is significantly bigger (1000x) of a bacterial strand compared to single ions, the diffusion constants are also assumed to be in the same range for both directions.

$$\lambda = \frac{k_f}{\sqrt{D_O}} + \frac{k_b}{\sqrt{D_R}} \tag{6.8.2}$$

The interfacial charge transfer of a redox couple is generally assumed to obey the Butler–Volmer kinetics [204]. As the floating bacteria can touch the bare electrode in the presented system it is assumed that a charge transfer of the pathogen to the electrode occurs. Based on this idea, the Butler Volmer equation has been used according to [205], and the following assumptions have been made:

- The solution resistance is estimated to be $R_s = 60$ Ohm (has been calculated

from the overall conductance of the solution)

- The polarization resistance of the electrode in contact with the bacterial strand is estimated to be R_p = 2600 Ohm (has been calculated according to [206])
- The double layer capacitance has been estimated to be C_d = 625 pF (based on [206])
- The correction factor for the exponent ν = -0.707175 is modified from the original version ([203]), has been 0.5 originally and is one of the parameters to be optimized by the fit function
- The parameter λ describes the Diffusion and transfer kinetics of the reaction partner and is optimized for the fit in Fig. 6.8 and set to be λ = 243.72 1/s (described in eq. 6.8.2)

Evaluating the theoretical behaviour compared to the experimental results is not straight-forward. Two main aspects have been observed when applying the Butler-Volmer equation to the measurement scheme of the bacterial sensor. First, the exponents of the frequency are off by about 0.2. Hence, the equation 6.8.1 has been modified with an correction parameter ν. Second, the imaginary part of the experiments of the Nyquist plot always results in positive values. Consequently, the instrinsic imaginary part of the last term of eq. 6.8.1 is regarded as positive. The original derivation of the expression for the impedance vs. the frequency of the theoretical behaviour relies on a Randles circuit [203]. However, the analytical description fits the taken data semi-well and therefore a more complex equivalent circuit is assumed. The presented data in 6.8 provides some evidence that the bacterial sensor can be described by the analytically derived, linearized Butler Volmer equation but further research needs to fine-tune this first attempt of mathematical interpretation.

6.9 Discussion

Chapter 6 aims to sense bacterial species in fluids. In order to find the best electrode structures for this purpose numerical simulations are performed.
Firstly, in figure 6.1 a conceptional proof in two dimensions is presented. The numerical study takes the material properties into consideration. Modeling a microorganism as a circle with different electrical properties and choosing the right length scales provides evidence that the dielectric field is sufficiently displaced. A first sensitivity of the system towards E. Coli like species is found although diffusional forces are regarded as omnidirectional and thus neglected [207].

Secondly, a set of possible materials for substrate, electrode, and connecting dielectric is investigated. Fig. 6.2 shows that the electrical field lines behave differently when switching the materials. From a visual inspection, the requirements for attraction are superior and best exploited with Al_2O_3.

Thirdly, a set of 3D models is exhibited in fig. 6.3. A slightly positive effect of guard electrodes are explored in fig. 6.4. A mathematical tool for more precise evaluation of arbitrary structures is defined in fig. 6.5 and tested in fig. 6.6. The electrical gradient fields change dramatically and also the forces that may act on pathogens consequently. Sharp edged Z and ZF- structures offer higher electrical gradients and appear higher ranked for the purpose of bacteria attraction. The big influence of variations in the electrode configuration validates the concept of the quality factor. Following a stringent systematical approach the new tool of quality factor led a ranking of the studied structures in table 6.1.

Lastly, an experimental proof is given in 6.8. Several bacteria concentrations can be differed when EIS is applied to the designed sensor system. The Nyquist plot has a indicates a dominant capacitative behaviour of the system. As the difference between the samples is relatively small, additional data processing is recommended to use for real-life application. The experimental data can be partly be described a modified Butler Volmer equation. Suggestions for modification include the λ parameter that accounts for diffusion and electron transfer rates when a E. Coli strand gets in direct interaction with an electrode. A more complex equivalent circuit is desireable that accounts for more effects like a possible deviation of the double layer capacity.
This chapter is a systematical study of the interplay between sensor design and expected real-life (EIS-) signal for the purpose of bacteria detection. The state-of-the-art is enhanced especially with the concept of the quality factor as an evaluation tool and its ability to assess otherwise unpredictable electrode geometries. A contribution lies in real-life recommendations for the layout and topologies of these sensor structures and a guideline what performances can be expected when turning this system into a commercial product.

Chapter 7

Ionic Sensors

7.1 Printed Ionic Sensor

In this chapter, a fully printable Na^+ ionic sensor is presented. The goal is a cost-intensive, additively manufacturable sensor that measures Na^+ concentrations in fluids.

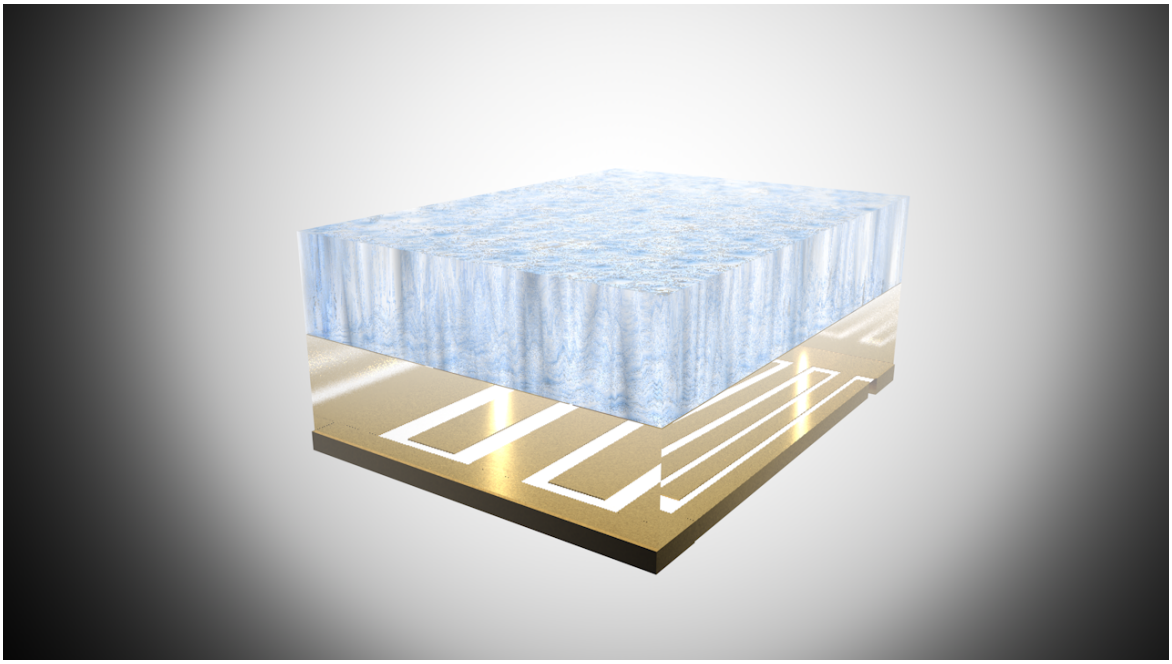

Figure 7.1: Concept of Bottom-up Designed Ionic Sensor with Fluid of Interest on Top. The transparent part in the center represents a functional, dielectric membrane influencing electrical fields that span between the golden electrode structures (bottom). Published in [77], ©IEEE 2021.

The chapter is based on the publication [77] and starts off with explaining the concept, schematising the experimental setup and detailing the role of FEM simulations in the geometrical design. The chapter continues by showing fabricated ion sensors and the corresponding experimental characterization and tests. More specifically, Electrochemical Impedance Spectoscopy (EIS) measurements are shown, and a possible

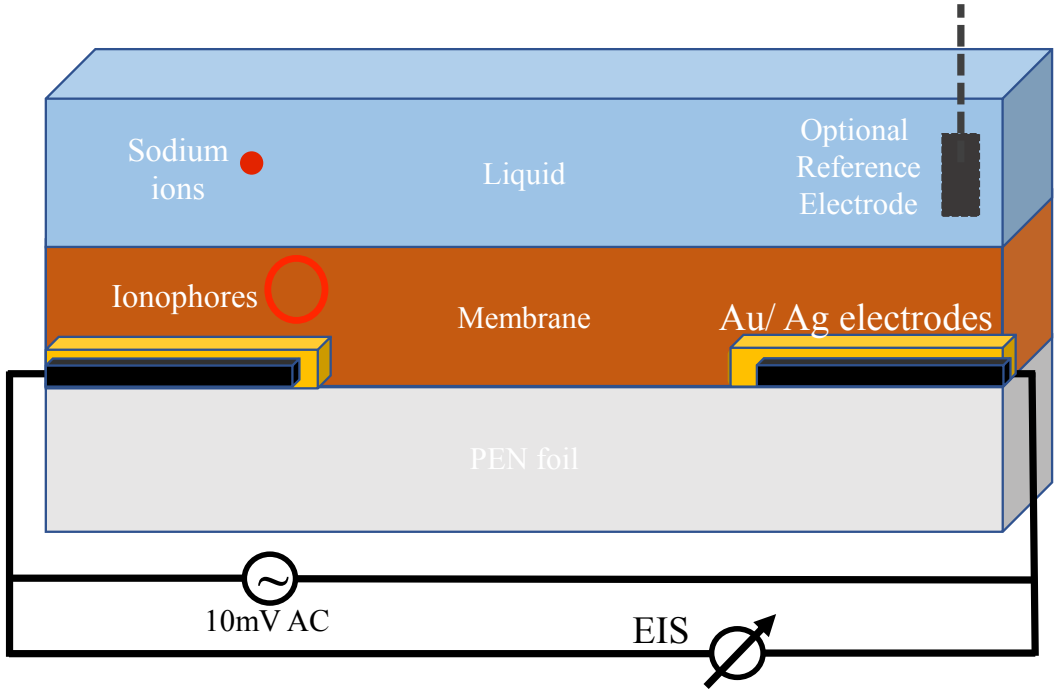

Figure 7.2: Working Principle based on Schematic Cross-section of the Ionic Sensor and Measurement Setup. The readout circuit needed for electrochemical impedance spectroscopy is hinted conceptionally. To obtain a constant potential in the fluid-of-interest a pseudo Pt-mesh reference electrode can be added. As the electrodes are not in direct contact with the fluid, a two-electrode measurement is preferred in order to circumvent the urgent need of the additional reference electrode. The red dots represent the ion of interest. The ionophores are covalently bound in the polymer membrane and have a local energetical minimum when a target ion is trapped. Adapted and originally published in [77].

way to calibrate the system is presented. Issues like cross-sensitivity towards other ionic species, drift, and possible detection limits are given. This second part of experimental results is concluded by experimentally produced Nyquist diagrams that are used for modelling an equivalent circuit. The model facilitates significantly the development of integrated read-out circuitry and opens the realm of Iot applications for electrochemical sensory systems.

7.2 Concept

First, the concept of the ionic sensor is presented. In figure 7.1 golden electrodes are directly below a sensitive membrane that physically separates the ions of interest of the bulk fluid vs. the optimized electric field and its polarizable elements. Electrochemical

Impedance Spectroscopy is utilized to derive the electrical properties of the membrane creating a measurable signal.
Figure 7.2 shows a simplified schematic of the sensor system that involves the electrical circuit as well. The main idea evolves around a bottom-up approach: Every part of the sensor is fully printable. Starting with a Polyethylennaphthalat (PEN) substrate, conductive electrodes are added in (arbitrary) structures via inkjet-printing. Next, a dielectric membrane containing an ion-specific ionophore is stacked and in direct contact with the fluid-of-interest. An optional Reference Electrode (RE) can be used to force the liquid to a certain electrical potential. However, the dielectric membrane, the covalently bound ionophores and their dipole moment seem to be the main cause of the measureable EIS signal. Hence, two-electrode setups are favored.

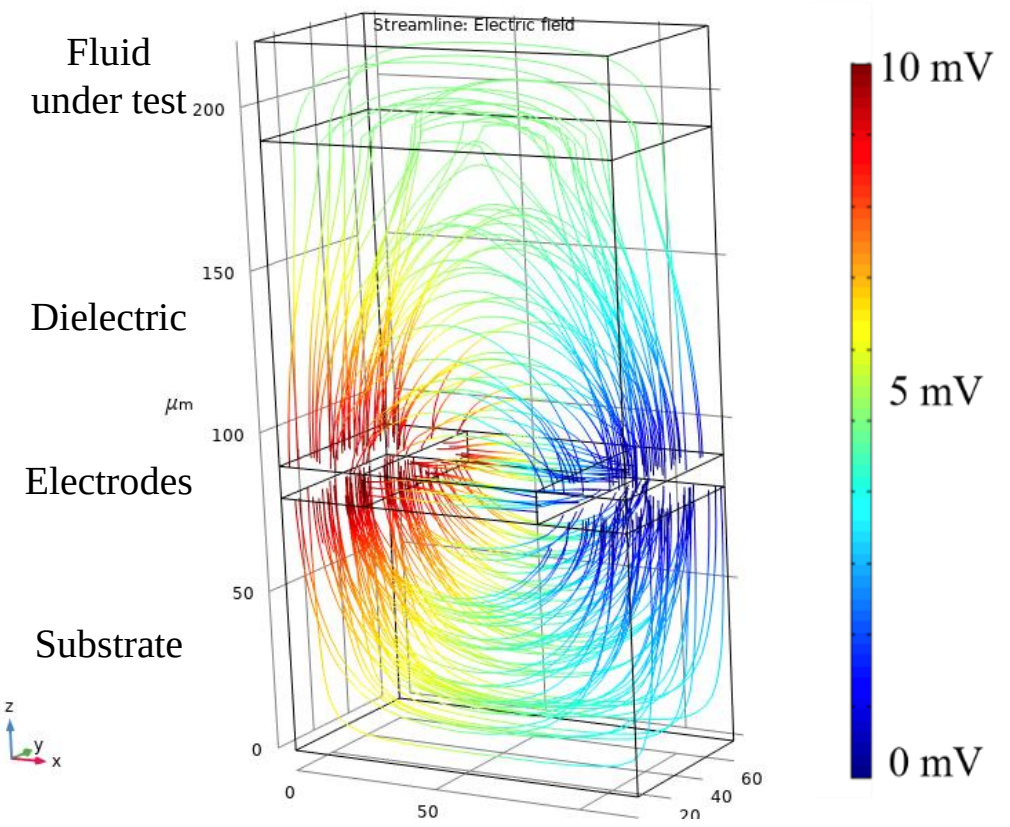

Figure 7.3: Defining Sensor Design via 3D FEM Simulation of the Electrical Field Distributions in a Surface Line Plot. Manifold sensor structures are assessed to find optimized parameters shown in Table 7.1 as well as screening the involved dielectric material properties. The color scale displays the applied potential. Published in [77], ©IEEE 2021.

For excitation, AC signals with small amplitudes like 10mV are applied to the sensor stack and a full EIS spectrum is deducted from the current response. Keeping the excitation signal amplitude low allows to stay outside the electroactive window, minimizing unwanted chemical reactions and hence parasitic currents.

The reader is kindly refered to chapter 4.1 for more details on the experimental setup.

7.3 FEM Simulation on Distributions of the Electrical Fields

Next, the design aspects of the sensor are evaluated. As mentioned in chapter 6, the geometrical design of the involved materials is crucial. In figure 7.3, finite-element simulations are performed and electrical field lines are displayed in an electrostatic case. As anticipated, the two metal electrodes in the center of the 3D simulation do not contain any field lines. The used dielectric membrane and dielectric substrate surrounding are transversed by coloured field lines. Minimizing the density of field lines in the actual fluid under test leads to high signal-to-noise ratios for the sensor system later on. It is used to make statements about crucial design parameters like the necessary height of the dielectric membrane.
Table 7.1 shows the final results for the optimized parameters that are derived from the FEM simulations. A set of optimal parameters is presented that offer high density of electrical field lines in the dielectric membrane. The membrane contains ionophores that exhibit high affinity towards an ion of interest that diffuses into the membrane.
The technological possible resolution of inkjet-printing is taken into account and defines electrode dimensions. The electrical properties of all the involved materials are fed to the electrostatic simulation, and consequently useful values for the height of the ion-selective-membrane deducted. As can be seen in Fig. 7.3 the electrodes are not traversed.
The infinite dielectric constant of the metal allows for the conclusion that the electrode (metal) design parameters like the electrode height should not heavily change the field distribution. Rather, the interplay between all involved dielectric layers define the electric field in the sensor stack.

7.4 Fabricated Sensors

The enhanced design parameters are used to manufacture the sensor stack via inkjet printing. Details on the materials and methods can be found in 4.1.
Figure 7.4 shows the fully printed sensor stack. Starting from a dielectric substrate, a flexible Polyethylennaphthalat (PEN) foil, conductive silver nanoparticle ink electrodes

Parameter	**Value**	**Unit**
Electrode Dimensions	100x60x30	µm
Electrode Distance	108	µm
Height of ISM	100	µm
Dielectric Constant of Substrate $\epsilon_{r,sub}$	3.2	-
Dielectric Constant of ISM ϵ_{r_s}	4.25	-
Dielectric Constant of aq. Solution $\epsilon_{r,sol}$	78	-

Table 7.1: Best Design Parameters based on FEM Simulations. The first row denotes assumed values for the FEM simulation of a single electrode finger (length, width, height). Published in [77], ©IEEE 2021.

are printed. The inks have been iteratively develeloped and its composition can be found in chapter 4.1.

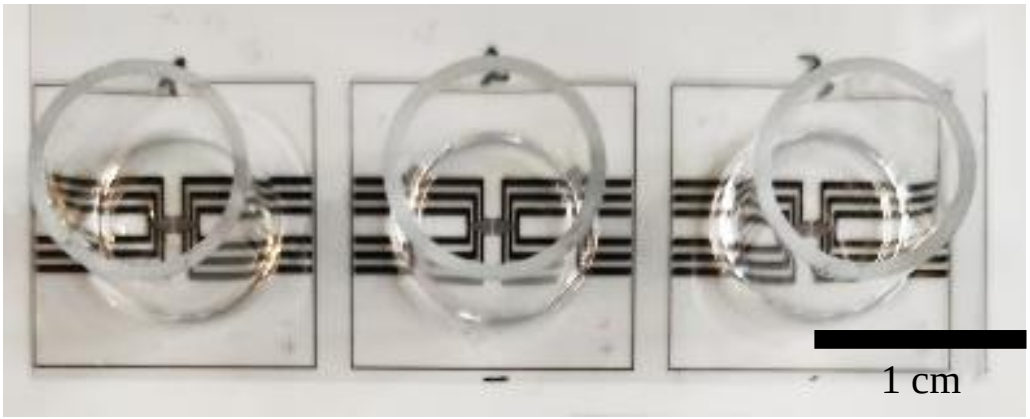

Figure 7.4: Additively Manufactured Sensors for Ion Detection of Na^+ with Glass Ring Encapsulation, ISM, and Printed Electrodes. Published in [77], ©IEEE 2021.

7.4.1 Electrochemical Impedance Spectroscopy

Next, electrochemical Impedance Spectroscopy is performed on the sensor samples. The eleven fabricated sensor samples show good adhesion between the layers and remain in stable condition when in direct contact with fluids. The Bode Plot in fig. 7.5 shows the absolute value of the impedance of the sensor towards the fluid-under-test of four Sodium-Ionophore based samples. The Na^+ concentration of the fluid is clearly distinguishable for a biological relevant range. The controls are a) the dry,

functional membrane and b) an infunctional, "reference" membrane that does contain any ion-specific ionophore. The results have been verified by a two-electrode as well as three-electrode setup. The latter involves a Ag/ AgCl- reference electrode that defines a potential to the fluid-under-test. On the one side, this allows for potentially more controllable and more accurate results. However, for biotech applications a two-electrode setup appeared to have (71.3 ± 0.7) MΩ of good usable dynamical range which is more than enough for our purpose. Also, being able to omit the toxic Ag coming from the Ag/ AgCl reference electrode is an immense advantage especially for any kind of in-vivo measurements.

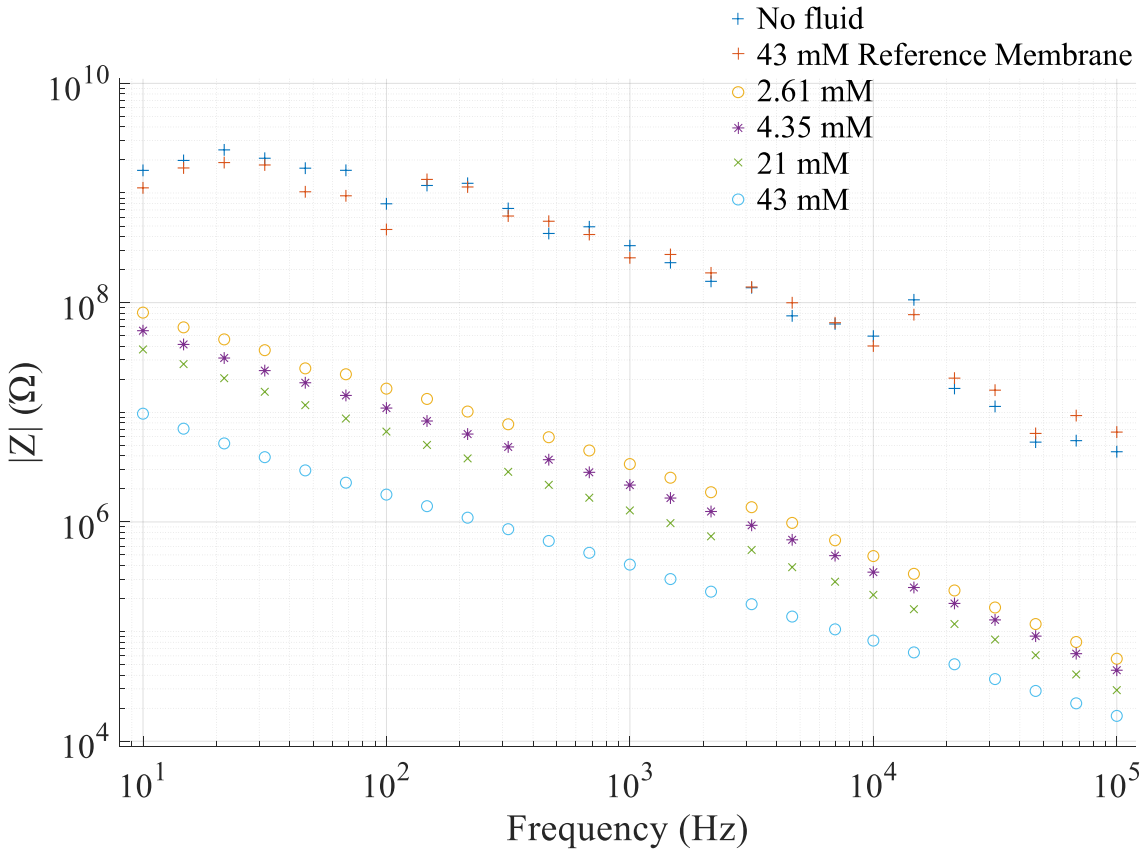

Figure 7.5: Impediometric response of an ionic sensor for different analyte concentrations c of Na+ and reference membrane without ionophore using fresh sample of Sodium Nitrate (AAS Standard). The frequency covers a wide range of the excitation signal with an constant ampltiude of 10 mV. Published in [77], ©IEEE 2021.

The samples have been pre-wetted for 1h. This leads to faster response times in the range of single seconds [77]. As chemical sensors are intrinsically slow compared to other electronics this is tolerable. The impedance of the "Reference Membrane" appears to be quite high but could be experimentally repeated. The main purpose of the Reference in this system is provide an addtional path for read-out purposes. Being able to substract the impedance signal from a reference can potentially improve

the Signal-to-Noise Ratio (SNR) and potentially circumvent undesired side-effects like extra parasitic capacitances. The corresponding phase data to Fig. 7.5 is given in the appendix A.2 but is hard to interpret. For this reason, the proposed measurement scheme does not rely on the phase data.

7.4.2 Calibration and Cross-Sensitivity

A deeper dive into the data allows to calibrate the system and underlines its versatility. Figure 7.6 A) shows that for the lower part of the frequency spectrum we obtain the best dynamic range between the solutions for the lower frequencies like $10 - 1000$ Hz. A conducted error analysis contains a generous estimate of the systematic errors (details can be found in the appendix). For the double-log plot linear fits can be used to calibrate and hence, predict unknown concentrations in a reasonable fashion.

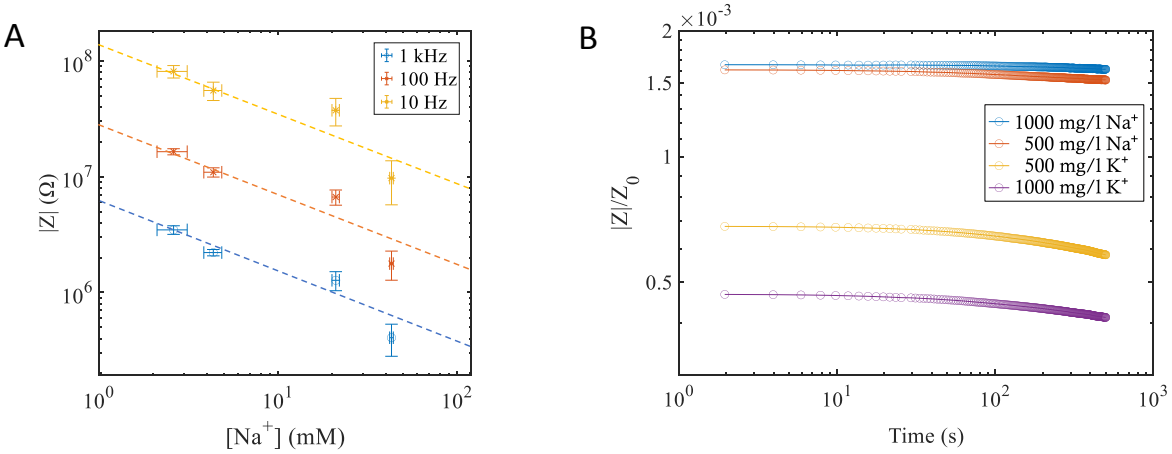

Figure 7.6: A) Dependence between the absolute value of the impedance |Z| and the target ion concentrations [Na^+] for Ionic Sensor. Three excitation frequencies are evaluated including the statistical and systematic errors calculated according to appendix A.3. B) Cross-Sensitivity of Ionic Sensor over time. Chemically similar K^+ ions are studied in contrast to Na^+. Published in [77].

Interestingly, the linear fit function works best the lower the excitation frequency is. A possible explanation can be found in the effects of capacitative behaviour of the system. The higher the frequency the stronger the influence of parasistic capacities gets in phase and magnitude of impediometric response.

7.4.3 Drift and Detection Limit

Figure 7.6 B shows a the normalized impedance Z/Z_0 over time. A slight drift is noticed as well as cross-sensitivity towards the most similar chemical element K^+. Na^+ and K^+ have nearly the same ionic radii and hence a very alike hydration sphere - making these elements react chemically (almost) the same. The fact that less impedance

is measured for K^+ is not straight-forward and unfortunately leads to the need of data processing in the further scape of this project. However, the clear separation between the signals emphasize the high specificity towards the most challenging ion, K^+. Importantly, a detection limit for Na^+ has been experimentally determined. 10nM are directly detectable in low frequencies.

On the other hand, the theoretical detection limit is estimated to be in a similar range, of roughly 10^{-8}M. This value is calculated by dividing the possible dynamic range through the distinguishable target concentration range. Assuming a very conservative approximation of being able to distinct only 10 Ω in the read-out electronics leads to an absolute analytical sensitivity of 17 ± 0.03 MΩ/mM. The calculation of the sensitivity is also detailed in the theory chapter 5.3.

7.4.4 Nyquist Diagram

After reviewing electrochemical aspects like drift the experimental results are used to derive an electrical model from the system.
Another way of representing EIS data is to use Nyquist Diagrams. The real part of the impedance is plotted against the imaginary part in figure 7.7. Three benchmark parameter of the discussed Randle's Circuit in chapter 5 are investigated with R_s being a resistor element and R_{ct} the resistor in parallel to the double layer capacity C_{dl}. The interpretation of this elements is the following:

- The solution resistance R_s can be depicted at the highest frequency when the real axis is crossed. It appears to go inversely proportional to the concentration of the target ion.
- R_{ct} is a purely real number and intersects with the real axis at low frequency as the sum of both R_s and R_ct
- Z_w symbolizes diffusional effects and is represented by the final straight line of the Nyquist plot.

The Nyquist plot in figure 7.7 shows fitted semi-circles that can be traced to interfaces like electrolyte-electrode. It can now be used to fit a equivalent circuit model to the experimental data which is detailed in the next chapter when following the rules above (and also shown in the graph). A semi-circle in a Nyquist Diagram can be interpreted as an interface. The interface is likely to be between electrode and electrolyte.

7.4.5 Modelling and Equivalent Circuit

In the scope of this thesis, only few requirements to the sensor system were made: Cheap, printable, sufficient resolution, and a controllable drift. FEM simulations help

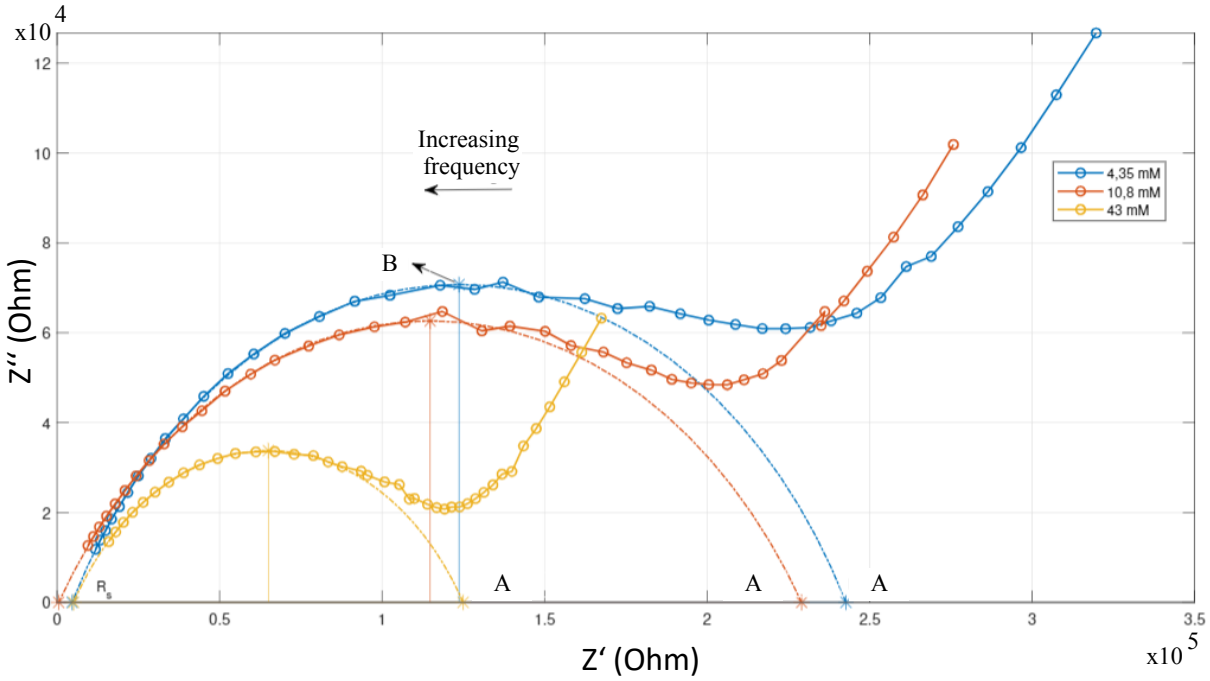

Figure 7.7: Nyquist Plot of Sodium Concentrations [Na^+]. The shown data refers to the sensors in Fig. 7.5 in a separate measurement with the PalmSens4 Potentiostat. The point A stands for $R_s + R_{ct}$, respectively. Point B labels $\omega + R_{ct} + C_{dl} = 1$. Modified from Bachelor Thesis [175], description in the text.

to define crucial design parameters and set rules on how to proceed. In turn, assumptions and approximations for material properties are made. The experimental results can be used to iterate some parts of the parameter space. One common approach in EIS is create an equivalent circuit model that provides circuit components for each material interface and its electrical properties. Figure 7.8 shows an equivalent circuit for the experimentally fabricated sensor system.
The electrolyte and the electrode, the membrane and their interface is modeled and the right values are stepwise iterated. Furthermore, Warburg impedances model diffusional limits that occur in electrochemical experiments due to a limited active electrode area and kinetic restraints. Parasitic capacities have been estimated to be in in pF- range. Interestingly, the ohmic resistance of the membrane itself was rather small (10^2 Ω).

7.4.6 Optimal Frequency and Amplitude of Excitation Signal

From figure 7.5 one can derive that the dynamic range of the output signal depends on the frequency of the excitation signal. In a series of experiments, the optimal frequency is derived to be around 80 to 100 Hz. Figure 7.9 shows the output impedance of the used membrane on solid state electrodes with exactly one frequency, 80 Hz. In fact, the amplitude of the excitation signal does not heavily change the sensor's output as can be seen in the bacteria sensor project as well (please compare figure 6.6a).

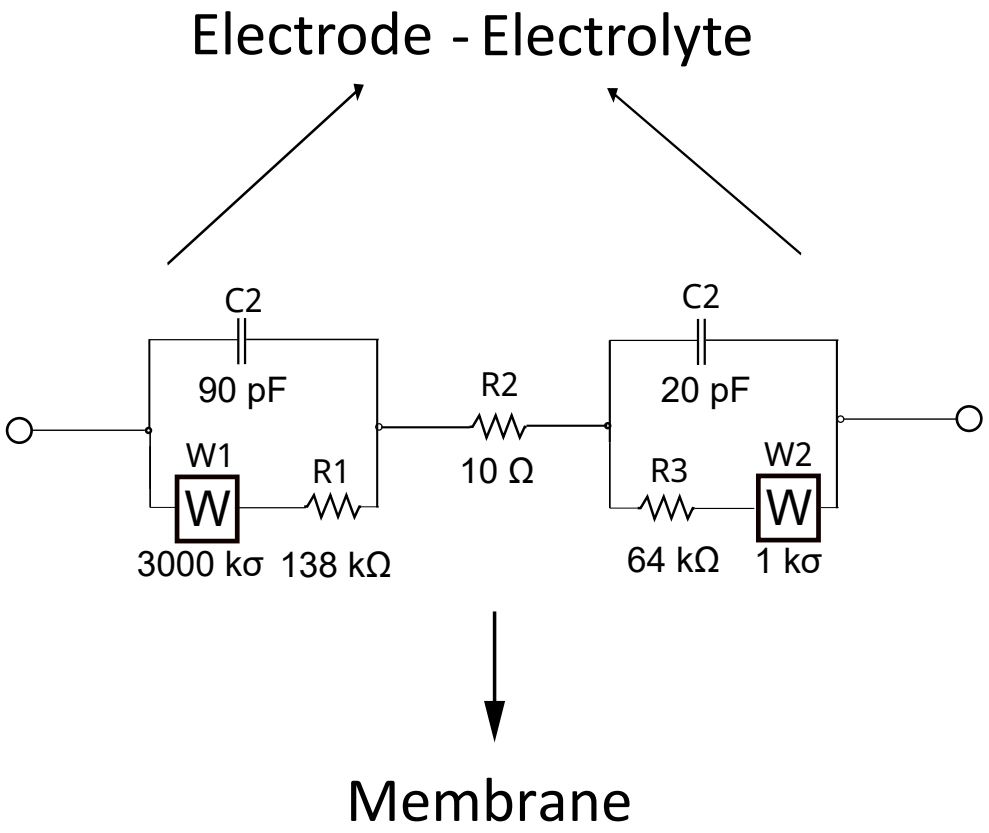

Figure 7.8: Equivalent Circuit Model obtained by fitting experimental EIS data.

Fig. 7.9 verifies a drift-like behaviour of the Sodium sensor. This means that when hitting the next cycle of measurement the original output signal does not fully recover. In order to learn more about this behaviour, more experiments about repeatability are provided in the next section.

7.4.7 Repeatability and Long-term Effects

The presented ink composition with the Sodium Ionophore in table 7.1 is now tested for its behaviour on solid-state electrodes. A step-like concentration change is given in figure 7.10. Three full-day measurements are performed and start from low Sodium concentrations to high ones. The x-axis reports the time. It is important to note here that a single frequency (80 Hz) is used instead of capturing a whole spectra. On the vertical axis the absolute value of the impedance output is shown.

The whole experimental procedure from Fig. 7.10 includes an eight minute cleaning cycle with Phosphate-Saline-Buffer (PBS) between the switch from higher to lower concentrations or vice versa. The cleaning also helped to minimize salt depositions on the active sensor area.

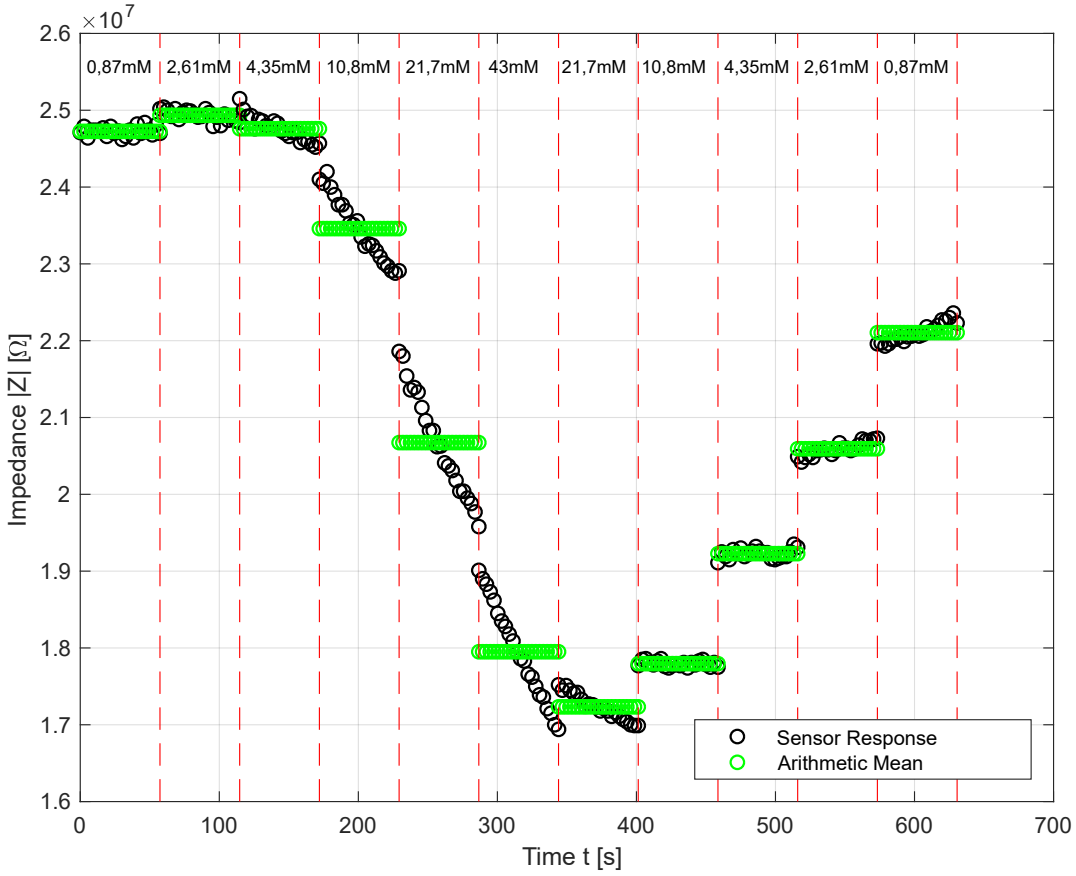

Figure 7.9: Behaviour of ion-selective-membrane on solid-state-electrodes when using a single, fixed excitation frequency of 80 Hz and a excitation amplitude of 50mV. The concentration values refer to Sodium. Data from [171] using the alternative approach for membrane characterization described in Fig. 4.3.

7.5 Discussion

Chapter 7.4.1 introduces the concept of a fully printable ionic sensor. FEM simulations pave the way for a better understanding of the electrical fields spanning between two micro-electrodes. The analyte changes the printable ion-selective-membrane (ISM) and its dielectric properties when getting in contact [77]. The performed AC-DC simulations show good penetration of the ISM by the electrical field, whereas the substrate as well as the aqueous testing solution are barely crossed [77]. This approach is beneficial for the signal-to-noise ratio. A full set of optimized design parameters are presented. An important observation is that the conducted FEM simulations suggest to keep the height of the ISM more or less equal to the distance of the electrodes. The deducted design parameters are then used for fabrication of the sensors.

The successful manufacturing of several prototypes validated the idea of ion-selective materials. EIS data showed distinguishable results for various Na^+ concentrations. The system provides a useable direct dynamic range of (71.3±0.7) MΩ for the relevant

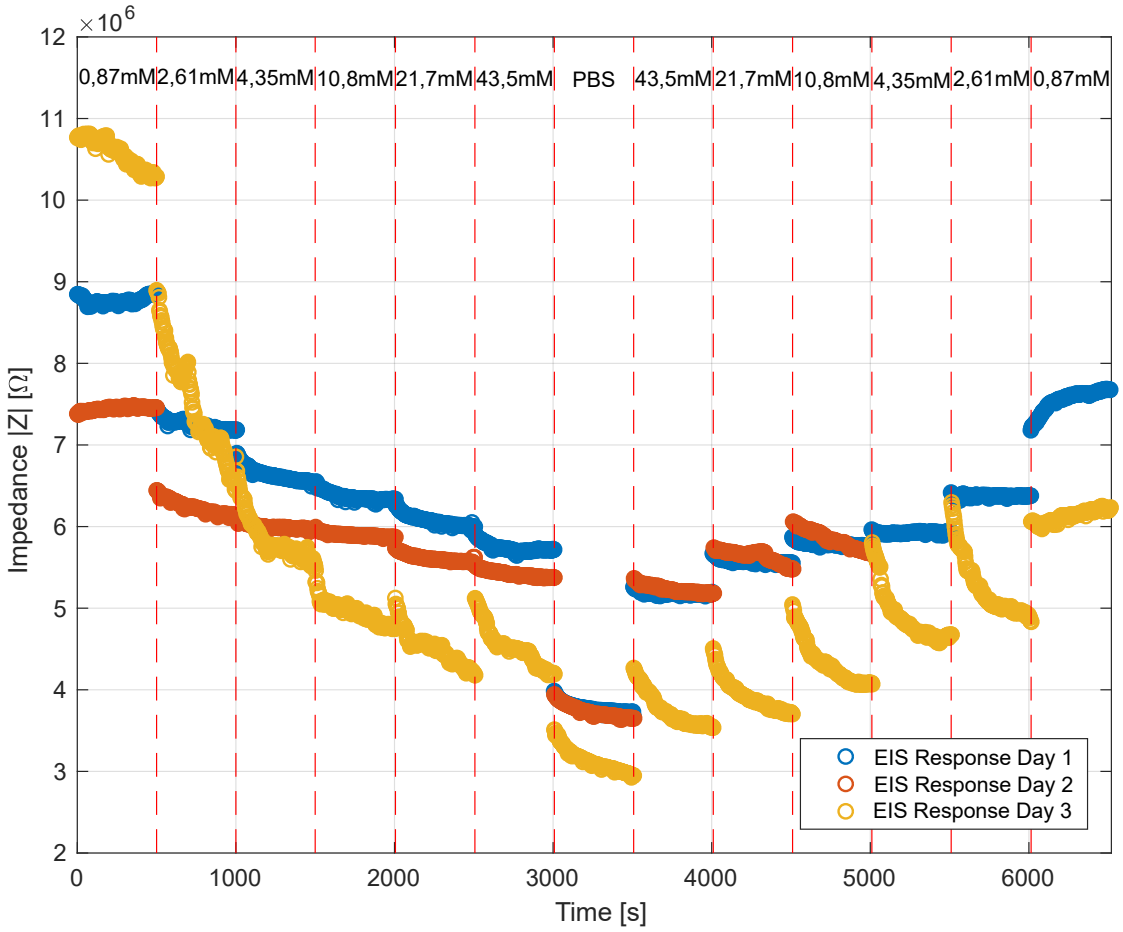

Figure 7.10: Repeatability Measurements and Long-term Effects on Ionic Sensor. Three all-day measurements are performed in PBS and Sodium Nitrate, respectively. The concentration values on top refer to Sodium ions. Data from [171] using the alternative approach for membrane characterization described in Fig. 4.3.

biological range of ion in fluids when using the magnitude of the impedance. In contrast, the corresponding phase data itself is challenging to interpret (can be seen in appendix A.2). Hence, the focus lays on the absolute value of the overall impedance $\|Z\|$. As described in chapter 5.2, the hypothesis that the polarization of the ionophores which are macromolecus compared to ionic radius of a single sodium ion, lead to a change of the applied displacement field.

Considering Fig. 7.6, lower frequencies like 100 Hz offer a better signal and a higher useable dynamic range. For frequencies below 1 kHz, a rather ohmic instead of capacitative behaviour is interpreted. For higher frequencies, this effect is reversed and capacitative components dominate the spectra. In electrochemistry, there are manifold effects that can take place when electrodes, fluids and dielectrics are involved: undefined potentials of the fluids over time, charge build-ups, incorperation of carbon monoxide into the fluid changing the pH - to name a few. Capacitative double

layer effects appear even in a perfectly equilibriated solution and a variety of reactions between electrode material and the involved chemicals lead to (nearly) unpredictable parasitic capacities and currents. To solve this issue, an additional reference membrane is introduced that experiences similar electrochemical effects. However, the reference membrane does not contain any ionophores and thus can be used as "baseline" in order to derive a "robust measurement scheme" [77].
Linear regression is then used to calibrate the sensor system. Cross sensitivity is researched when switching to K^+. Even though in the measurement solutions, the same counter-ion is used (Nitrate AAS-Standard, dilution series) Sodium and Potassium can be differentiated by one order of magnitude in the impedance signal |Z| and appears to be controllable. As mentioned, several non-linear effects appear in electrochemical experiments. By using a small, non-destructive excitation signal a small-signal model is applied. However, the response time seem to be limited to diffusional process. The wetting of the membrane does increase its size (by up to 30%) and also limits binding rates of the ionophore-analyte system.
Figure 7.9 and Figure 7.10 show the ion-selective membrane's properties when in contact with solid-state-electrode and fixed excitation signals. On the on hand side, a visible offset of the output impedance appears. As the offset is significant advanced data processing has to circumvent this issue. A clear repeatability of the measurement is shown in Figure 7.10 but the few percent offset have to managed by smart data processing techniques. The sensor responses appear to follow exponential functions (like diffusional processes) and this can be an aspect to be exploited for future work. Finally, the response times are in the range of seconds to single minutes which fit biotech applications.

Chapter 8

Summary and Discussion

The main achievements of this thesis and its corresponding publications are:

- Design, Modeling and Fabrication of fully functional ion sensor
- Proposing a theoretical background to the sensing scheme
- Proposing an enhanced equivalent circuit model based on experimental results
- Advanced characterization of sensor to pave the way for integrated read-out electronics
- Development of experimental setup for read-out
- Design, Modeling and characterization of EIS-based bacterial sensor
- Introducing a mathematical tool to evaluate arbitrary electrode designs in FEM simulations
- Inventing a new jet-able ink enabling additive manufacturing of previous bulky and expensive ion sensors
- Experimentally verifying the approach of EIS for sensor applications

A few topics of discussion arise from the experimental data.

8.1 Optimal Frequency of Operation

The EIS spectra in Fig. 7.5 show a clear distinction of Sodium ions in solution. The magnitude of the impedance unfolds in a well interpretable spectrum. In contrast, the obtained phase data is very hard to interpret and thus not used is the argumentation line of the sensor's mode of operation (see appendix for phase data). Also, the spectra show a dynamic range of impedance over the frequency. As a consequence, a single frequency with the highest range of measurable output impedances appears to

be supreme. Future data processing could be simplified by only operating the sensor system at a single, optimal frequency providing the best possible resolution. Figure 7.6 hints on this by choosing low frequencies below 1 kHz for calibration. In fact, an optimal operating frequency appeared to be 80 Hz. Circumventing possible noise of external sources in the range of 50 or 60 Hz, this low frequency of 80 Hz offers a high, useable dynamic range and measurement times that are not very fast but adequate for chemical measurements and their time scale of ms or even single seconds.

8.2 Sensor Behaviour Depending on Frequency Domain

The spectra in Figure 7.5 also show that the system's behaviour depends on the operated frequency domain. The equivalent circuit shown in fig. 7.8 hints on a more complex behaviour and signal contributions of a variety of influences like interfaces and their effects like capacitative Helmholtz layers. However, two trends emerge in the sensor response. In the lower frequencies, the purely ohmic part appears to dominate the response. Going into higher frequencies for the excitation signal leads to more dominant capacitative behaviour.

8.3 Interpretation of Real vs. Imaginary Part of EIS data

Electrochemical Impedance Spectroscopy provides not only the purely ohmic part but also the imaginary part as output variable. In the case of bacteria sensing both outputs are useable and the interpretation is straight forward when Nyquist plots are chosen as representation (compare figure 6.8. However, in the case of ionic sensing the imaginary part appears to be very challenging to interpret. An example is given in the appendix A.2 showing the non-linear change of the phase throughout the frequency range of 10 Hz to 100 kHz. It appears that the phase of the ionic EIS sensor reflects multiple effects that are presented in the theory chapter 5. Hence, the argumentation how to realize a measurement scheme for an ionic sensor does not rely on the phase data.

8.4 Drift

A common issue with electrochemical sensors is the degradation of the sensor signal over time. The experiments show a lifetime of the printed ionic sensors of more than six months. Drift effects occur due to the highly non-linear electrochemical environment.

For instance, the potential of the fluid itself changes over time as gases like carbon dioxid are absorbed. This leads to change of the pH in the fluid affecting a majority of the involved reactions at room temperature. The sensor system comprises a phase boundary of the liquid state to the solid state of the functional membrane. The latter is regarded as not perfectly defined. The polymer membrane is permeable and swells when in contact with the liquid of interest. The system operates rarely in a perfect equilibrium. This can be circumvented by using a small-signal model. However, this approach is only an approximation. It can be improved by taking kinetics of higher order into account. The environment itself is defined by the application. In the case of sweat sensing many constituents (like a variety of ions) are present in the fluid-of-interest. A temperature decrease of the sample could be beneficial for the measurement but cooling seems to be impractical and cost intensive. More research needs to include long-time studies of the developed sensor systems to verify the longevity, especially the functionalized parts like the membrane. Based on this the application space can be adjusted accordingly.

8.5 Cross-Sensitivity

The applications are also defined by the cross-sensitivities of the sensor. Rather niche applications like a Sodium sensor for semiconductor processes can be realized with low sensitivities towards other ions. Nevertheless, biotech applications are more challenging in the sensor setup. Sodium and other ionic species are important biomarkers but the environment of measurement is intrinsicaly more difficult for electrochemical measurements. The richness of proteins, molecules, single ions, acids that nature provides in biological substances lead to a very complex environment for direct measurements. Many unwanted "reaction partners" can interfere with the desired output.
Potassium is chemically extraordinary similar to Sodium in its ionic radii, hydration sphere and chemical properties. In Figure 7.6B), the sensor response to the two nearly perfectly dissociated ions is presented while providing the same counterion, nitrate. A clear distinction is visible, however, more research on selectivity coefficients towards other ionic species and interferences needs to be done before moving to biological fluids like sweat or urine.

8.6 Detection Limit

Crucial for the sensor performance are not only the sensitivities towards undesired substances but also the detection limits of the developed sensor systems. 10 nM of Na^+ are experimentally verified to be the lowest concentration to be distinguished. Signal processing techniques have not been applied in the scope of this work but can potentially push this limit even further. Especially Principal-Component-Analysis

(PCA) is regarded as a powerful tool in this context. In spite of that it can be stated that the biological relevant concentration range is fully covered with this detection limit. Human cells operate with concentrations of Sodium and Potassium in the range of 1 to 150 mM which lays several orders of magnitude higher.

8.7 Challenges in Fabrication

The manufactured sensors can be seen in Fig. 7.4. FEM simulations (compare fig. 7.3) have led to optimized design parameters. The set of parameter in table 7.1 does not perfectly match the dimensions that can be easily ink-jet printed. In concrete terms, this refers to the height of the functional membrane. While the FEM simulations predict a optimum of 100 µm, it is non-trivial to achieve this physical dimension. Inkjet printing allows easily to create $1-10$ µm with developed inks with the necessary viscosity to be printable in the first place. The stacking of layers cannot be done endlessly but suffers from layer mismatch and the need of UV curing to harden the layer below. Day et. al used drop-casting on impediometric Potassium sensors and dealt with thin membrane heights of 1 µm [30] which is common. An important conclusion can be drawn here. First, the used FEM model is not perfect. Second, the exact relationship between the membrane height, electrode distance, the involved dielectric constants of functional and non-functional parts of the system remains not fully understood but can rather be seen as an approximation. The highly non-linear system is approximated by the small-signal model. The role of higher harmonics appear to play a role and can be considered in future approaches. This idea is elaborated in section 9 even further.

8.8 Challenges in Data Acquisition

Low available sample volumes (e.g. in sweat analysis) can pose serious issues for the data acquisitions. The measurement conditions outside the lab entail evaporation of the liquids being able to change ionic contents quickly. Evaporation the of the sample is non-trivial to solve and is enhanced when dealing with low volumes below 500 µL. Salt depositions can appear on the active sensor area and falsify measurements. The use of microfluidics can minimize evaporation effects and create a more controllable measurement environment but also adds to the complexity of the system as well as to the costs of fabrication. The packaging method that is shown in figure 7.4 can be improved and the concept of additive manufacturing (see Fig. 7.1) suits well the integration of microfluidics as defined reaction chambers can significantly enhance the stability of environmental parameters. Also, the data interpretation is more challenging compared to the simple output voltage of an potentiometric sensor. For instance, the phase data of ionic sensors is challenging to understand. In appendix A.2, the

phase data for the Sodium sensor shows non-linear behaviour throughout the whole excitation frequency range from 100 Hz to 100 kHz (please compare Fig. A.1). Consequently, the argumentation relies fully on the the magnitude of the impedance sensor neglecting the additional information of the phase.
Future research should focus on a few topics to develop the sensor systems even further. The printability of the developed inks is fine and under control. Recent progress has shown that the acrylate approach works also on another deposition platform and with other cartridges. An aspect where future research has to improve is the homogeneity of the dielectric functional membranes.

A central point is to test other ionophores that have been presented in A.1. Especially heavy metal ionophores are of interest due to their toxicity and occurance in e.g. drinking water. Also, the alkali metals are of significant importance for our biological systems and offer manifold application the biotech realm.

Chapter 9

Conclusion and Outlook

9.1 Future Improvements and Research Opportunities

In the following chapter, some conclusions are drawn from the findings. First of all, the range of additional ionophores is emphasized (please see table A.1). The sensor system can be extended to this great variety of selective molecules. Especially heavy metals are of great interest. They show toxicity for humans and animals and can be prevented by a wide use of biosensors in drinking water applications.

Next, the system can be developed further in terms of data processing. A key feature for future work can be the analysis of data in the Laplace plane [208]. The idea evolves around higher harmonics that arise when measureing the device. The current response is like the excitation signal sinusoidal at a chosen frequency. In this work, the current-potential relation has been linearized. The used Taylor-expansion also gives terms of higher harmonics. To experimentally measure them, a circuit with tuned amplifiers or lock-in amplifiers is needed but can extend the available information significantly [208].

9.2 Electrical Tongue Concept

Possible applications are given in chapter 1.2 but one concept should be highlighted: Combining several ionic sensors with different target ions into a sensor array presents a "electrical nose" or "electrical tongue" approach (the reader is kindly refered to [209] for an historic background behind this idea). As electrochemical sensors tend to have cross-sensitivities this approach succeeds in overcoming these drawbacks. The presented work allows for tiny scales of fabrication (down to 20 µm feature size) and an optimized ink is likely to push this barrier even further with ink-jet techniques. The possibility to integrate the read-out electronics can significantly reduce production

costs of chemical sensors. Their use in everyday objects like drinking water taps could be realized, and contribute to a sustainable world.

9.3 Impact on Environment

Recycling and waste management begins in the concept phase of production. The work aims to minimize material usage by using a high-resolution inkjet printing method. PVC membranes can leach and especially solvent residues can be problematic when contaminating the fluid of interest [210]. Compared to common PVC membranes, less constituents are used and the fabrication process allows for precise deposition of energy in form of UV pulse. This benefits a precise curing process and minizes leaching effects. In addition, the used materials are chosen to as bio-compatible as possible and degradable after their life cycle. Recent reports evaluate the leaching of PVC membranes, show significant leaching and recommend cyto-toxicity assays in an early stage of sensor development [211].

Chapter 10

List of publications, patents and supervised theses

- Pfeffer, Christian; Zips, Sabine; Müllner, Ernst; Hefele, Markus; Kreupl, Franz; Wolf, Bernhard; Wolfrum, Bernhard; Brederlow, Ralf: A Cost-Effective, Impediometric Na_+-Sensor in Fluids. IEEE Sensors, Volume: 5, Issue: 6, June 2021, 2021
URL: https://ieeexplore.ieee.org/document/9387556

- Pfeffer, Christian; Liang, Yue; Grothe, Helmut; Wolf, Bernhard; Brederlow, Ralf: Towards Easy-to-Use Bacteria Sensing: Modeling and Simulation of a New Environmental Impedimetric Biosensor in Fluids. Sensors 2021, 21, 1487. https://doi.org/10.3390/s21041487
URL: https://www.mdpi.com/1424-8220/21/4/1487

- Pfeffer, Christian and Zips, Sabine; Method of Forming an acrylate-based ionic sensor and corresponding apparatus
EPO Patent Application 20182319.2, 2020,
URL: https://worldwide.espacenet.com/patent/search?q=pn%3DEP3929576A1

- Hefele, Markus; Müllner, Ernst; Brederlow, Ralf; Lösel, Andreas; Meier, Sebastian; Pfeffer, Christian; Kreupl, Franz; Wolf, Bernhard: Integrated multipurpose analog front-end for electrochemical ISFET sensors In: 2019 17th IEEE International New Circuits and Systems Conference (NEWCAS) (2019). pp. 1-4.
DOI: 10.1109/NEWCAS44328.2019.8961291
URL: https://ieeexplore.ieee.org/document/8961291

Unpublished/ in Preparation:
- Pfeffer, Christian; Ochs, Matthias, Zhang, Lei and Brederlow, Ralf: Tackling Drawbacks of Electrochemical Sensors based on EIS using Neural Network Techniques
- Pfeffer, Christian; Zhang, Lei; Oefelein, Raphael; Brederlow, Ralf: A Theoretical Backbone for Impedance Spectroscopy Based Sensing for Bacteria in Fluids

Conferences and Summer Schools

- Guimera, Carmen Milian; Narag, Jadze Princeton Casilana; Monastyreckis, Gediminas; Pfeffer, Christian: Oral Drug Delivery
Flexible Coatings on Flexible Foils
Poster Presentation DTU Copenhagen, PhD Summer School: Micro and Nano Sensors (2021)

- EuroSensors 2020, Lecce, Italy: Submitted contribution but cancelled due to Corona Pandemic

- Markus Hefele, Christian Pfeffer, Sebastian Meier, Ernst Müllner, Helmut Rink, Franz Kreupl, Ralf Brederlow
MCU-Supported Electrochemical Sensors for pH and pX
CoC Industry Day 2019

Supervised Theses

Jakob Frey, Advanced Impedance Spectroscopy in FEM simulations for Sensory Purposes, Master Thesis (Title may differ), 2022

Aymen Nasri, Preventing Bacterial Infections: Simulation and Design of a New Sensor System, Bachelor Thesis, 2021

Yue Liang, Simulation and Development of a New Environmental Impediometric Biosensor, Master Thesis, 2020

Emna Azek, (Fully Printed) Ion Selective Sensors for Biotech and Life Science, Bachelor Thesis, 2020

Felix Naunheimer, Ion Selective Sensors for Biotech and Life Science (Wafer-Level), Bachelor Thesis, 2020

Eva-Maria Korek, Development of an Electrochemical Microsensor for Monitoring Biomarkers in Sweat for Healthcare Applications, Master Thesis, 2020

Elisabetta Mahmutovic, Characterization of all CMOS Integrated 3D-Extended Metal Gate ISFETs, Bachelor Thesis, 2019

Niklas Fauth, Demo and Read-out Circuit for Electrochemical Sensor (Internship), 2018

Appendix A

Appendix

A.1 List of Developed and Commercialized Ionophores

The following list is the extensive study on developed and commercially availabe Ionophores. Table A.1 is discussed in chapter 2.6.

Table A.1: List of Developed and Commercialized Ionophores

Target Ion	Chemical Structure and Trade Name
Cadmium	
Cadmium ionophore I	N,N,N',N'-Tetrabutyl-3,6-dioxaoctanedi(thioamide), ETH 1062
Calcium	
Calcium Ionophore	A23187 - Antibiotic A 23187, Calimycin
Calcium Ionophore I	(-)-(R,R)-N,N'-Bis-[11-(ethoxycarbonyl)undecyl]-N,N',4,5-tetramethyl-3,6-dioxaoctane-diamide, Diethyl N,N'-[(4R,5R)-4,5-dimethyl-1,8-dioxo-3,6-dioxaoctamethylene]bis(12-methylaminododecanoate), ETH 1001
Calcium Ionophore	A23187 hemimagnesium salt - A23187 hemimagnesium salt, Antibiotic A 23187 hemimagnesium salt, Calcimycin hemimagnesium salt, Calimycin hemimagnesium salt

Table A.1 continued from previous page

Target Ion	Description
Calcium ionophore II	N,N,N',N'-Tetra[cyclohexyl]diglycolic acid diamide, N,N,N',N'-Tetracyclohexyl-3-oxapentanediamide, ETH 129
Calcium ionophore III	Antibiotic A 23187, Calcium Ionophore A23187, Calimycin
Calcium ionophore IV	N,N-Dicyclohexyl-N',N'-dioctadecyl-3-oxapentanediamide, N,N-Dicyclohexyl-N',N'-dioctadecyl-diglycolic diamide, ETH 5234
Calcium ionophore V	10,19-Bis[(octadecylcarbamoyl)methoxyacetyl]-1,4,7,13,16-pentaoxa-10,19- diazacycloheneicosane, K23E1
Ionophore A23187	4-Bromo-A23187, 4-Bromo-calcimycin
Carbonate	
Carbonate ionophore II	1-(Dodecylsulfonyl)-4-trifluoroacetylbenzene, ETH 6019
Carbonate ionophore IV	4-Butyl-α,α,α-trifluoroacetophenone
Carbonate ionophore VII	N,N-Dioctyl-3α,12α-bis(4-trifluoroacetylbenzoyloxy)-5β-cholan-24-amide
Cesium	
Cesium ionophore II	4-tert-Butylcalix[6]arene-hexaacetic acid hexaethyl este
Cerium(III) Ionophore	2-Aminobenzothiazole, 2-Benzothiazolamine
Chloride	
Chloride ionophore I	meso-Tetraphenylporphyrin manganese(III)-chloride complex
Chloride ionophore II	4,5-Dimethyl-3,6-dioctyloxy-o-phenylene-bis(mercurytrifluoroacetate), ETH 9009

Table A.1 continued from previous page

Target Ion	Description
Chloride ionophore III	3,6-Didodecyloxy-4,5-dimethyl-o-phenylene-bis(mercury chloride), ETH 9033
Chloride ionophore IV	4,5-Bis-[N'-(butyl)thioureido]-2,7-di-tert-butyl-9,9-dimethylxanthene
Copper	
Copper(II) ionophore I	o-XBDiBDTC, o-Xylylenebis(N,N-diisobutyldithiocarbamate)
Copper(II) Ionophore IV	N,N,N',N'-Tetracyclohexyl-2,2'-thiodiacetamide
Cyanide	
Cyanide Ionophore II	Magnesium phthalocyanine, Phthalocyanine magnesium salt
Lead ionophore II	MBDiBDTC, S,S'-Methylenebis(N,N-diisobutyldithiocarbamate)
Lead ionophore IV	tert-Butylcalix[4]arene-tetrakis(N,N-dimethylthioacetamide)
Hydrogen	
Hydrogen ionophore V	Calix[4]-aza-crown
Hydrogen ionophore I	Hydrogen ionophore I, Tridodecylamine
Hydrogen ionophore II	4-Nonadecylpyridine, ETH 1907, Proton ionophore II
Hydrogen sulfite ionophore I	ETH 5444, Octadecyl 4-formylbenzoate
Hydrogen ionophore I	Tridodecylamine
Iron(III) ionophore VI	1-(4-Dimethylaminophenyl)-2-(6-phenanthridinyl)ethanone

Table A.1 continued from previous page

Target Ion	Description
Lithium	
Lithium ionophore I	N,N'-Diheptyl-N,N',5,5-tetramethyl-3,7-dioxanonanediamide, ETH 149
Lithium ionophore IV	5-Butyl-5-ethyl-N,N,N',N'-tetracyclohexyl-3,7-dioxaazelaic diamide, ETH 2137, N,N,N',N'-Tetracyclohexyl(2-butyl-2-ethyltrimethylenedioxy)diacetamide
Lithium ionophore VI	6,6-Dibenzyl-1,4,8-11-tetraoxacyclotetradecane, 6,6-Dibenzyl-14-crown-4
Lithium ionophore VIII	N,N,N',N',N",N"-Hexacyclohexyl-4,4',4"-propylidynetris(3-oxabutyramide)
Magnesium	
Magnesium ionophore I	ETH 1117, Magnesium-ligand, N,N'-Diheptyl-N,N'-dimethyl-1,4-butanediamide
Magnesium ionophore II	ETH 5214, N,N"-Octamethylene-bis(N'-heptyl-N'-methyl-methylmalonamide
Magnesium ionophore III	ETH 4030, N,N"-Octamethylene-bis(N'-heptyl-N'-methylmalonamide)
Magnesium ionophore IV	ETH 7025, N,N',N"-Tris[3-(heptylmethylamino)-3-oxopropionyl]-8,8'-iminodioctylamine
Magnesium ionophore VI	1,3,5-Tris[10-(1-adamantyl)-7,9-dioxo-6,10-diazaundecyl]benzene, ETH 5506
Magnesium ionophore VII	4,13-[Bis(N-adamantylcarbamoyl)acetyl]-1,7,10,16,tetraoxa-4,13-diazacyclooctadecane, K22B5
Mercury	

Table A.1 continued from previous page

Target Ion	Description
Mercury ionophore I	1,10-Dibenzyl-1,10-diaza-18-crown-6, 7,16-Dibenzyl-1,4,10,13-tetraoxa-7,16-diazacyclooctadecane, N,N'-Dibenzyl-4,13-diaza-18-crown-6
Nitrate (NO_3)	
Nitrate Ionophore VI	9-Hexadecyl-1,7,11,17-tetraoxa-2,6,12,16-tetraazacycloeicosane
	Tridodecylmethylammonium nitrate, Methyltridodecylammonium nitrate
	Tetraoctylammonium nitrate
Nitrite(NO_2)	
Nitrite ionophore I	Cyanoaqua-cobyrinic acid heptakis(2-phenylethyl ester)
Nitrite ionophore VI	(SP-4-2)-[[2,2'-[1,2-Phenylenebis[(nitrilo-κN)methylidyne]]bis[4,6-bis(1,1-dimethylethyl)phenolato-κO]](2-)]cobalt, N,N'-Bis(3,5-di-tert-butylsalicylidene)-1,2-benzenediaminocobalt(II), N,N'-Bis-(3,5-di-tert-butylsalicylidene)-o-phenylenediamine cobalt(II), Cobalt(II) tert-butyl-salophen
Perchlorate	
Perchlorate ionophore I	Dichloro-tetraphenylporphyrinato-phosphorus(V)-chloride
Potassium	
Potassium ionophore I	Valinomycin, Cyclo(L-Val-D-HyIva-D-Val-L-Lac-)3: HyIva = α-Hydroxyisovaleric acid, Lac = Lactic acid
Potassium ionophore II	BB15C5, Bis[(benzo-15-crown-5)-4'-ylmethyl] pimelate

Table A.1 continued from previous page

Target Ion	Description
Potassium ionophore III	2-Dodecyl-2-methyl-1,3-propanediyl bis[N-[5'-nitro(benzo-15-crown-5)-4'-yl]carbamate], BME 44
Silver	
Silver ionophore IV	O,O"-Bis[2-(methylthio)ethyl]-tert-butylcalix[4]arene
Silver ionophore VII	(3α,5β,12α)-3-{[(2,2'-Bithiophen)-5-ylcarbonyl]oxy}-12-{{2-{[(diphenylamino)thioxomethyl]thio}acetyl}oxy}-N,N-dioctyl-cholan-24-amide
Sodium	
Sodium ionophore I	ETH 227, N,N',N"-Triheptyl-N,N',N"-trimethyl-4,4',4"-propylidynetris(3-oxabutyramide)
Sodium ionophore II	ETH 157, N,N'-Dibenzyl-N,N'-diphenyl-1,2-phenylenedioxydiacetamide
Sodium ionophore III	ETH 2120, N,N,N',N'-Tetracyclohexyl-1,2-phenylenedioxydiacetamide
Sodium ionophore IV	2,3:11,12-Didecalino-16-crown-5, 2,6,13,16,19-Pentaoxapentacyclo[18.4.4.47,12.01,20.07,12]dotriacontane, DD-16-C-5
Sodium ionophore VI	Bis[(12-crown-4)methyl] dodecylmethylmalonate, Dodecylmethylmalonic acid bis[(12-crown-4)methyl ester]
Sodium ionophore VIII	Bis[(12-crown-4)methyl] 2,2-didodecylmalonate
Sodium ionophore V	4-Octadecanoyloxymethyl-N,N,N',N'-tetracyclohexyl-1,2-phenylenedioxydiacetamide, ETH 4120
Sodium ionophore X	4-tert-Butylcalix[4]arene-tetraacetic acid tetraethyl ester

Table A.1 continued from previous page

Target Ion	Description
Tin	
Tin(II) ionophore I	2,3,11,12-Dibenzo-1,4,7,10,13,16-hexaoxacyclooctadeca-2,11-diene, 6,7,9,10,17,18,20,21-Octahydrodibenzo[b,k][1,4,7,10,13,16]hexaoxacyclooctadecene, DB18C6, Dibenzo-18-crown-6
Zinc	
Zinc ionophore I	Tetrabutylthiuram disulfide
Zinc ionophore IV	Potassium hydrotris(N-tert-butyl-2-thioimidazolyl)borate, [TmBut]K
Zinc ionophore I	Tetrabutylthiuram disulfide
Zinc ionophore IV	Potassium hydrotris(N-tert-butyl-2-thioimidazolyl)borate, [TmBut]K
Further Ionophores	
Nickel ionophore II	4,4',4",4"'-(Porphine-5,10,15,20-tetrayl)tetrakis(benzoic acid), meso-Tetraphenylporphine-4,4',4",4"'-tetracarboxylic acid
Phthalate Ionophore I	(Sn(IV)[OEP]Cl2), 2,3,7,8,12,13,17,18-Octaethyl-21H,23H-porphine tin(IV) dichloride, Sn(IV)-octaethylporphyrine dichloride
Thulium Ionophore I	2,2'-Diaminodiphenyl disulfide, 2,2'-Dithiodianiline, Bis(2-aminophenyl) disulfide
Fluoride ionophore I	Bis(fluorodioctylstannyl)methane
Erbium(III) Ionophore I	N'-(2-Hydroxy-1,2-diphenylethylidene)benzohydrazide
Manganese(II) ionophore II	2,2'-Bis(salicylideneamino)azobenzene
Ammonium ionophore	Nonactin

Table A.1 continued from previous page

Target Ion	Description
Ammonium ionophore I	Ammonium ionophore, Nonactin
Bisulfite ionophore	4-[4-(Dioctylamino)-phenylazo]-3-nitro-benzaldehyde, Chromoionophore CR-514

Table A.1: Developed and Commercialized Ionophores. Based on [212].

A.2 Phase Data of Ion Sensor

EIS measurements can be displayed in different types of plots. Fig. A.1 displays the phase of an ionic sensor when wetted in 20 minutes of Sodium Nitrate Standard Solution (21 mM). As the phase data does not show a linear behaviour, it is neglected for the purpose of ion sensing.

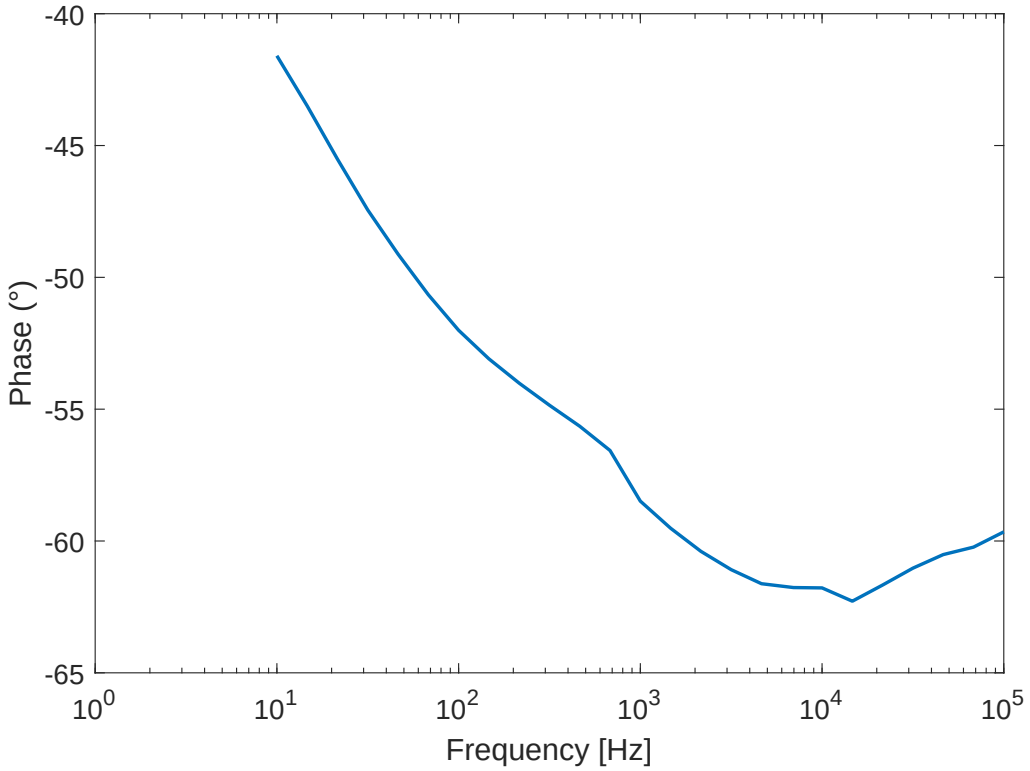

Figure A.1: Phase Data of EIS- Measurements on Ionic Sensor. The phase data shows non-linear behaviour across the whole excitation frequency range. The data is challenging to interpret and hence the argumentation of the ionic sensor does not rely on it.

A.3 Error Analysis

The calculated errors in EIS data consist out of systematical and statistical errors. The used potentiostat Biologic VSP-300 is generously estimated to have 1% of systematic error in the relevant range of 10 Hz to 100 kHz. Also, the performed dilution series is assumed to have an error of 2%. Statistical errors are considered by assuming normal distribution and calculating the standard deviations around the mean μ in eq. A.3.1

$$SD(X) = \sqrt{Var(X)} = \sqrt{E(X-\mu)^2} \tag{A.3.1}$$

For calculated parameters, like sensitivity, Gaussian error propagation is used to derive the standard error as can be seen in eq.A.3.2. Δ_Z corresponds to the ohmic measurement range, and Δ_D corresponds to the available concentration range, respectively.

$$SE(X) = \frac{\epsilon_{sys}}{\Delta_Z\,[\Omega]} + \frac{\epsilon_{sys}}{\Delta_D\,[mM]} \tag{A.3.2}$$

Calibration curve

A.4 Quality Factor Code in Matlab

The code for the quality factor is also published on Github. It has been developed with Yue Liang in the framework of a joint publication [131].

```
function GradientHist
    h=figure('Position',[50,200,1800,800]);

    button1 = uicontrol('Style', 'pushbutton', ...
        'String', 'select Gradient Data 1',...
        'Position', [120 60 150 40],...
        'Callback', @GetfileA);

    button2 = uicontrol('Style', 'pushbutton', ...
        'String', 'Start',...
        'Position', [1300 20 180 60],...
        'Callback', @Analyse);
    button3= uicontrol('Style', 'pushbutton', 'String', 'Clear',...
        'Position', [1500 20 180 60],...
        'Callback', 'cla');

    button4 = uicontrol('Style', 'pushbutton', ...
        'String', 'select Gradient Data 2',...
        'Position', [350 60 150 40],...
        'Callback', @GetfileB);



    textUpper=uicontrol('Style','text',...
        'Position',[850 40 160 40],...
        'String','Upper Input');

    Upper = uicontrol('Style', 'edit', ...
        'String', '1e-6',...
```

```
    'Position', [850 20 160 40]);

textLower=uicontrol('Style','text',...
    'Position',[650 40 160 40],...
    'String','Lower Input');

Lower = uicontrol('Style', 'edit', ...
    'String', '0',...
    'Position', [650 20 160 40]);

textBin=uicontrol('Style','text',...
    'Position',[1050 40 160 40],...
    'String','Bin Number');

BinNum = uicontrol('Style', 'edit', ...
    'String', '100',...
    'Position', [1050 20 160 40]);




axis1 = axes('Units' , 'pixels' , 'Position',[70 150 800 600]);
axis2 = axes('Units' , 'pixels' , 'Position',[950 150 800 600]);



function GetfileA(~ ,~)
    %choose the file that you would analyse
    [name,path]=uigetfile('~.mat');
    filename = [path,name];
    setappdata(h,'filename1',filename)

    textData1=uicontrol('Style','text',...
        'Position',[120 20 150 40],...
        'String',name);


end

function GetfileB(~ ,~)
```

```
    %choose the file that you would analyse
    [name,path]=uigetfile('~.mat');
    filename = [path,name];
    setappdata(h,'filename2',filename)

    textData2=uicontrol('Style','text',...
        'Position',[350 20 150 40],...
        'String',name);


end

function Analyse(~,~)

    currentUpper=str2double(get(Upper,'String'));
    currentLower=str2double(get(Lower,'String'));
    currentBin=str2double(get(BinNum,'String'));

    %%
    filename1= getappdata(h,'filename1')
    Data_1=importdata(filename1);

    Data_1_x = Data_1(:,1);
    Data_1_y = Data_1(:,2);
    Data_1_z = Data_1(:,3);
    Data_1_value = Data_1(:,4);

    [m,n]=find(isnan(Data_1));

    Invalid_data_1=Data_1(m,:);
    Data_1(m,:)=[];

    k=find(Data_1(:,4)<=0 | Data_1(:,4)>=5e-6 );
    Overrange_Data_1=Data_1(k,:);

    Data_1(k,:)=[];
    Data_1_opt=Data_1;


    x1 = Data_1_opt(:,1);
```

```
y1= Data_1_opt(:,2);
z1= Data_1_opt(:,3);
v1= Data_1_opt(:,4);

%%
filename2= getappdata(h,'filename2')
Data_2=importdata(filename2);

[m,n]=find(isnan(Data_2));

Invalid_data_2=Data_2(m,:);
Data_2(m,:)=[];

k=find(Data_2(:,4)<=0 | Data_2(:,4)>=5e-6 );
Overrange_Data_2=Data_2(k,:);

Data_2(k,:)=[];
Data_2_opt=Data_2;


x2 = Data_2_opt(:,1);
y2 = Data_2_opt(:,2);
z2= Data_2_opt(:,3);
v2= Data_2_opt(:,4);
%%
set (h,'CurrentAxes',axis1);
edges = linspace(currentLower,currentUpper,currentBin);
hist = histogram(v1);
hist.NumBins=currentBin;
hist.BinEdges = [edges (currentUpper+1e-6)];
hist.Normalization = 'countdensity';


title('Gradient1')
ylabel('Count');
xlabel('Value');
hold on

set (h,'CurrentAxes',axis2);
```

```
        edges = linspace(currentLower,currentUpper,currentBin);
        hist = histogram(v2);
        hist.NumBins=currentBin;
        hist.BinEdges = [edges (currentUpper+1e-6)];
        hist.Normalization = 'countdensity';

        title('Gradient2')
        ylabel('Count');
        xlabel('Value');
        hold on


       hold on

      end


end
```

Appendix B

Acknowledgements

This PhD thesis is the summary of four years of academic work. Without a doubt, this was only made possible by a range of great people that I would like to thank in this occasion.
Prof. Ralf Brederlow, I would like to thank you for being an excellent advisor, mentor and Doktorvater. After four years I still had the impression that I can learn professional as well as personal skills. Thank you for your patience in the beginning, keeping your faith in me, hikes in the alps and all discussions about technology, politics, and life.
I would to thank Prof. Franz Kreupl for your mentorship and life lessons, Prof. Bernhard Wolf for great advice, for the passion about being a real interdisciplinary scientist and for teaching me the human approach about being a supervisor. I thank Bernhard Wolfrum for excellent scientific help and career advice.
I would like to thank my HES colleagues, Max, Markus and Moritz, and my industry mentor Ernst Müllner. Max, thank you for being a great collegue and friend, and for the joint bouldering. Markus, thank you for bringing me to CCC.
I thank Sabine Zips for your being a friend and for professional help when I needed it the most. Your group with Leroy and Lennart was great!
I thank Matthias Ochs, Markus Dietl, Eva Korek, Vartika Verma, Carl Riehm, Helmut Grothe, Tauseef Siddiqui, Iris Artinger and Carola Kabdebo and Marco Schewa for being great collegues.
I would like to thank Domatec GmbH, especially Raphael, Andreas, and Robert Priller for a great collaboration concerning the bacterial sensor project. I thank Anika, Rainer, and Szabolcs for technical assistance and IT support!
I thank my Bachelor and Master students, and interns: Niklas, Elisabetta, Yue, Felix, Emna, Nabila, Aymen, Ömer, Lei and Jakob! Thank you for everything!
I thank my friends Theresa and Robert for kind, motivational words and help with Latex! Robert, I can't thank you enough for your help in Matlab, Python and Latex! Philip, thank you for showing empathy when I needed it the most! Thank you -Theresa Wessendorf for being a great room mate and keeping the good mood up!
I would like to thank Verena for showing me the benefits of studying!

I would like to thank Amelie for showing me that perspective matters. I thank Jonas for being a friend when in need! Kili, thank you for great times together during my PhD. Thank you, Hannah.
Furthermore I would like to thank Ludwig, Felix and Steffi for shared working times, an additional desk and kind words. Thank you Nils for help with vectorgraphics!
Great thanks goes to my parents Christine and Josef for their support and believe in me!

Bibliography

[1] United Nations. *United Nations Sustainable Development Summit 2015*. https://sustainabledevelopment.un.org/post2015/summit. [Online; accessed 14-Jan-2022]. 2015.

[2] United Nations. *Transforming our world: the 2030 Agenda for Sustainable Development*. https://sdgs.un.org/2030agenda. [Online; accessed 14-Jan-2022]. 2022.

[3] Wei Gao et al. "Fully integrated wearable sensor arrays for multiplexed in situ perspiration analysis". In: *Nature* 529.7587 (2016), pp. 509–514.

[4] Adam Hulanicki, Stanislav Glab, and FOLKE Ingman. "Chemical sensors: definitions and classification". In: *Pure and applied chemistry* 63.9 (1991), pp. 1247–1250.

[5] Alan D McNaught, Andrew Wilkinson, et al. *Compendium of chemical terminology*. Vol. 1669. Blackwell Science Oxford, 1997.

[6] IJ Higgins and CR Lowe. "Introduction to the principles and applications of biosensors". In: *Philosophical Transactions of the Royal Society of London. B, Biological Sciences* 316.1176 (1987), pp. 3–11.

[7] Saumya Joshi. "Flexible biosensors using solution processable devices". Dissertation. München: Technische Universität München, 2019.

[8] KN Mikhel'son and MA Peshkova. "Ionophore-based chemical sensors: developments and prospects". In: *Usp. Khim.* 84 (2015), pp. 555–578.

[9] Anant Agarwal and Jeffrey Lang. *Foundations of analog and digital electronic circuits*. Elsevier, 2005.

[10] Vijay Deep Bhatt. "Solution-Processable Carbon Nanotube Devices for Biosensing Applications". Dissertation. München: Technische Universität München, 2018.

[11] G. G. Guilbault. "Recommendations for publishing manuscripts on ion-selective electrodes". In: *Pure and Applied Chemistry* 53.10 (1981), pp. 1907–1912.

[12] Rui You et al. “Ultrasensitive micro ion selective sensor arrays for multiplex heavy metal ions detection”. In: *Microsystem Technologies* 25.3 (2019), pp. 845–849.

[13] Yuzhou Shao, Yibin Ying, and Jianfeng Ping. “Recent advances in solid-contact ion-selective electrodes: functional materials, transduction mechanisms, and development trends”. In: *Chem. Soc. Rev.* 49 (13 2020), pp. 4405–4465.

[14] Yi Heng Cheong, Liya Ge, and Grzegorz Lisak. “Highly reproducible solid contact ion selective electrodes: Emerging opportunities for potentiometry – A review”. In: *Analytica Chimica Acta* 1162 (2021), p. 338304.

[15] Nicolas Moser et al. “ISFET Arrays for Lab-on-Chip Technology: A Review”. In: *2019 26th IEEE International Conference on Electronics, Circuits and Systems (ICECS)*. 2019, pp. 57–60.

[16] Nicolas Moser et al. “ISFETs in CMOS and Emergent Trends in Instrumentation: A Review”. In: *IEEE Sensors Journal* 16.17 (2016), pp. 6496–6514.

[17] Silvestre Salas-Rodríguez et al. “Recent advances of Ion Sensing based on Flexible Low Temperature Thin Film Transistors”. In: *2021 IEEE Latin America Electron Devices Conference (LAEDC)*. 2021, pp. 1–4.

[18] Soumendu Sinha and Tapas Pal. “A comprehensive review of FET-based pH sensors: materials, fabrication technologies, and modeling”. In: *Electrochemical Science Advances* n/a.n/a (), p. 2100147.

[19] SM Goetz et al. “Organic field-effect transistors for biosensing applications”. In: *Organic Electronics* 10.4 (2009), pp. 573–580.

[20] Nada Mzoughi et al. “Characterization of novel impedimetric pH-sensors based on solution-processable biocompatible thin-film semiconducting organic coatings”. In: *Sensors and Actuators B: Chemical* 171 (2012), pp. 537–543.

[21] M Brischwein et al. “Ultrathin Electrochemical Chemo-and Biosensors”. In: *Ed. VM Mirsky* (2004), pp. 159–180.

[22] J. Wiest et al. “Intelligent Mobile Lab for Metabolics in Environmental Monitoring”. In: *Analytical Letters* 39.8 (2006), pp. 1759–1771.

[23] Martin Brischwein et al. “5 Toward Printable Lab-on-for Cell Analytics”. In: *Biological and Medical Sensor Technologies* (2017), p. 125.

[24] Leland C Clark Jr and Champ Lyons. “Electrode systems for continuous monitoring in cardiovascular surgery”. In: *Annals of the New York Academy of sciences* 102.1 (1962), pp. 29–45.

[25] Srinjoy Mitra and David RS Cumming. *CMOS Circuits for Biological Sensing and Processing*. Springer, 2017.

[26] A.J. Bard and L.R. Faulkner. *Electrochemical Methods: Fundamentals and Applications*. Wiley, 2000, 368ff.

[27] Andreas Hierlemann and Henry Baltes. "11 - Semiconductor-Based Chemical Microsensors". In: *MEMS*. Ed. by Jan G. Korvink and Oliver Paul. Norwich, NY: William Andrew Publishing, 2006, pp. 567–666.

[28] Martin Matthäus Aicher. "Entwicklung von Ca2+ und Mg2+ Sensoren in Mikrotechnologie". Dissertation. München: Technische Universität München, 2017.

[29] Nicole Jaffrezic-Renault and Sergei V Dzyadevych. "Conductometric microbiosensors for environmental monitoring". In: *Sensors* 8.4 (2008), pp. 2569–2588.

[30] C. Day et al. "Impedance-based sensor for potassium ions". In: *Analytica Chimica Acta* 1034 (2018), pp. 39–45.

[31] Asma Bananezhad et al. "Large-scale fabrication of flexible solid-state reference electrodes". In: *Journal of Electroanalytical Chemistry* 847 (2019), p. 113241.

[32] AA Shul'ga, B Ahlers, and K Cammann. "Ion-selective conductometric microsensors based on the phenomenon of specific salt extraction". In: *Journal of Electroanalytical Chemistry* 395.1-2 (1995), pp. 305–308.

[33] K Cammann et al. "New sensing principles for ion detection". In: *Sensors and Actuators B: Chemical* 35.1-3 (1996), pp. 26–31.

[34] U Trebbe et al. "A new calcium-sensor based on ion-selective conductometric microsensors–membranes and features". In: *Fresenius' Journal of Analytical Chemistry* 371.6 (2001), pp. 734–739.

[35] KN Mikhelson and MA Peshkova. "Advances and trends in ionophore-based chemical sensors". In: *Russian Chemical Reviews* 84.6 (2015), p. 555.

[36] Mohamed Braiek et al. "A conductometric sensor for potassium detection in whole blood". In: *Sensors and Actuators B: Chemical* 235 (2016), pp. 27–32.

[37] Manju Gerard, Asha Chaubey, and B.D. Malhotra. "Application of conducting polymers to biosensors". In: *Biosensors and Bioelectronics* 17.5 (2002), pp. 345–359.

[38] Pedro Estrela et al. "Optical biosensors". In: *Essays in Biochemistry* 60.1 (June 2016), pp. 91–100.

[39] Chen Chen and Junsheng Wang. "Optical biosensors: An exhaustive and comprehensive review". In: *Analyst* 145.5 (2020), pp. 1605–1628.

[40] John R Moody and Thomas W Vetter. "Development of the ion exchange-gravimetric method for sodium in serum as a definitive method". In: *Journal of research of the National Institute of Standards and Technology* 101.2 (1996), p. 155.

[41] Ikuo Satoh. “Calorimetric Biosensing of Heavy Metal Ions with the Reactors Containing the Immobilized Apoenzymes”. In: *Annals of the New York Academy of Sciences* 613.1 (1990), pp. 401–404.

[42] Ikuo Satoh. “”An apoenzyme thermistor microanalysis for zinc (II) ions with use of an immobilized alkaline phosphatase reactor in a flow system””. In: *Biosensors and Bioelectronics* 6.4 (1991), pp. 375–379.

[43] Ikuo Satoh. *Advances in Molecular and Cell Biology, 15 B*. 1996.

[44] Qiancheng Zhao et al. “Ion permeation and mechanotransduction mechanisms of mechanosensitive piezo channels”. In: *Neuron* 89.6 (2016), pp. 1248–1263.

[45] Lord Rayleigh. “On Waves Propagated along the Plane Surface of an Elastic Solid”. In: *Proceedings of the London Mathematical Society* s1-17.1 (1885), pp. 4–11.

[46] Khasim Cali, Elena Tuccori, and Krishna C. Persaud. “Chapter Eighteen - Gravimetric biosensors”. In: *Odorant Binding and Chemosensory Proteins*. Ed. by Paolo Pelosi and Wolfgang Knoll. Vol. 642. Methods in Enzymology. Academic Press, 2020, pp. 435–468.

[47] David B Go et al. “Surface acoustic wave devices for chemical sensing and microfluidics: a review and perspective”. In: *Analytical methods* 9.28 (2017), pp. 4112–4134.

[48] Min-Hee Kim, In-Keun Yu, and Seong-Ho Choi. “Development of an Ionic Quartz Crystal Microbalance (QCM) Sensors for the Detection of Na+ and K+ in Human Urine”. In: *Sensor Letters* 17.9 (2019), pp. 671–679.

[49] Ye Chang et al. “Detection of volatile organic compounds by self-assembled monolayer coated sensor array with concentration-independent fingerprints”. In: *Scientific reports* 6.1 (2016), pp. 1–12.

[50] Yi Zhang et al. “Film bulk acoustic resonators (FBARs) as biosensors: A review”. In: *Biosensors and Bioelectronics* 116 (2018), pp. 1–15.

[51] Amir Rahafrooz and Siavash Pourkamali. “Resonant MEMS sensors for detection of aqueous heavy metal ions with Sub-ppm resolution”. In: *2008 IEEE International Conference on Electron Devices and Solid-State Circuits*. 2008, pp. 1–4.

[52] Changgeng Liu et al. “Micromachining techniques in developing high-frequency piezoelectric composite ultrasonic array transducers”. In: *IEEE Transactions on Ultrasonics, Ferroelectrics, and Frequency Control* 60.12 (2013), pp. 2615–2625.

[53] Marcel Thränhardt et al. “Sensing physical fluid properties with CMUT arrays”. In: *2009 IEEE International Ultrasonics Symposium*. 2009, pp. 763–766.

[54] William A Catterall. "Neurotoxins that act on voltage-sensitive sodium channels in excitable membranes". In: *Annual Review of Pharmacology and Toxicology* 20.1 (1980), pp. 15–43.

[55] Sigma Aldrich. *Sodium ionophore X, Selectophore (TM)*. https://www.sigmaaldrich.com/DE/de/product/sial/71747andhttps://www.sigmaaldrich.com/DE/de/product/sial/19731. [Online; accessed 14-Jan-2022]. 2022.

[56] Mohammed Zourob, Sauna Elwary, and Anthony PF Turner. *Principles of bacterial detection: biosensors, recognition receptors and microsystems*. Springer Science & Business Media, 2008.

[57] Hach. *Sension+ 9650 Sodium Ion Selective Electrode (ISE)*. https://www.hach.com/sension-9650-sodium-ion-selective-electrode-ise-sensor-only/product-details?id=7640597363. [Online; accessed 14-Jan-2022]. 2022.

[58] Thermo Scientific. *Thermo Scientific™ Orion™ Plastic-Membrane ISE Sensor Modules*. https://www.fishersci.at/shop/products/thermo-scientific-orion-plastic-membrane-ise-sensor-modules/10749741. [Online; accessed 14-Jan-2022]. 2022.

[59] Mettler Toledo. *DX223-Na Sodium half-cell*. https://www.mt.com/de/en/home/products/Laboratory_Analytics_Browse/Product_Family_Browse_titrators_main/Product_Family_Titration_Sensors/Titration_Ion_Selective_sensors_Fami/Sodium_Electrode.html. [Online; accessed 14-Jan-2022]. 2022.

[60] George Eisenman, Donald O. Rudin, and James U. Casby. "Glass Electrode for Measuring Sodium Ion". In: *Science* 126.3278 (1957), pp. 831–834.

[61] Xylem1. *ISE sensor for ammonium - WTW*. hhttps://www.xylemanalytics.com/en/general-product/id-152/ise-sensor-for-ammonium---wtw. [Online; accessed 14-Jan-2022]. 2022.

[62] Chun-Ze Lai et al. "Subnanomolar detection limit application of ion-selective electrodes with three-dimensionally ordered macroporous (3DOM) carbon solid contacts". In: *Journal of Solid State Electrochemistry* 13.1 (2009), pp. 123–128.

[63] Lajos Höfler et al. "Limitations of current polarization for lowering the detection limit of potentiometric polymeric membrane sensors". In: *Analytical chemistry* 81.9 (2009), pp. 3592–3599.

[64] MetroOhm. *Sodium-selective glass electrode*. https://www.metrohm.com/en/products/60501100?__cf_chl_f_tk=9YlMhSOy6s2TD.qqJj7fdz.z1Jy2TrYCNPVg6C0gNf0-1642190207-0-gaNycGzNCJE7. [Online; accessed 14-Jan-2022]. 2022.

[65] Konstantin N Mikhelson. "Ion-Selective Electrodes with Crystalline Membranes". In: *Ion-Selective Electrodes*. Springer, 2013, pp. 113–124.

[66] Mohd Zeeshan et al. “Fabrication of a lead ion selective membrane based on a polycarbazole Sn (iv) arsenotungstate nanocomposite and its ion exchange membrane (IEM) kinetic studies”. In: *RSC Advances* 11.7 (2021), pp. 4210–4220.

[67] L. Gilbert et al. “Development of an amperometric, screen-printed, single-enzyme phosphate ion biosensor and its application to the analysis of biomedical and environmental samples”. In: *Sensors and Actuators B: Chemical* 160.1 (2011), pp. 1322–1327.

[68] I.S. Kucherenko et al. “Electrochemical biosensors based on multienzyme systems: Main groups, advantages and limitations – A review”. In: *Analytica Chimica Acta* 1111 (2020), pp. 114–131.

[69] N. Conrath et al. “A novel enzyme sensor for the determination of inorganic phosphate”. In: *Analytica Chimica Acta* 309.1 (1995), pp. 47–52.

[70] Sagir Alva, Lee yook heng, and Ahmad Musa. “Screen-Printed Potassium Ion Sensor Fabricated from Photocureable and Self-Plasticized Acrylic Film”. In: *Journal of Physical Science* (Jan. 2006).

[71] Qi Zhang et al. “Plasticizer-Free Thin-Film Sodium-Selective Optodes Inkjet-Printed on Transparent Plastic for Sweat Analysis”. In: *ACS Applied Materials & Interfaces* 12.23 (2020), pp. 25616–25624.

[72] Li Guang and Xu Hui. *Full-solid potassium ion sensor and preparation method thereof*. CN101871912A. June 2010.

[73] Hongjie Jiang et al. “Inkjet-printed Solid-state Potentiometric Nitrate Ion Selective Electrodes for Agricultural Application”. In: *2019 IEEE SENSORS*. 2019, pp. 1–4.

[74] Boris Lakard. “Electrochemical Biosensors Based on Conducting Polymers: A Review”. In: *Applied Sciences* 10.18 (2020).

[75] Ya-nan Zhang et al. “Optical fiber sensors for measurement of heavy metal ion concentration: A review”. In: *Measurement* 158 (2020), p. 107742.

[76] John F. Alder et al. “Communication. An optical potassium ion sensor”. In: *Analyst* 112 (8 1987), pp. 1191–1192.

[77] Christian Pfeffer et al. “A Cost-Effective, Impediometric Na+-Sensor in Fluids”. In: *IEEE Sensors Letters* 5.6 (2021), pp. 1–4.

[78] E. Barsoukov and J.R. Macdonald. *Impedance Spectroscopy: Theory, Experiment, and Applications*. Wiley, 2005, 29ff.

[79] Md Eshrat E. Alahi and Subhas Chandra Mukhopadhyay. “Detection Methodologies for Pathogen and Toxins: A Review”. In: *Sensors* 17.8 (2017).

[80] Ellen Cesewski and Blake N Johnson. “Electrochemical biosensors for pathogen detection”. In: *Biosensors and Bioelectronics* (2020), p. 112214.

[81] Max Maurin. “Real-time PCR as a diagnostic tool for bacterial diseases”. In: *Expert Review of Molecular Diagnostics* 12.7 (2012), pp. 731–754.

[82] P Rajapaksha et al. “A review of methods for the detection of pathogenic microorganisms”. In: *Analyst* 144.2 (2019), pp. 396–411.

[83] Simon Toze. “PCR and the detection of microbial pathogens in water and wastewater”. In: *Water Research* 33.17 (1999), pp. 3545–3556.

[84] Saima Hameed, Lijuan Xie, and Yibin Ying. “Conventional and emerging detection techniques for pathogenic bacteria in food science: A review”. In: *Trends in Food Science and Technology* 81 (2018), pp. 61–73.

[85] Phillip Belgrader et al. “PCR detection of bacteria in seven minutes”. In: *Science* 284.5413 (1999), pp. 449–450.

[86] Hannah Kleyer, Robin Tecon, and Dani Or. “Resolving Species Level Changes in a Representative Soil Bacterial Community Using Microfluidic Quantitative PCR”. In: *Frontiers in Microbiology* 8 (2017).

[87] Olivier Lazcka, F Javier Del Campo, and F Xavier Munoz. “Pathogen detection: A perspective of traditional methods and biosensors”. In: *Biosensors and bioelectronics* 22.7 (2007), pp. 1205–1217.

[88] Satish Kumar Pandey, Girish Chandra Mohanta, and Parveen Kumar. “Chapter 6 - Development of Disposable Sensor Strips for Point-of-Care Testing of Environmental Pollutants”. In: *Advances in Nanosensors for Biological and Environmental Analysis*. Ed. by Akash Deep and Sandeep Kumar. Elsevier, 2019, pp. 95–118.

[89] S Sieuwerts, FA De Bok, and E Mols. “de vos WM, Vlieg JE”. In: *A simple and fast method for determining colony forming units. Letters in applied microbiology* 47.4 (2008), pp. 275–8.

[90] B Wolf et al. “Cell meets Silicon: Mikrosensorarrays für biomedizinische Forschung, Diagnostik und pharmazeutisches Screening”. In: *Bulletin des Schweizerischen Elektrotechnischen Vereins, des Verbandes Schweizerischer Elektrizitatswerke* 94.19 (2003), pp. 11–15.

[91] Angela M Otto et al. “Chips statt Mäuse: Zellen auf bioelektronischen Sensorchips als Alternative zu Tierversuchen”. In: *ALTEX* 21.3 (2004), pp. 70–76.

[92] Angela M Otto et al. “Analysis of drug action on tumor cell metabolism using electronic sensor chips”. In: *Archiv der Pharmazie: An International Journal Pharmaceutical and Medicinal Chemistry* 337.12 (2004), pp. 682–686.

[93] Volker Lob et al. “Cell-based assays: mikrosensorarray-basiertes screening an lebenden Zellen und Geweben”. In: *Biospektrum* 11 (2005), pp. 511–512.

[94] Thomas Geisler et al. “Automated multiparametric platform for high-content and high-throughput analytical screening on living cells”. In: *IEEE Transactions on automation science and engineering* 3.2 (2006), pp. 169–176.

[95] Lisa D Sprague et al. “Multiparametric sensor-chip based technology for monitoring metabolic activity: A proof-of-principle study with live tissue.” In: *Clinical Laboratory* 52.7-8 (2006), pp. 375–384.

[96] M Brischwein et al. “Planar ruthenium oxide sensors for cell-on-a-chip metabolic studies”. In: *Chemia Analityczna* 54.6 (2009), p. 1193.

[97] Markus Hefele et al. “Measuring fluorescence-lifetime and bio-impedance sensors for cell based assays using a network analyzer integrated circuit”. In: *Biosensors and Bioelectronics* 129 (2019), pp. 292–297.

[98] Mirko Lehmann et al. “Simultaneous measurement of cellular respiration and acidification with a single CMOS ISFET”. In: *Biosensors and Bioelectronics* 16.3 (2001), pp. 195–203.

[99] T Schwarzenberger et al. “Impedance sensor technology for cell-based assays in the framework of a high-content screening system”. In: *Physiological measurement* 32.7 (2011), p. 977.

[100] Martin Brischwein et al. “Electric cell-substrate impedance sensing with screen printed electrode structures”. In: *Lab on a Chip* 6.6 (2006), pp. 819–822.

[101] Cornelia Pfister et al. “Estimation of dynamic metabolic activity in micro-tissue cultures from sensor recordings with an FEM model”. In: *Medical & biological engineering & computing* 54.5 (2016), pp. 763–772.

[102] K Ziemiecka et al. “Scientific description of an in vitro model of secondary caries test new bio-impedance detection method based on microbial marker.” In: *Pol. J. Environ. Stud.* 22 (2013), pp. 67–73.

[103] Dujuan Li et al. “Label-free capacitive immunosensor based on quartz crystal Au electrode for rapid and sensitive detection of Escherichia coli O157: H7”. In: *Analytica chimica acta* 687.1 (2011), pp. 89–96.

[104] B Serra et al. “Lectin-modified piezoelectric biosensors for bacteria recognition and quantification”. In: *Analytical and bioanalytical chemistry* 391.5 (2008), pp. 1853–1860.

[105] Richard M White and Fred W Voltmer. “Direct piezoelectric coupling to surface elastic waves”. In: *Applied physics letters* 7.12 (1965), pp. 314–316.

[106] Maria-Isabel Rocha-Gaso et al. “Surface generated acoustic wave biosensors for the detection of pathogens: A review”. In: *Sensors* 9.7 (2009), pp. 5740–5769.

[107] Tara Elkin et al. “Immuno-carbon nanotubes and recognition of pathogens”. In: *ChemBioChem* 6.4 (2005), pp. 640–643.

[108] Yi Lin et al. “Carbon nanotubes for immunomagnetic separation of Escherichia coli O157: H7”. In: *Journal of nanoscience and nanotechnology* 6.3 (2006), pp. 868–871.

[109] Jinseok Heo and Susan Z Hua. “An overview of recent strategies in pathogen sensing”. In: *Sensors* 9.6 (2009), pp. 4483–4502.

[110] Robert Nißler et al. “Remote near infrared identification of pathogens with multiplexed nanosensors”. In: *Nature communications* 11.1 (2020), pp. 1–12.

[111] Sungkyu Seo et al. “Microelectrical noise detector for rapid, specific, and sensitive identification of bacteria”. In: *Journal of Vacuum Science & Technology B: Microelectronics and Nanometer Structures Processing, Measurement, and Phenomena* 24.6 (2006), pp. 3133–3138.

[112] A-E Depince-Berger et al. “New tools in cytometry”. In: *Morphologie* 100.331 (2016), pp. 199–209.

[113] Maik Herbig et al. “Label-free imaging flow cytometry for analysis and sorting of enzymatically dissociated tissues”. In: *Scientific reports* 12.1 (2022), pp. 1–17.

[114] Lena Ganda Saptalena, Andriy Kuklya, and Ursula Telgheder. “Gas chromatography–differential mobility spectrometry and gas chromatography–mass spectrometry for the detection of coliform bacteria”. In: *International Journal of Mass Spectrometry* 388 (2015), pp. 17–25.

[115] Ji Young Lee et al. “Label-free detection of single living bacteria via electrochemical collision event”. In: *Scientific reports* 6.1 (2016), pp. 1–6.

[116] Cristina Quintelas et al. “Near-infrared spectroscopy for the detection and quantification of bacterial contaminations in pharmaceutical products”. In: *International journal of pharmaceutics* 492.1-2 (2015), pp. 199–206.

[117] Susann Meisel et al. “Assessment of two isolation techniques for bacteria in milk towards their compatibility with Raman spectroscopy”. In: *Analyst* 136.23 (2011), pp. 4997–5005.

[118] Yu Liu et al. “Label and label-free based surface-enhanced Raman scattering for pathogen bacteria detection: A review”. In: *Biosensors and Bioelectronics* 94 (2017), pp. 131–140.

[119] Paul Béland, Oleksiy Krupin, and Pierre Berini. “Selective detection of bacteria in urine with a long-range surface plasmon waveguide biosensor”. In: *Biomedical optics express* 6.8 (2015), pp. 2908–2922.

[120] Mariateresa Ferone et al. “Microbial detection and identification methods: Bench top assays to omics approaches”. In: *Comprehensive Reviews in Food Science and Food Safety* 19.6 (2020), pp. 3106–3129.

[121] SJ Park et al. *Detection of microorganisms using terahertz metamaterials Sci.* 2014.

[122] Leopold Kremser, Dieter Blaas, and Ernst Kenndler. “Capillary electrophoresis of biological particles: Viruses, bacteria, and eukaryotic cells”. In: *ELECTROPHORESIS* 25.14 (2004), pp. 2282–2291.

[123] Meera J Desai and Daniel W Armstrong. “Separation, identification, and characterization of microorganisms by capillary electrophoresis”. In: *Microbiology and molecular biology reviews* 67.1 (2003), pp. 38–51.

[124] L.A. Kartsova et al. “Capillary electrophoresis as a powerful tool for the analyses of bacterial samples”. In: *TrAC Trends in Analytical Chemistry* 134 (2021), p. 116110.

[125] Hui-min Neoh et al. “Pulsed-field gel electrophoresis (PFGE): A review of the “gold standard” for bacteria typing and current alternatives”. In: *Infection, Genetics and Evolution* 74 (2019), p. 103935.

[126] Robert K Selander et al. “Methods of multilocus enzyme electrophoresis for bacterial population genetics and systematics”. In: *Applied and environmental microbiology* 51.5 (1986), pp. 873–884.

[127] B.R. Jennings and V.J. Morris. “Light scattering by bacteria. II. Size and electrical properties of E. Coli”. In: *Journal of Colloid And Interface Science* 49.1 (1974). cited By 17, pp. 89–97.

[128] Dietmar Puchberger-Enengl et al. “Microfluidic concentration of bacteria by on-chip electrophoresis”. In: *Biomicrofluidics* 5.4 (2011), p. 044111.

[129] Michie Yasuda and Michael Peter Shiaris. “Differentiation of bacterial strains by thermal gradient gel electrophoresis using non-GC-Clamped PCR primers for the 16S–23S rDNA intergenic spacer region”. In: *FEMS Microbiology Letters* 243.1 (Feb. 2005), pp. 235–242.

[130] Ronghui Zhou, Ping Wang, and Hsueh-Chia Chang. “Bacteria capture, concentration and detection by alternating current dielectrophoresis and self-assembly of dispersed single-wall carbon nanotubes”. In: *Electrophoresis* 27.7 (2006), pp. 1376–1385.

[131] Christian Pfeffer et al. “Towards Easy-to-Use Bacteria Sensing: Modeling and Simulation of a New Environmental Impedimetric Biosensor in Fluids”. In: *Sensors* 21.4 (2021).

[132] Sumihiro Koyama et al. “Attachment and detachment of living microorganisms using a potential-controlled electrode”. In: *Marine Biotechnology* 15.4 (2013), pp. 461–475.

[133] Albert Saavedra et al. “Attachment of Leptospirillum sp. to chemically modified pyrite surfaces. Fast and simple electrochemical monitoring of bacterial-mineral interactions”. In: *Hydrometallurgy* (2020), p. 105534.

[134] Sumihiro Koyama et al. “Electrical retrieval of living microorganisms from cryopreserved marine sponges using a potential-controlled electrode”. In: *Marine Biotechnology* 17.5 (2015), pp. 678–692.

[135] Sumihiro Koyama and Takao Yoshida. “Electrical Collection of Membrane-intact and Dehydrogenase-positive Symbiotic Bacteria from the Deep-sea Bivalve Calyptogena Okutanii”. In: *Electrochemistry* 84.5 (2016), pp. 358–360.

[136] Anil K Deisingh and Michael Thompson. “Detection of infectious and toxigenic bacteria”. In: *Analyst* 127.5 (2002), pp. 567–581.

[137] Douglas A Boehm, Philip A Gottlieb, and Susan Z Hua. “On-chip microfluidic biosensor for bacterial detection and identification”. In: *Sensors and Actuators B: Chemical* 126.2 (2007), pp. 508–514.

[138] Andrea Carbonaro et al. “Cell characterization using a protein-functionalized pore”. In: *Lab on a Chip* 8.9 (2008), pp. 1478–1485.

[139] Paulo A. Raymundo-Pereira et al. “A Nanostructured Bifunctional platform for Sensing of Glucose Biomarker in Artificial Saliva: Synergy in hybrid Pt/Au surfaces”. In: *Biosensors and Bioelectronics* 86 (2016), pp. 369–376.

[140] Xuanhong Cheng et al. “Cell detection and counting through cell lysate impedance spectroscopy in microfluidic devices”. In: *Lab on a Chip* 7.6 (2007), pp. 746–755.

[141] Joseph C Liao et al. “Use of electrochemical DNA biosensors for rapid molecular identification of uropathogens in clinical urine specimens”. In: *Journal of clinical microbiology* 44.2 (2006), pp. 561–570.

[142] Olivier Laczka et al. “Detection of Escherichia coli and Salmonella typhimurium using interdigitated microelectrode capacitive immunosensors: the importance of transducer geometry”. In: *Analytical chemistry* 80.19 (2008), pp. 7239–7247.

[143] Lei Yao et al. “CMOS capactive sensor system for bacteria detection using phage organisms”. In: *2008 Canadian Conference on Electrical and Computer Engineering*. IEEE. 2008, pp. 000877–000880.

[144] Liju Yang et al. “Interdigitated microelectrode (IME) impedance sensor for the detection of viable Salmonella typhimurium”. In: *Biosensors and bioelectronics* 19.10 (2004), pp. 1139–1147.

[145] Liang Su et al. “Microbial biosensors: A review”. In: *Biosensors and Bioelectronics* 26.5 (2011), pp. 1788–1799.

[146] Alberto Olmo and Alberto Yúfera. “Computer Simulation of Microelectrode based Bio-Impedance Measurements with COMSOL.” In: *Biodevices*. 2010, pp. 178–182.

[147] Pubchem Database Entry CID 2724889. *4-tert-Butylcalix[4]arene-tetraacetic acid tetraethyl ester*. https://pubchem.ncbi.nlm.nih.gov/compound/2724889. [Online; accessed 02-Apr-2022]. 2022.

[148] Ceradrop. *CERADROP, a MGI Group Company: All-in-one State-of-the-art Digital Materials Deposition Platform - CeraPrinter F-Serie*. http://www.ceradrop.com/en/products/f-serie/andhttp://www.ceradrop.com/content/uploads/2016/04/CeraPrinter_F-Serie.pdf. [Online; accessed 18-Feb-2022]. 2022.

[149] Sabine Zips. “Printing technologies for bioelectronic applications and organs-on-chips”. Dissertation. München: Technische Universität München, 2021.

[150] IM Hutchings et al. *Fundamentals of Inkjet Printing*. John Wiley and Sons, Ltd. 2015.

[151] L Jay Deiner and Thomas L Reitz. “Inkjet and aerosol jet printing of electrochemical devices for energy conversion and storage”. In: *Advanced Engineering Materials* 19.7 (2017), p. 1600878.

[152] Yang Guo et al. “Inkjet and inkjet-based 3D printing: connecting fluid properties and printing performance”. In: *Rapid Prototyping Journal* (2017).

[153] Akira Asai. “Three-Dimensional Calculation of Bubble Growth and Drop Ejection in a Bubble Jet Printer”. In: *Journal of Fluids Engineering-transactions of The Asme* 114 (1992), pp. 638–641.

[154] Herman Wijshoff. “The dynamics of the piezo inkjet printhead operation”. In: *Physics reports* 491.4-5 (2010), pp. 77–177.

[155] Brian Derby. “Inkjet printing of functional and structural materials: fluid property requirements, feature stability, and resolution”. In: *Annual Review of Materials Research* 40 (2010), pp. 395–414.

[156] Naoki Morita et al. “Inkjet printheads”. In: *Fundamentals of Inkjet Printing: The Science of Inkjet and Droplets. Weinheim, Germany: Wiley-VCH Verlag GmbH & Co. KGaA* (2016).

[157] JE Fromm. “Numerical calculation of the fluid dynamics of drop-on-demand jets”. In: *IBM Journal of Research and Development* 28.3 (1984), pp. 322–333.

[158] Sabine Zips et al. “Direct Stereolithographic 3D Printing of Microfluidic Structures on Polymer Substrates for Printed Electronics”. In: *Advanced Materials Technologies* 4.3 (2019), p. 1800455.

[159] Jonathan Stringer and Brian Derby. “Formation and stability of lines produced by inkjet printing”. In: *Langmuir* 26.12 (2010), pp. 10365–10372.

[160] Dan Soltman and Vivek Subramanian. “Inkjet-printed line morphologies and temperature control of the coffee ring effect”. In: *Langmuir* 24.5 (2008), pp. 2224–2231.

[161] PJ Smith et al. “Direct ink-jet printing and low temperature conversion of conductive silver patterns”. In: *Journal of materials science* 41.13 (2006), pp. 4153–4158.

[162] Paul C Duineveld. “The stability of ink-jet printed lines of liquid with zero receding contact angle on a homogeneous substrate”. In: *Journal of Fluid Mechanics* 477 (2003), pp. 175–200.

[163] Stephen H Davis. “Moving contact lines and rivulet instabilities. Part 1. The static rivulet”. In: *Journal of Fluid Mechanics* 98.2 (1980), pp. 225–242.

[164] Stefano Schiaffino and Ain A Sonin. “Formation and stability of liquid and molten beads on a solid surface”. In: *Journal of fluid mechanics* 343 (1997), pp. 95–110.

[165] Sabine Zips et al. “Fully printed μ-needle electrode array from conductive polymer ink for bioelectronic applications”. In: *ACS applied materials & interfaces* 11.36 (2019), pp. 32778–32786.

[166] COMSOL Multiphysics® COMSOL. “AC/DC Module User’s Guide COMSOL Multiphysics®v. 5.5. COMSOL”. In: *COMSOL Multiphysics® v. 5.5. COMSOL AB* (2018).

[167] Philippe Bühlmann, Ernö Pretsch, and Eric Bakker. “Carrier-based ion-selective electrodes and bulk optodes. 2. Ionophores for potentiometric and optical sensors”. In: *Chemical Reviews* 98.4 (1998), pp. 1593–1688.

[168] Christian Pfeffer and Sabine Zips. *Method of Forming an Acrylate-based Ionic Sensor and Corresponding Apparatus*. Application 20182319.2. June 2020.

[169] Daehwan Jang, Dongjo Kim, and Jooho Moon. “Influence of fluid physical properties on ink-jet printability”. In: *Langmuir* 25.5 (2009), pp. 2629–2635.

[170] Gareth H McKinley and Michael Renardy. “Wolfgang von Ohnesorge”. In: *Physics of Fluids* 23.12 (2011), p. 127101.

[171] Felix Naunheimer. “Ion Selective Sensors for Biotech and Life Science (Bachelor Thesis)”. Technische Universität München, 2021.

[172] S. Meier et al. “Patterning Platinum by Selective Wet Etching of Sacrificial Pt-Al Alloy”. In: *2020 4th IEEE Electron Devices Technology Manufacturing Conference (EDTM)*. 2020, pp. 1–4.

[173] PalmSens. *PalmSens4 Potentiostat Product Page*. https://www.palmsens.com/product/palmsens4/. [Online; accessed 14-Jan-2022]. 2022.

[174] Biologic Sciences Instruments. *Biologic VSP 300 Potentiostat*. https://www.biologic.net/products/vsp-300/. [Online; accessed 14-Jan-2022]. 2022.

[175] Emna Azek. “Fully Printed Ion Selective Sensors for Biotech and Life Science (Bachelor Thesis)”. Technische Universität München, 2021.

[176] A.J. Bard and L.R. Faulkner. “Electrochemical Methods: Fundamentals and Applications”. In: 2nd edition. Wiley, 2000, 368ff.

[177] Ed Vitz et al. *Hydration of Ions*. https://chem.libretexts.org/Bookshelves/General_Chemistry/Book%3A_ChemPRIME_(Moore_et_al.)/11%3A_Reactions_in_Aqueous_Solutions/11.04%3A_Hydration_of_Ions. [Online; accessed 02-Apr-2022]. 2022.

[178] Declan A Doyle et al. “The structure of the potassium channel: molecular basis of K+ conduction and selectivity”. In: *Science* 280.5360 (1998), pp. 69–77.

[179] E. Glueckauf. “The influence of ionic hydration on activity coefficients in concentrated electrolyte solutions”. In: *Trans. Faraday Soc.* 51 (0 1955), pp. 1235–1244.

[180] Robert H Stokes and Robert A Robinson. “Ionic hydration and activity in electrolyte solutions”. In: *Journal of the American Chemical Society* 70.5 (1948), pp. 1870–1878.

[181] Peter Debye and Hans Falkenhagen. “Dispersion of the conductivity and dielectric constants of strong electrolytes”. In: *Physikalische Zeitschrift* 29.121-132 (1928), pp. 401–426.

[182] P Debye. “Part I. Dielectric constant. Energy absorption in dielectrics with polar molecules”. In: *Transactions of the Faraday Society* 30 (1934), pp. 679–684.

[183] James Clerk Maxwell. “VIII. A dynamical theory of the electromagnetic field”. In: *Philosophical transactions of the Royal Society of London* 155 (1865), pp. 459–512.

[184] Attay Kovetz et al. *The principles of electromagnetic theory*. CUP Archive, 1990.

[185] JM Jin. “The Finite Element Method in Electromagnetics. 2nd (ed.) Wiley”. In: *John Wiley and Sons* (2002).

[186] David Keun Cheng et al. *Field and wave electromagnetics*. Pearson Education India, 1989.

[187] Branko D Popović. *Introductory engineering electromagnetics*. Addison-Wesley Publishing Company, 1971.

[188] João Pedro A Bastos and Nelson Sadowski. *Magnetic materials and 3D finite element modeling*. CRC press, 2013.

[189] COMSOL Multiphysics® COMSOL. "AC/DC Module User's Guide COMSOL Multiphysics®v. 5.5. COMSOL". In: *COMSOL Multiphysics® v. 5.5. COMSOL AB* (2018), 93ff.

[190] Klaus J Vetter and Sidney Barnatt. "Electrochemical Kinetics: Theoretical Aspects". In: *Journal of the Electrochemical Society* 115.8 (1968), 262CA.

[191] Edmund J.F. Dickinson and Andrew J. Wain. "The Butler-Volmer equation in electrochemical theory: Origins, value, and practical application". In: *Journal of Electroanalytical Chemistry* 872 (2020). Dr. Richard Compton 65th birthday Special issue, p. 114145.

[192] Haoqing Zhang, Honglong Chang, and Pavel Neuzil. "DEP-on-a-Chip: Dielectrophoresis Applied to Microfluidic Platforms". In: *Micromachines* 10.6 (2019).

[193] Herbert Ackland Pohl. "Some Effects of Nonuniform Fields on Dielectrics". In: *Journal of Applied Physics* 29.8 (1958), pp. 1182–1188.

[194] Herbert A. Pohl. "The Motion and Precipitation of Suspensoids in Divergent Electric Fields". In: *Journal of Applied Physics* 22.7 (1951), pp. 869–871.

[195] Herbert Ackland Pohl. "Dielectrophoresis". In: *The behavior of neutral matter in nonuniform electric fields* (1978).

[196] Herman P Schwan. "Electrical properties of tissue and cell suspensions". In: *Advances in biological and medical physics*. Vol. 5. Elsevier, 1957, pp. 147–209.

[197] Ronald Pethig. "Dielectric properties of biological materials: Biophysical and medical applications". In: *IEEE transactions on electrical insulation* 5 (1984), pp. 453–474.

[198] Nurhaslina Abd Rahman, Fatimah Ibrahim, and Bashar Yafouz. "Dielectrophoresis for Biomedical Sciences Applications: A Review". In: *Sensors* 17.3 (2017).

[199] Liju Yang. "A Review of Multifunctions of Dielectrophoresis in Biosensors and Biochips for Bacteria Detection". In: *Analytical Letters* 45.2-3 (2012), pp. 187–201.

[200] Akihiko Irimajiri, Tetsuya Hanai, and Akira Inouye. "A dielectric theory of "multi-stratified shell" model with its application to a lymphoma cell". In: *Journal of theoretical biology* 78.2 (1979), pp. 251–269.

[201] Tyler Shake et al. “Embedded passivated-electrode insulator-based dielectrophoresis (EπDEP)”. In: *Analytical and bioanalytical chemistry* 405.30 (2013), pp. 9825–9833.

[202] Raphael Oefelein. “Analyse und Bewertung eines Impedanzsesnorszur Bakteriendetektion in Verdunstungskuehlanlagen (Bachelor Thesis)”. Hochschule Weihenstephan Triesdorf Fakultaet Bioingenieurwissenschaften in cooperation with domatec GmbH, 2021.

[203] Su-Moon Park and Jung-Suk Yoo. *Peer reviewed: electrochemical impedance spectroscopy for better electrochemical measurements*. Anal. Chem. 2003, 75, 21, 455 A–461 A. 2003.

[204] Peng Bai and Martin Z Bazant. “Charge transfer kinetics at the solid–solid interface in porous electrodes”. In: *Nature communications* 5.1 (2014), pp. 1–7.

[205] J Alvarez-Ramirez et al. “Non-Linear First-Harmonic Balance to Compute the Electrochemical Impedance of Butler-Volmer Equation”. In: *Journal of The Electrochemical Society* 165.9 (2018), H517.

[206] Gamry Instruments. *Basics of Electrochemical Impedance Spectroscopy*. ttps://www.gamry.com/application-notes/EIS/basics-of-electrochemical-impedance-spectroscopy/. [Online; accessed 14-Jan-2022]. 2022.

[207] Zbigniew Adamczyk. “Diffusion of Particles”. In: *Encyclopedia of Colloid and Interface Science*. Berlin, Heidelberg: Springer Berlin Heidelberg, 2013, pp. 247–247.

[208] A.J. Bard and L.R. Faulkner. “Electrochemical Methods: Fundamentals and Applications”. In: 2nd edition. Wiley, 2000, 419ff.

[209] G. Pioggia et al. “A composite sensor array impedentiometric electronic tongue: Part I. Characterization”. In: *Biosensors and Bioelectronics* 22.11 (2007), pp. 2618–2623.

[210] Krzysztof Maksymiuk, Emilia Stelmach, and Agata Michalska. “Unintended Changes of Ion-Selective Membranes Composition—Origin and Effect on Analytical Performance”. In: *Membranes* 10.10 (Sept. 2020), p. 266.

[211] Rocío Cánovas et al. “Cytotoxicity Study of Ionophore-Based Membranes: Toward On-Body and in Vivo Ion Sensing”. In: *ACS Sensors* 4.9 (2019). PMID: 31448593, pp. 2524–2535.

[212] Sigma Aldrich. *Available Ionophores*. https://www.sigmaaldrich.com/. [Online; accessed 14-Jan-2022]. 2022.